AVERTISSEMENT

Ce document est le fruit d'un long travail approuvé par le jury de soutenance et mis à disposition de l'ensemble de la communauté universitaire élargie.

Il est soumis à la propriété intellectuelle de l'auteur. Ceci implique une obligation de citation et de référencement lors de l'utilisation de ce document.

D'autre part, toute contrefaçon, plagiat, reproduction illicite encourt une poursuite pénale.

Contact : ddoc-theses-contact@univ-lorraine.fr

LIENS

Code de la Propriété Intellectuelle. articles L 122. 4
Code de la Propriété Intellectuelle. articles L 335.2- L 335.10
http://www.cfcopies.com/V2/leg/leg_droi.php
http://www.culture.gouv.fr/culture/infos-pratiques/droits/protection.htm

03INPL106N

INSTITUT NATIONAL POLYTECHNIQUE DE LORRAINE
ECOLE NATIONALE SUPERIEURE DES INDUSTRIES CHIMIQUES
LABORATOIRE DES SCIENCES DU GENIE CHIMIQUE DU CNRS

THESE

présentée à l'INPL
Ecole Doctorale Ressources, Procédés, Produits, Environnement
en vue d'obtenir le titre de Docteur
de l'Institut National Polytechnique de Lorraine
Spécialité: Génie des Procédés

par Wenli SONG

Service Commun de la Documentation
INPL
Nancy-Brabois

Contrôle de l'émission de composés organiques volatils par adsorption en lit fluidisé circulant

---

Thèse en co-tutelle avec
Institute of Process Engineering, Chinese Academy of Sciences, Beijing, Chine

Soutenue à Pékin, le 12 décembre 2003

Jury

Hongzhong LI, Professeur, Institute of Process Engineering, CAS, Beijing (rapporteur)
Weiyang FEI, Professeur, Université Tsinghua, Beijing
Jinghai LI, Profe[illegible], CAS, Beijing, (directeur de thèse)
John DODDS, P[illegible]naux (rapporteur)
Lingai LUO (M[illegible]Chambéry (co-directeur de thèse)
Daniel TONDEU[illegible]Nancy (directeur de thèse)

D 136 035260 4

Invités
Xigang YUAN, Professeur, Université de Tianjin, Tianjin
Michel SARDIN, Professeur, Institut National Polytechnique de Lorraine, Nancy

136035 2604

03 INPL 106 N

VOC Emission Control by Circulating Fluidized Bed Adsorption

[T] 2003 SONG W.

Dissertation Submitted to

Institut National Polytechnique de Lorraine

Doctoral School: Resources, Processes, Products, Environment

in fulfillment of the requirement for the degree of

Doctor of INPL
Domain: Process Engineering

by

Wenli SONG

Defended on December 12, 2003, in BEIJING

Jury

Hongzhong LI, Professor, Institute of Process Engineering, CAS, Beijing (referee)
Weiyang FEI, Professor, Tsinghua University, Beijing
Jinghai LI, Professor, Institute of Process Engineering, CAS, Beijing, (supervisor)
John DODDS, Professor, Ecole des Mines d'Albi-Carmaux, France (referee)
Lingai LUO (Mrs), Professor, Université de Savoie, Chambéry, France (co-supervisor)
Daniel TONDEUR, Research Director at CNRS, Nancy, France (supervisor)

Invited guests
Xigang YUAN, Professor, Tianjin University, Tianjin
Michel SARDIN, Professor, Institut National Polytechnique de Lorraine, Nancy, France

RESUME

Contrôle de l'émission de Composés Organiques Volatils (COV) par adsorption en lit fluidisé circulant

Les composés organiques volatils (COV) sont les polluants gazeux les plus courants émis par les industries chimiques, pétrochimiques et parachimiques, mais également par des activités artisanales comme le nettoyage, la peinture, et par les transports. La majorité des procédés de capture par adsorption développés pour un contexte industriel sont des technologies à lit fixe. Quelques procédés utilisant des lits fluidisés multi-étagés ont vu le jour pour traiter des gaz dilués, mais l'utilisation d'un lit fluidisé circulant n'a fait l'objet d'aucune étude publiée à ce jour.

Les lits fluidisés circulants (LFC) fonctionnent en régime dit de "fluidisation rapide", avec un fort débit de solide et de gaz. Par ailleurs, les transferts solide-gaz de matière et de chaleur sont très rapides et l'on est dans des conditions quasi-isothermes. Ces caractéristiques font du LFC une alternative potentiellement intéressante aux procédés existants. Il reste à démontrer que l'on peut obtenir des degrés d'épuration poussés dans ce type d'appareils. Par ailleurs, le manque de modèle satisfaisant pour les écoulements et les transferts, le manque de méthodologie de simulation et d'expérimentation étaient des obstacles à la conception, au dimensionnement, à l'extrapolation, et à l'évaluation de ce procédé.

Le présent travail se propose de combler (en partie au moins) ces manques. On présentera successivement le modèle d'équilibre d'adsorption et sa détermination expérimentale, les expériences d'adsorption en CFB et leur interprétation, la modélisation de l'aéraulique du système gaz-particules dans le contacteur, le transfert de matière gaz-particules, et la modélisation du processus global d'adsorption dans le contacteur.

Les isothermes d'adsorption pour le système-modèle Toluène-Ambersorb 600 ont été mesurées et sont bien représentées par une équation de type Dubinin-Astakhov.

Un modèle mono-dimensionnel de moyenne complexité est mis en place pour l'écoulement gaz-solide. Il combine le modèle EMMS (Energy Minimization Multi-Scale) que l'on a modifié à l'aide d'une hypothèse simplificatrice, et qui fournit la répartition locale des domaines diphasiques dense et dilué, et le modèle de Kunii et Levenspiel pour la distribution axiale de la fraction volumique globale de gaz. Ce nouveau modèle donne accès à des grandeurs comme les fractions volumiques des domaines denses et dilués, les fractions volumiques solides et gaz internes à ces domaines, et les vitesses relatives dans tous ces domaines. À partir de là, on peut calculer les coefficients de transfert externes globaux gaz-solide. Une étude paramétrique montre comment la formation d'agglomérats (domaine dense) influence l'adsorption. Le transfert de matière est accéléré par une vitesse superficielle élevée du gaz et un débit faible de circulation du solide.

Ce modèle mono-dimensionnel est alors confronté aux résultats expérimentaux, et l'on définit des critères d'efficacité. Ainsi, on peut dire par exemple que l'efficacité de la phase solide est de 56 % (taux moyen de saturation de l'adsorbant) lorsque l'efficacité de la phase gazeuse est de 99 % (% d'abattement de la pollution). Cette efficacité du solide peut être augmentée par l'étagement du contacteur (deux contacteurs en série par exemple), ce qui permet également de diminuer le taux de recirculation du solide et la charge du désorbeur.

Enfin, on discute la possibilité d'effectuer dans une configuration de LFC des opérations équivalentes aux procédés en lit fixe classiques de TSA et de PSA (Adsorption modulée en température ou en pression).

Mots Principaux: Lit fluidisé circulant, Adsorption, Transfert de matière

Composés Organiques Volatils (COV)

摘要

挥发性有机物的循环流化床吸附净化

挥发性有机物(Volatile Organic Compounds, VOCs)是石油、化工及其相关行业排放的最常见的空气污染物。目前，已有几种采用多层鼓泡流化床的低浓度 VOCs 吸附处理工艺进入工业应用，但还没有采用循环流化床进行吸附净化处理的报道。

循环流化床(Circulating Fluidized Bed, CFB)通常操作在高气固通量的快速流态化状态下。循环流化床内的传热速率很高，可以达到几乎等温的工况。相对于鼓泡流化床，循环流化床内的气固接触效率更好，操作气速也更高，所以循环流化床吸附工艺应该是 VOCs 污染控制的一条可选择的新途径。目前还没有循环流化床吸附过程得到工业应用，其主要原因是对于循环流化床内气固流动和传递过程缺乏了解，及因此造成的循环流化床反应器的设计、预测和评价的困难。

本文对涉及 VOCs 的循环流化床吸附净化工艺的吸附等温线、循环流化床提升管内的流体动力学、气固之间的传质以及循环流化床内的吸附过程进行了研究。建立了间歇操作的 CFB 吸附实验装置，在不同条件下进行了 CFB 吸附实验。

采用重量法测量了 Ambersorb 600/甲苯体系的吸附等温线，在实验温度范围内它可以用 Dubinin-Astakhov 方程描述。

用修改的 EMMS 局部模型与 Kunii 和 Levenspiel 的夹带模型相结合，建立了描述循环流化床提升管内气固流动的一维模型。从而得到了描述床内各处聚团相与稀相具体结构的结构与流动参数，并讨论了操作条件的影响。在此基础上建立了 EMMS 传质模型用于计算气固间外传质系数。研究证明，循环流化床内聚团的存在是影响气固传质的主要因素。外部传质系数随表观气速的增加或固体循环速率的减小而提高。

所建立的一维吸附模型可以较好的描述循环流化床提升管内的吸附过程。表观气速的增加将使吸附质浓度沿床高的下降速度减慢，而固体循环速率的增加将使吸附质浓度沿床高的下降速度加快；对于 Ambersorb 600/甲苯体系，在气相效率

为99%时，固相效率为56%；采用多级循环流化床吸附系统可以增加吸附器的固相效率，同时也可以降低吸附剂的再生循环流量，即再生器的负荷。

本文还讨论了循环流化床吸附器基本参数的设计步骤；并对循环流化床变温、变压吸附净化系统的设计进行了讨论。

关键词：循环流化床，吸附，传质，挥发性有机物 (VOC)

ABSTRACT

Volatile Organic Compounds (VOC) Emission Control by Circulating Fluidized Bed Adsorption

Volatile Organic Compounds (VOCs) are the most common air pollutants emitted from chemical, petrochemical and allied industries. Several adsorption systems employing multi-stage bubble fluidized bed have been developed and operated in practice for dilute VOCs emission control, but no such process with CFB reactors has been reported.

The CFB are usually operated in the fast fluidization regime with high gas and solids throughput. The heat transfer inside the CFB is much faster and nearly isothermal conditions could be obtained. With improved gas–solid contacting and higher operation velocity than in a bubble fluidized bed, the CFB adsorption process is thus an alternative for emission reduction of dilute VOCs. Despite the advantages, the CFB reactor has not been used in industries for adsorption process until now. This mainly results from the lack of knowledge of hydrodynamics and transfer process involved in the CFB reactor, entailing difficulties in design, in extrapolation, in evaluation of performances.

In this study, we discussed the adsorption isotherm of adsorbate/adsorbent system, the hydrodynamics of gas and solid adsorbent particles in CFB riser, the mass transfer between gas and solid particle and the adsorption process inside the riser. The adsorption experiments with CFB test unit were also conducted.

The adsorption isotherm measurement for Ambersorb 600/toluene system has been conducted and the isotherm can be presented very well by Dubinin-Astakhov equation.

A one-dimensional model for gas-solid two-phase flow in a CFB riser has been established by combining the modified Energy Minimization Multi-Scale (EMMS) model describing the local hydrodynamics and Kunii and Levenspiel's entrainment model for axial voidage distribution. This new model was then used to estimate variables such as solid volume fraction and size of clusters, gas and solid velocities, and slip velocities between gas and solid particles and between dilute and cluster phases. Based on this, the external mass transfer coefficient between gas and solid particles was obtained. The research results shows that, the formation of clusters has significant influence on the mass transfer process. Higher superficial gas velocity and lower solid circulating rate will result in higher external mass transfer coefficient between gas and solid particle

The proposed one-dimensional adsorption model can be used to describe the adsorption

process in CFB riser. The higher superficial gas velocity and lower solid circulating rate will result in slower VOCs concentration reduction along the riser. For Ambersorb 600/toluene system, the experimental results show that while maintaining gas phase efficiency at 99%, the solid phase efficiency could reach 56%. The multi-stage CFB adsorber will increase the solid phase efficiency, reducing the adsorbent regeneration re-circulating rate and also the load of regenerator.

The design procedures for the CFB adsorber were discussed; the possible designs of CFB-PSA system and CFB-TSA system for emission control were also presented.

KEY WORDS: Circulating Fluidized Bed, Adsorption, Mass Transfer,
Volatile Organic Compounds (VOC)

CONTENTS

1. INTRODUCTION.....1
1.1. VOCs Emissions And Controlling Legislations.....1
1.1.1. VOCs Emissions.....2
1.1.2. VOCs Emissions Controlling Legislations.....2
1.2 Fluidized Bed Adsorption Process.....3
1.2.1. Earlier Practice.....3
1.2.2. Recent Development.....5
1.2.3. Circulating Fluidized Bed Adsorption Process.....6
1.3 Purposes of the Research.....6

2. ADSORPTION ISOTHERM.....9
2.1. Adsorption Isotherm Models.....9
2.1.1. Langmuir Isotherm.....9
2.1.2. Freundlich Isotherm.....10
2.1.3. Dubinin-Astakhov Equation.....10
2.2. Adsorbent and Adsorbate.....11
2.3. Experimental Setup and Procedures.....12
2.3.1. Experimental Setup.....12
2.3.2. Experimental Procedures.....13
2.3.3. Estimation of Weight Measurement Error.....14
2.4. Experimental Results and Discussions.....15
2.4.1. Experimental Results.....15
2.4.2. Data Fitting with Different Isotherms.....16
2.4.3. Isosteric Heat of Adsorption.....22
2.5. Conclusions.....24

3. CFB ADSORPTION EXPERIMENTS.....25
3.1. Experimental Setup.....25
3.1.1. CFB Unit.....25
3.1.2. The Gas Supply System.....26
3.1.3. The Solid Circulating System.....28

3.1.4. Gas Sampling and Pressure Sampling.....29
3.1.5. Measurement of Gas Phase Concentration.....30
3.1.6. Measurement of Axial Voidage Distribution.....31
3.2. Experimental Procedures.....32
3.2.1. Preparatory Operation.....32
3.2.2. Experimental Operations and Measurements.....32
3.2.3. Operation Conditions and Experimental Results.....34

4. BREAKTHROUGH CURVES.....37
4.1. Mathematical Model.....37
4.2. The Validation of Assumptions.....38
4.2.1. Influence of Inlet VOCs Concentrations.....38
4.2.2. Influence of Solid Circulation Rate.....39
4.2.3. The Influence of Regeneration on Adsorbent.....42
4.3. Discussion and Conclusions.....44
4.3.1. Dimensionless Analysis.....44
4.3.2. Conclusions.....45

5. HYDRODYNAMICS OF CFB RISER.....47
5.1. Characteristics of Circulating Fluidized Bed.....47
5.1.1. Introduction.....47
5.1.2. Characteristics of CFB Riser.....49
5.2. Local Hydrodynamics – the EMMS Model.....50
5.2.1. Introduction.....50
5.2.2. The Three Scales and Interactions.....50
5.2.3. Force and Mass Balance.....54
5.2.4. Energy Resolution and System Stability Conditions.....56
5.2.5. Analytical Solution of EMMS Model.....57
5.3. Axial Hydrodynamics - Voidage Distribution.....70
5.3.1. Two Types of Axial Voidage Distribution.....70
5.3.2. Estimation of Bed Voidage at Bottom.....72
5.3.3. Estimation of Axial Voidage Distribution.....72
5.3.4. One Dimensional Hydrodynamics in CFB Riser.....73
5.4. Conclusions.....79

6. GAS/SOLID MASS TRANSFER.....81
6.1. External Mass Transfer.....81
6.1.1. Mass Transfer Between Gas And Solid Particles.....81
6.1.2. Gas/Solid Mass Transfer in CFB Riser.....83
6.2. Intraparticle Mass Transfer In Porous Adsorbent.....89
6.2.1. Pore Diffusion.....89
6.2.2. Surface Diffusion.....91
6.2.3. Mass Transfer Within Adsorbent Particles.....92
6.3. Gas/Solid Mass Transfer In CFB Riser.....93
6.3.1. Overall Mass Transfer Coefficient.....93
6.3.2. Gas Dispersion.....95
6.4. Conclusions.....96

7. VOCs ADSORPTION IN CFB RISER 97
7.1. Adsorption In CFB Riser.....98
7.1.1. One Dimensional Adsorption Model 98
7.1.2. Simplified Analytical Solution.....101
7.1.3. Influence of Operation Conditions.....102
7.2. Design of CFB Adsorber (Riser).....104
7.2.1. Determination of Basic Parameters.....104
7.2.2. Gas and Solid Efficiencies.....105
7.2.3. Multi Stage Adsorber.....106
7.3. Design of CFB Adsorption Process.....109
7.3.1. CFB-PSA System.....109
7.3.2. CFB-TSA System.....110
7.4. Conclusions.....112

8. CONCLUSIONS AND PROSPECTS.....113

NOMENCLATURE.....117
REFERENCES.....121
ABOUT THE AUTHER.....127
ACKNOWLEDGEMENT.....129

1. INTRODUCTION

Volatile Organic Compounds (VOCs) are the most common air pollutants emitted from chemical, petrochemical and allied industries. VOCs are among the main sources of photochemical reaction in the atmosphere leading to various environmental hazards. Adsorption is one of the most effective methods of controlling VOCs emission. The adsorption processes for VOCs emission control are traditionally carried out with fixed-bed reactors but, due to the increase of reactor size, the classical cylindrical columns become impractical when high-flow-rate streams need to be treated. Less conventional geometries and technologies such as stacks of shallow beds, adsorbing rotors, etc. have then to be used. In this context, fluidized bed processes can be considered as an alternative. They should have advantages over fixed-beds for emission control of the dilute VOCs at high flow rate, as then the adsorption process can be operated continuously with high velocities. Several adsorption systems employing a multi-stage bubble fluidized bed for dilute VOC emission control have been developed and operated in practice, but no such process with CFB reactors has been reported.

This work is involved in the development of a new CFB adsorption process for control of dilute VOCs emission.

1.1. VOCs Emissions and Controlling Legislations

According to the Council Directive of the European Union[1], "Volatile Organic Compound shall mean any organic compound having at 293.15 K a vapour pressure of 0.01 kP_a or more, or having a corresponding volatility under the particular conditions of use."

Volatile Organic Compounds include most solvent thinners and liquid fuels. VOCs are the most common air pollutants emitted from chemical, petrochemical and allied industries, and include aliphatic hydrocarbons, alcohols, ketones, aromatic hydrocarbons, aldehydes and chlorinated hydrocarbons. Table 1-1 lists some common VOCs substances[2, 3].

Table 1-1 Common VOCs [2]

Serial Number	Volatile Organic Compounds
1	Acetaldehyde
2	Acetone
3	Benzene
4	Carbon tetrachloride
5	Ethyl acetate
6	Ethylene glycol
7	Formaldehyde
8	Heptane
9	Hexane
10	Isopropyl alcohol
11	Methyl ethyl ketone
12	Methyl chloride
13	Monomethyl ether
14	Naphthalene
15	Styrene
16	Toluene, Xylene

1.1.1. VOCs Emissions

In France, the VOCs emission was approximately 2.1 Mt in 2000[4]. Fig. 1-1 shows the VOCs emissions from different sources in France. The majority of VOCs is produced from industries by evaporative process during manufacturing and the processing including solvents (26.4%) and transportation (25.8%).

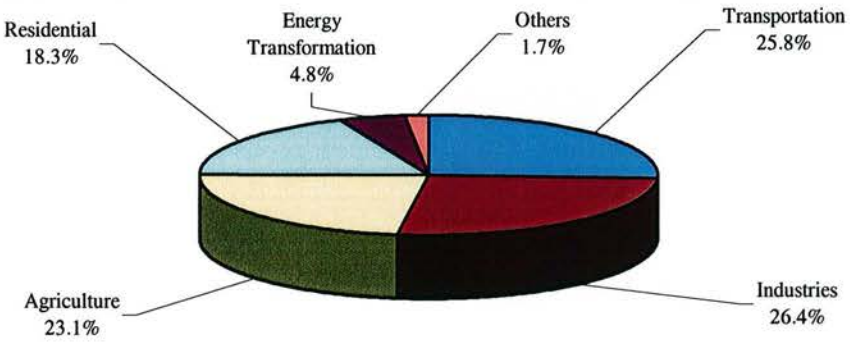

Fig. 1-1 VOCs Emissions From Different Sectors (France)

In China, VOCs are not categorized separately as a sort of substances, therefore no statistical data of VOCs emission have been reported.

1.1.2. VOCs Emissions Controlling Legislations

It is necessary to limit and control VOCs emissions because they affect the change of climate, the growth and decay of plants, and the health of human beings and all animals. Regulations on controlling organic vapour pollutants in air have been issued world wide. According to Council Directive 1999/13/EC of 11 March 1999, the VOCs discharge limits are between 2mg/Nm^3 and 20mg/Nm^3 for different VOCs substances and mass flow rates, while they are 50mg/Nm^3 and 150mg/Nm^3 for the existing abatement equipment.

Befor 1996, there was no national legislation for most VOCs emission discharge in China. A new national air pollutants discharge control legislation (GB16297-1996) became effective in 1997 in which the emission control for 14 VOCs, including benzene (17/12 mg/Nm^3), toluene (60/40 mg/Nm^3), xylene (90/70 mg/Nm^3), methanol, methanal, aldehyde etc. have been required. Since then, the VOCs control equipment employing activated carbon fixed bed adsorption process have been developed in China, usually with small gas flow rate.

1.2. Fluidized Bed Adsorption Process

Deep within the collective chemical engineering psyche is the feeling that continuous processes are always better than batch operation ones. This feeling, though not always legitimate, spurs continuing research and experimentation in adsorption processes. Different continuous fluidized bed adsorption process has been designed to handle process streams with large flow rate, or to maintain the uniform temperature in the adsorber, where fluidized bed process do appear superior to traditional fixed bed process.

1.2.1. Earlier Practice

During the last 50 years, several attempts have been made at commercializing continuous fluidized bed adsorption process. Courtaulds Ltd. developed a multi-stage fluidized bed adsorption process in the 1950's and the first plant was commissioned in 1959 to recover 1.2 tons/h of CS_2 from 400,000 m^3/h of air[5]. The system (Fig. 1-2) consisted of a bubble fluidized bed adsorber, a moving bed desorber with direct steam regeneration and a conventional bucket elevator to circulate the solids. The five-stage adsorber had a bed diameter of 11.6m with the height of 13.7m. Circulation of activated carbon adsorbent was 23 tons/h, and 90-95% of the entering CS_2 was removed from the air stream.

In China, a similar fluidized bed adsorption process (Fig. 1-3a) was developed by the Institute of Chemical Metallurgy, Chinese Academy of Sciences to remove dichloroethane, $C_2H_4Cl_2$, from exhaust gas in the 1970's. The system consisted of a multi-stage bubble fluidized bed adsorber and a fluidized bed desorber with steam regeneration. The adsorbent particles are pneumatically recirculated back to the adsorber and no mechanical device is used to control the circulation of solids[6], [7].

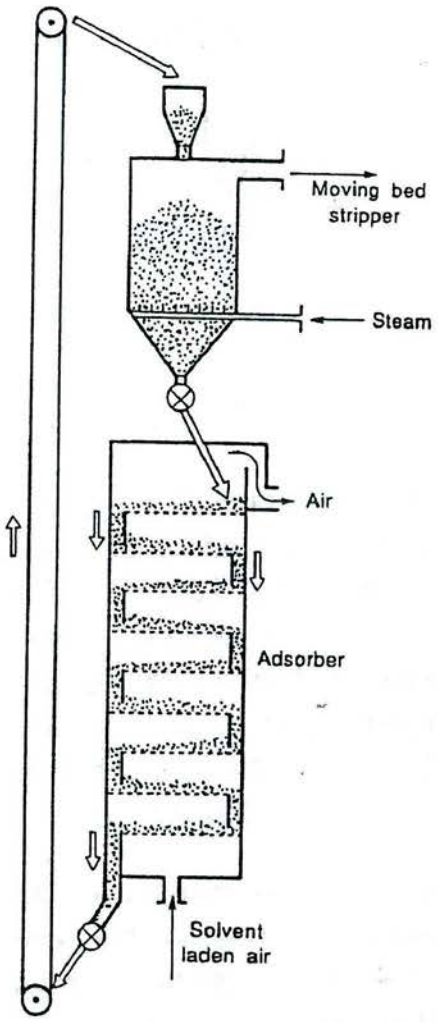

Fig. 1-2 Fluidized Bed Adsorber

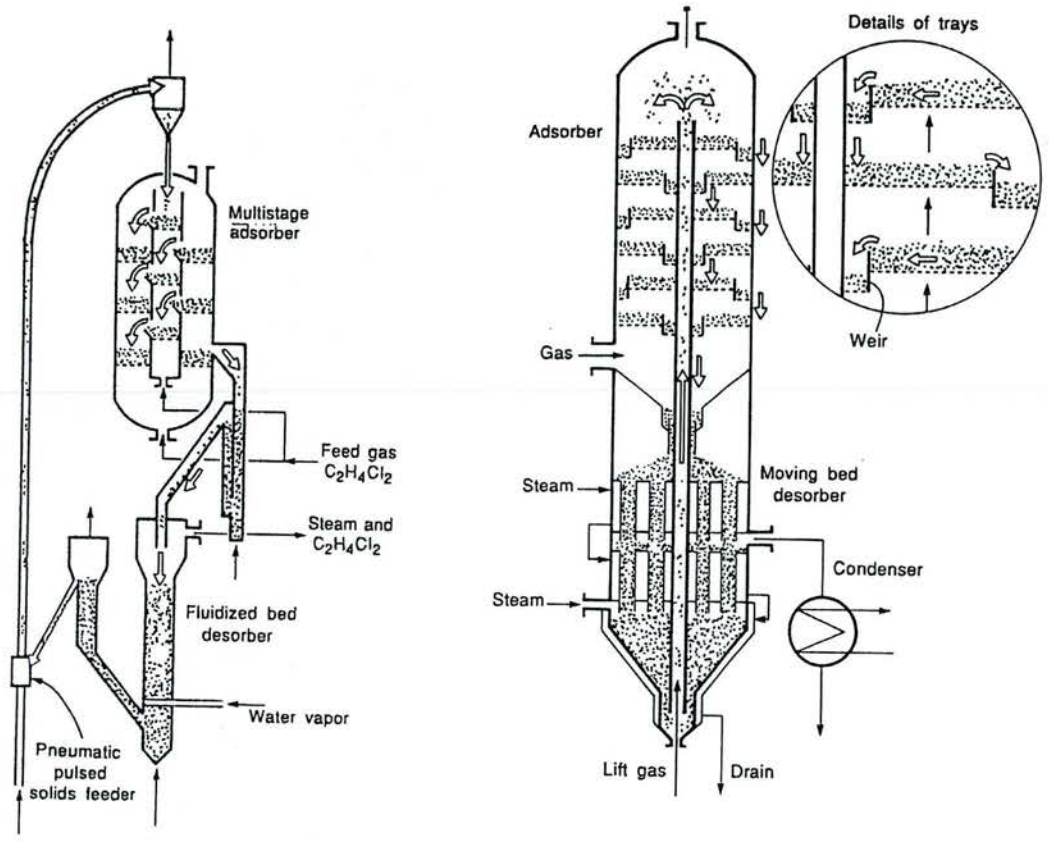

Fig. 1-3 Fluidized Bed Adsorption Process

A much more compact design of the continuous adsorption process with a multi-stage fluidized bed adsorber and a moving bed desorber was developed by Kureha Chemical Co. of Japan and later sold in the United States as the Purasiv HR process (Fig. 1-3b) for hydrocarbon removal from vent streams[8]. The process was designed to remove solvent or odorous material from 4000 – 60,000 m^3/h of fuel gas and higher concentration of solvent was obtained with indirect heating in the desorber. The adsorbent material is spherical active carbon manufactured from petroleum pitch with a diameter of 0.7mm.

One of the barrier issues associated with the commercialization of fluidized bed adsorption process is the severe attrition or weight loss of adsorbents in the fluidized bed. And this may be the reason why fluidized bed adsorption process has not been widely used in industry. More recently, several fluidized bed adsorption processes for VOCs control have been reported and are described below. The key to the successful commercialization of fluidized bed process has been the development of rugged and innovatively shaped forms of adsorbents.

1.2.2. Recent Development

POLYAD pre-concentration/solvent-recovery system (Fig. 1-4), developed by Weatherly Inc., has been in commercial use since 1988[9], [10]. The system employs a multi-stage fluidized bed adsorber and a multi-stage fluidized bed desorber for pre-concentration or a moving bed desorber for solvent recovery. The pre-concentration unit is used where solvent, at low VOC concentrations (<1200mg/Nm^3), is removed from a large exhaust air flow(>1.7×10^5 Nm^3/h) and concentrated into a smaller flow. An air flow can normally be concentrated 10 – 50 times, depending on the inlet VOC concentration and type and mixture of the VOCs. The solvent recovery unit is used where solvent recovery and reuse are feasible. The solvent is concentrated to a level where it can be condensed by ordinary cooling water. The thermal swing desorption is used with hot air for pre-concentration and with steam for solvent recovery. The most recent development of this process is the use of microwave for desorption, done by American Purification Inc. VOCs saturated adsorbent is regenerated continuously in a microwave desorption chamber. An inert gas is used to ensure an explosion-proof atmosphere for the regeneration process.

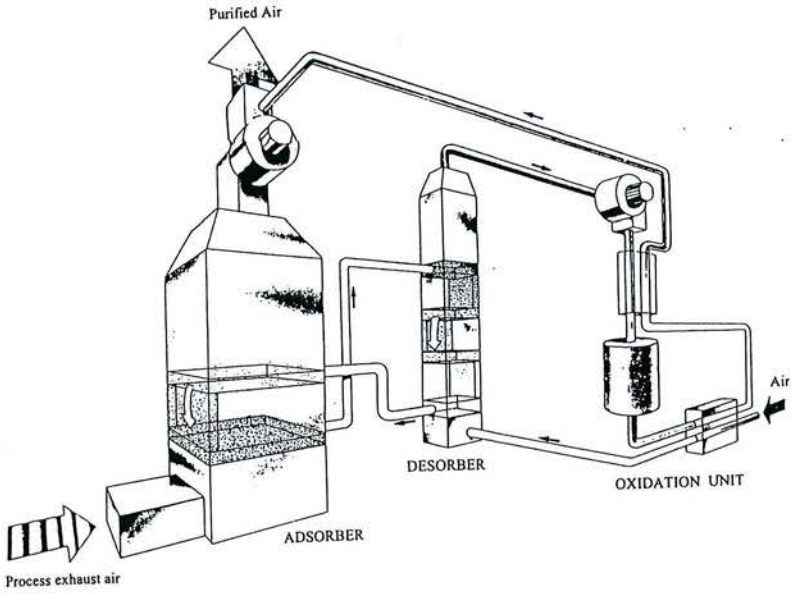

Fig. 1-4 Polyad pre-concentration-Incineration system

Another example, FluiSorb system, was developed by REECO for VOC emission control[11]. Both adsorber and desorber are multi-stage fluidized bed reactors. The process can be used on process streams ranging from 8.5×10^4 to 8.5×10^6 Nm^3/h containing VOC concentrations from 8000 to 4,000 mg/Nm^3 (200-1000ppm). A very high concentration factor, 1000:1 has been reported for the system with the removal efficiency of 99% for VOCs including ethyl lactate.

Environmental C&C Inc. and Rohm and Haas Company have also performed experimental research on the continuous VOC control with fluidized bed adsorber and moving bed desorber [12]. The experimental results show that, very high removal

efficiencies (>97%) have been achieved for VOC's mixtures including ethanol, IPA and ethyl lactate, or methyl ethyl ketone and toluene, while reasonable removal efficiency (>70%) for methanol has been observed.

The adsorbents employed in the above described process are mainly polymeric or carbonized polymeric adsorbents. They are specially developed for VOC control with fluidized bed process. The adsorbents are usually perfectly spherical shaped with high attrition resistance and hydrophobic surface property. The characteristics and manufacturers of the adsorbents are listed in Table 1-2.

Table 1-2 Characteristics of Adsorbents

ADSORBENT	PROCESS	MANUFACTURE	SURFACE PROPERTY	CRUSH STRENGTH/ ATTRITION RATE
AMBERSORB 600	-	ROHM & HAAS COMPANY	HYDROPHOBIC	>1000g/BEAD
SYNTTETIC CARBON	HYBRID	REECO	HYDROPHOBIC	<2% PER YEAR
BONOPRE 1120	POLYAD	WEATHERLY INC.	-	500g/BEAD
DOWEX OPTIPORE V493	POLYAD	DOW CHEMICAL COMPANY	-	-

1.2.3. Circulating Fluidized Bed Adsorption Process

It seems that all the new developed VOCs control systems employ exclusively multi-stage fluidized bed adsorber with Temperature Swing Adsorption (TSA) process. Until now, only one circulating fluidized bed (CFB) adsorption process has been reported, not for purification process like VOCs control, but for bulk separation[13]. It is a process for CO_2 recovery from power plant flue gas, employing both temperature and pressure swing with two CFB reactors, one as adsorber and the other as desorber. The process was also studied with computer simulation[14].

1.3. Purposes of the Research

The CFB are usually operated in the fast fluidization regime with high gas and solids throughput. The heat transfer inside the CFB is much faster and nearly isothermal conditions could be obtained. With improved gas–solid contacting and higher operation velocity than in a bubbling fluidized bed, the CFB adsorption process is thus an alternative for emission reduction of dilute VOCs.

Despite the advantages, the CFB reactor has not been used in industries for adsorption process until now. This mainly results from the lack of knowledge of hydrodynamics and transfer process involved in the CFB reactor, entailing difficulties in design, in extrapolation, in evaluation of performances. The aim of this study is to provide some basic tools to analyze the VOCs adsorption process inside the CFB riser, including the hydrodynamics of gas/solid two phase flow and the mass transfer process between gas

and solid adsorbent. From there, one can discuss the influence of operating parameters on the performance of the adsorber. These are the fundamentals for the design and operation of CFB adsorption process. The possible designs for temperature swing adsorption and pressure swing adsorption process with CFB adsorber are also presented.

2. ADSORPTION ISOTHERM

The adsorption isotherm is the fundamental information for the understanding of adsorption process. The experimental results of the isotherm measurement will supply not only the quantitative knowledge of the adsorbate/adsorbent system, but also the mechanism of adsorption and the properties of the adsorbent surface. A number of theories for the adsorption isotherm have been developed based on various assumptions concerning the nature of adsorbed phase and the thermodynamic perspective. In this study, the adsorption isotherm measurement is performed with gravimetric technique for Ambersorb 600/Toluene system and three adsorption equilibrium models are employed for analyzing the experimental data.

2.1. Adsorption Isotherm Models

2.1.1. Langmuir Isotherm

The Langmuir isotherm describes monolayer adsorption on homogeneous flat surface. The basic assumptions for Langmuir isotherm include [15]: 1. The adsorbed molecule or atom is held at definite, localized sites; 2. Each site can accommodate one and only one molecule or atom; 3. The adsorption energy is constant over all sites (homogeneous surface) and there is no interaction between neighboring adsorbate. Based on the concept of dynamic equilibrium between the rate of adsorption and desorption, the isotherm equation is derived:

$$\frac{q}{q_m} = \frac{k_L C}{1 + k_L C} \tag{2-1}$$

Equation (2-1) is the Langmuir isotherm, q is the amount adsorbed in mass per unit mass of adsorbent and q_m is the maximum adsorbed adsorbate corresponding to monolayer coverage. k_L is the Langmuir constant (or Henry's constant) and the temperature dependence of k_L is $e^{Q/RT}T^{-1/2}$, where Q is the heat of adsorption. C is the gas phase adsorbate concentration. Langmuir isotherm reduces to Henry's law, $q/q_m=k_LC$, when the adsorbate concentration C is very low, that is the amount adsorbed increases linearly with concentration, a constraint by statistical thermodynamics. When the adsorbate concentration is sufficiently high, the amount adsorbed reaches the saturation capacity measured by q_m.

2.1.2. Freundlich Isotherm

The Freundlich isotherm is one of the earliest empirical equations and the name of this

isotherm is due to the fact that it was used extensively by Freundlich [16]. The isotherm can also been obtained by considering Langmuir isotherm on a heterogeneous surface [17]. Freundlich's isotherm takes the form of:

$$q = k_F C^{1/n} \tag{2-2}$$

The Freundlich isotherm is generally used to describe the adsorption of gas solid systems having heterogeneous surface, provided the range of adsorbate concentration is not too wide as the isotherm equation does not have a proper Henry's law behavior at low concentration, and it does not have a finite limit when adsorbate concentration is sufficiently high. The parameters k_F and n are dependent on temperature [18]. While the Freundlich exponent $1/n$ is considered a linear function of temperature ($1/n=aT$), the functional form of temperature dependence of Freundlich coefficient k_F is in the form of $k_F=a\ Exp(-b\ T)$.

2.1.3. Dubinin-Astakhov Equation

Many investigators indicated that the potential theory is useful for adsorption equilibria of organic vapors on microporous materials such as activated carbon. The isotherm derived from the potential theory have found utility in interpreting adsorption by capillary condensation and pore filling.

Activated carbon has a very complex structure with pores ranging from macropores (>50nm) to micropores (<2nm). It is this micropore network where most of adsorption capacity resides. Because of the pore size comparable to the dimension of adsorbate molecule, the adsorption mechanism in micropore is completely different from that on a surface of a large pore, where adsorption occurs by a layering process. In micropores, the mechanism is due to micropore filling because of the adsorption force field encompassing the entire volume of micropore [19]. Such an enhancement in the adsorption potential would lead to higher heat of adsorption in micropore compared to that on a surface. Another difference between the two mechanisms is, in the case of surface layering, the chemical potential of the adsorption is independent of the amount adsorbed, while in the case of micropore filling the chemical potential is a function of amount adsorbed [20].

Dubinin-Astakhov equation, based on adsorption potential theory can be expressed as:

$$W = W_0 \exp\left[-\left(\frac{A}{\beta E_0}\right)^m\right] \tag{2-3}$$

$$A = RT \ln\left(\frac{C_{sat}}{C}\right) \tag{2-4}$$

where W is the volume of the adsorbate in the micropore and W_0 is the maximum volume that the adsorbate can occupy, which equals micropore volume. A is the adsorption potential, E_0 is the characteristic energy of reference adsorbate and β is the similarity coefficient. C_{sat} is the saturation concentration of adsorbate vapor at

temperature T. The Dubinin-Astakhov equation is applicable only to relatively non-polar surfaces.

2.2. Adsorbent and Adsorbate

A carbonaceous adsorbent Ambersorb 600, a product of Rohm and Haas Company, is used for the study. It is produced by pyrolyzing the highly sulphonated styrene/divinylbenzene macroreticular ion exchange resin with a patented process. The adsorbents are in the form of small spherical beads with high attrition resistance and uniform particle diameter, which are desirable for fluidized bed applications. The other important feature is the hydrophobic surface nature of the adsorbent, so it could also be used with high relative humidity conditions. The particle density of the adsorbent is 751 kg/m^3. The other physical and chemical properties are given in Table 2-1.

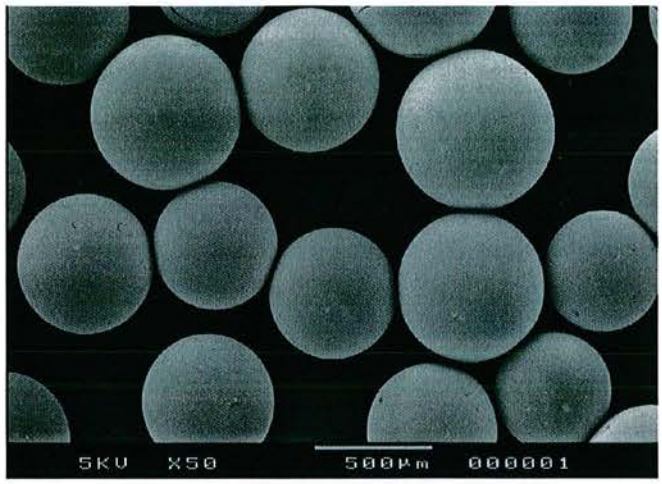

Fig. 2-1 Ambersorb 600 Carbonaceous Adsorbent

Table 2-1. Properties of Ambersorb 600 Adsorbent [21]

Characteristics	Value
Particle Size Distribution	0.21mm ~ 1.26mm
Mean Particle Diameter	0.65 mm
BET Surface Area	580 m^2/g
Bulk Density	0.54 g/ cm^3
Crush Strength	> 1000 g/bead
Pore Size Distribution	
Micropore Volume	0.22 cm^3/g
Mesopore Volume	0.17 cm^3/g
Macropore Volume	0.21 cm^3/g
Total Pore Volume	0.60 cm^3/g
Water Adsorption (at 81% relative humidity)	5 %

The VOC substance used for the isotherm measurement is toluene, due to its environmental significance. The physical and chemical properties of Toluene are listed in Table 2-2[22].

Table 2-2. Physical and Chemical Properties of Toluene

Characteristics	Value
Mole Weight	92.14 (kg/kmol)
Boiling Point	110.6(°C)
Liquid Density (25°C)	9.36 (kmol/m^3)
Saturation Pressure	
25 °C	3.79 (kPa)
120 °C	131.6 (kPa)

2.3. Experimental Setup and Procedures

2.3.1. Experimental Setup

The adsorption isotherm measurement is performed with gravimetric technique. The experimental setup is illustrated in Fig. 2-2. The main instrument used for the weight measurement is a magnetic suspension balance, a product of RUBOTHERM. As the weight to be measured is transmitted from a closed metal measuring chamber by means of a magnetic suspension coupling to a normal balance, which is in ambient conditions, the measuring chamber could be operated under high pressures and high temperatures. The measurement could be proceeded both manually and automatically by a computer. The specifications of the balance are listed in table 2-3[23].

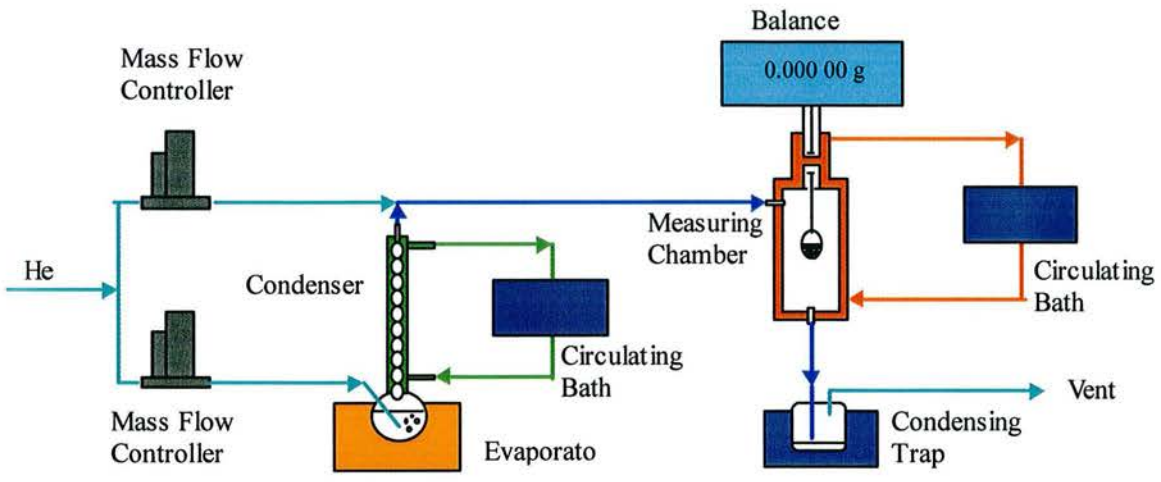

Fig. 2-2 Isotherm Measurement Setup

Table 2-3. Balance Specifications

Characteristics	Value
Measuring Weight	5 ~ 30 g
Resolution	0.01 mg
Relative Error	≤ 0.002% of measured value
Pressure Range	Vacuum and up to 100 bar
Temperature Range	-80 °C ~ 250 °C
Force-measuring Device	METTLER AT 261

Helium is used as carrier gas and divided into two streams: one as the evaporation stream and the other as the dilution stream. Inside the evaporator, liquid VOC is evaporated by heating and carried out by the evaporation stream. After flow through a condenser, the VOC saturated gas stream under certain temperature is obtained as the temperature in the condenser is precisely controlled by a Circulating Bath. Two Mass Flow Controllers (BROOKS, 5850TR) are used to adjust the flow rates of the Helium streams. By adjusting the temperature of condenser and the flow rate of evaporation/dilution helium streams, a gas stream with desired VOC concentration is obtained and used for the isotherm measurement.

Another circulating bath with a temperature stability of 0.05 °C is used to control the temperature of the measuring chamber of the balance. The temperature is measured in the measuring chamber just bellow the adsorbent sample with a Pt100 temperature probe. Accuracy of the temperature measurement is 0.05K.

A condensing trap, which is cooled down to –10 °C by an immersion bath, is also used to collect the Toluene in the gas stream after the balance, before being vented out.

2.3.2. Experimental Procedures

Before the experiment, the Ambersorb 600 adsorbent was kept in an oven at 180 °C for several days to desorb the possible adsorption. About 1 gram adsorbent is added into a metal basket hanging up at the middle of the measuring chamber of the balance. Helium is first introduced into the measuring chamber continuously with the flow rate of 100 ml/min. After both the temperature of the chamber and the weight of the adsorbent are settled, the balance reading is recorded and the weight of adsorbent is obtained by deducing the weight of components of balance holding the sample that was measured before at the same conditions.

The Helium stream with desired Toluene concentrations is then switched into the measuring chamber of the balance while the total flow rate is kept about the same as before. Isotherm data at this concentration is obtained with the weight increase up to the equilibrium. This process may take several days at lower concentration conditions. The Toluene concentration is then increased by increasing the Helium flow rate of evaporation stream and decreasing the flow rate of dilution stream, while the

temperature is kept as the same. The isotherm data is thus obtained for each Toluene concentration.

After one set of isotherm data is obtained for a desired temperature, the adsorbent sample is changed and this process is then repeated with other temperatures.

2.3.3. Estimation of Weight Measurement Error

For Isotherm measurement with magnetic suspension balance, the measured quantities are the balance reading (w_r) and temperature. Due to the buoyancy effects acting on the adsorbent and the components of the balance holding the sample, the weight of measuring object (w) is actually the sum of balance reading and the buoyancy of the atmosphere. That is:

$$w_r = w - V\rho_g \quad or \quad w = w_r + V\rho_g \tag{2-5}$$

If the density of gas (ρ_g) and the volume of the measuring object (V) remain constant during the measurement, then the buoyancy effect could be omitted, as what we want is the weight increase of measuring object and the influence of buoyancy is eliminated during the calculation.

$$w_{r1} - w_{r2} = (w_1 - V_1\rho_1) - (w_2 - V_2\rho_2) = w_1 - w_2 \tag{2-6}$$

During the isotherm measurement the density of gas and the volume of the measuring object are not constant, so the influence of buoyancy should be considered. The absolute error of weight measurement could be estimated as:

$$\Delta w = \frac{\partial w}{\partial w_r}\Delta w_r + \frac{\partial w}{\partial V}\Delta V + \frac{\partial w}{\partial \rho}\Delta\rho = \Delta w_r + \rho\Delta V + V\Delta\rho \tag{2-7}$$

The relative error of weight measurement is:

$$\frac{\Delta w}{w} = \frac{\Delta w_r}{w} + \frac{\rho\Delta V}{w} + \frac{V\Delta\rho}{w} \tag{2-8}$$

The first term in equation (2-8) is the measurement error of the balance. The rest two terms are the influence of buoyancy due to the change of gas phase density and adsorbed adsorbate volume. The volume of measuring object consists of two parts: the volume of adsorbent and the volume of the components of the balance holding the sample. If these two volumes are considered unchanged during the adsorption experiment, then the adsorption of the adsorbate substance on the adsorbent will increase the volume of gas displacement. Assuming the adsorbate has liquid density, the increased volume could be estimated. The maximum volume increase ($0.17cm^3$) occurs at low temperature (25^oC) and higher toluene concentration conditions.

During the measurement of an adsorption isotherm at certain temperature, the Toluene

concentration is changed from 840 mg/Nm^3 to 1670 mg/Nm^3, this also change the density of Toluene/Helium mixture. Again the maximum gas density change (0.0144 kg/m^3) occurs at lower temperature (25°C) and higher toluene concentration conditions.

The calculated result with experimental conditions shows that the maximum relative errors du to the influence of buoyancy is 0.0004%; it is the same order of magnitude as the relative error of the balance (0.0002%). So the relative error for the weight measurement is 0.0006% in the experiments and the corresponding maximum absolute error is 0.0096 mg.

2.4. Experimental Results and Discussions

2.4.1. Experimental Results

The isotherm measurements of Ambersorb 600/Toluene system have been performed with different Toluene concentrations at different temperatures (25 °C, 80 °C, 120 °C and 140 °C). The gas phase concentration of Toluene is between 800 mg/Nm^3 and 20000 mg/Nm^3. Fig. 2-3 shows the experimental results of isotherm measurement.

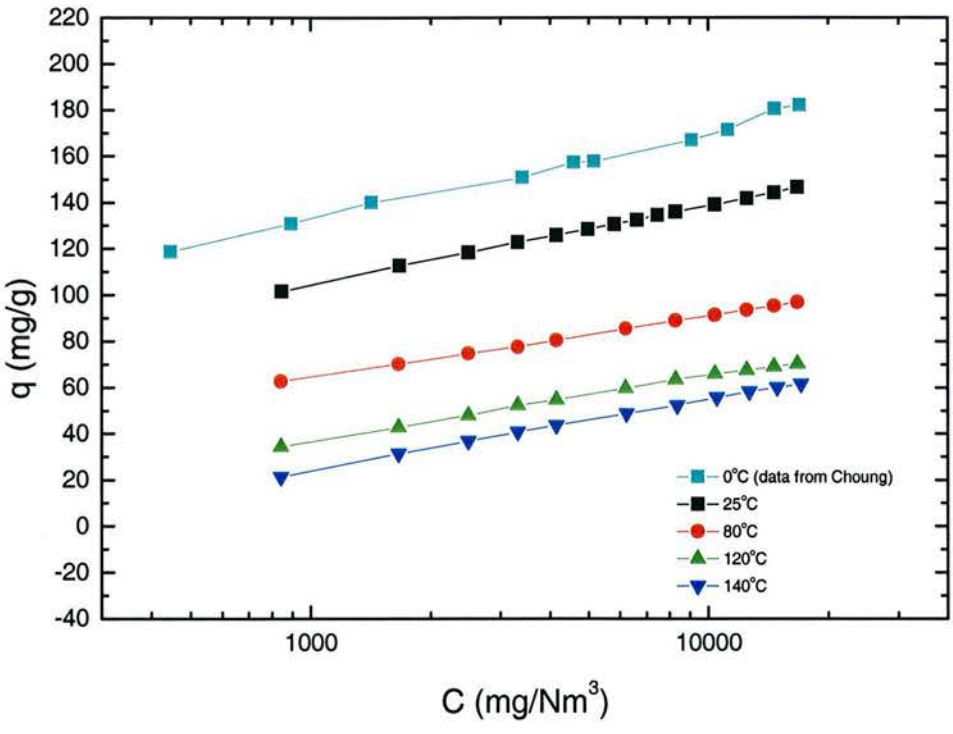

Fig. 2-3 Equilibrium Isotherm of Toluene/Ambersorb 600

Choung et al.[24] also measured the isotherm of Ambersorb 600/Toluene system based on

static volumetric technique. The tests are conducted between 0 °C and 75 °C with a much wider concentration range. Their measurement results agree well with this test results in the overlapped temperature and concentration range, as shown in Fig. 2-4. Choung's experimental results of isotherm measurement at 0 °C within the overlapped concentration range are also included in Fig. 2-3 and will be used in the following data processing and discussion.

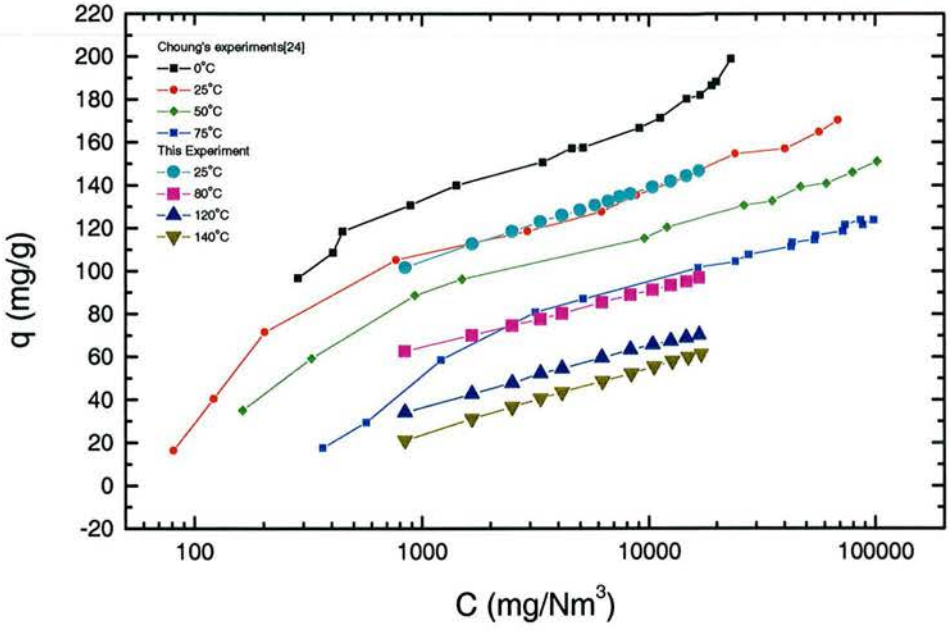

Fig. 2-4 Comparison of Isotherm Measurement Results

2.4.2. Data Fitting with Different Isotherms

The experimental equilibrium data are fitted with different equilibrium models, based on least-square method. That is the parameters are selected so that the sum of the squares of the deviations of the theoretical values from the experimental points for a range of independent variables becomes minimum.

Langmuir isotherm was first selected to describe the experimental data, as it is the most widely used isotherm. Equation (2-1) can be also rewritten as:

$$\frac{1}{q} = \frac{1}{k_L q_m}\frac{1}{C} + \frac{1}{q_m} \tag{2-9}$$

It is linear relationship between $1/q$ and $1/C$. The intercept is $1/q_m$ and the slope is $1/k_L q_m$. Table 2-4 gives the linear regression results with Langmuir Isotherm, in which, R is the correlation coefficient and SD is the standard deviation.

Table 2-4. Linear Regression Results with Langmuir Isotherm

Temperature K	$1/q_m$(g/mg)	$1/k_L q_m$(g/Nm^3)	R	SD
273.15	3.298	0.0054	0.9988	1.651
298.15	4.951	0.00663	0.99939	1.173
353.15	8.698	0.00996	0.99936	2.063
393.15	18.502	0.01332	0.99944	2.592
413.15	32.439	0.01465	0.99905	3.776

Fig. 2-5 shows the experimental (points) and fitted result (line) from linear regression for different temperatures. It is obvious that q_m is not a constant, but varied with temperature and the temperature dependence of k_L is not $e^{Q/RT}T^{-1/2}$. To eliminate the influence of density variation with temperature, q_m is expressed as $q_m=\rho v_m$. The variation of v_m and k_L with temperature are illustrated in Fig. 2-6.

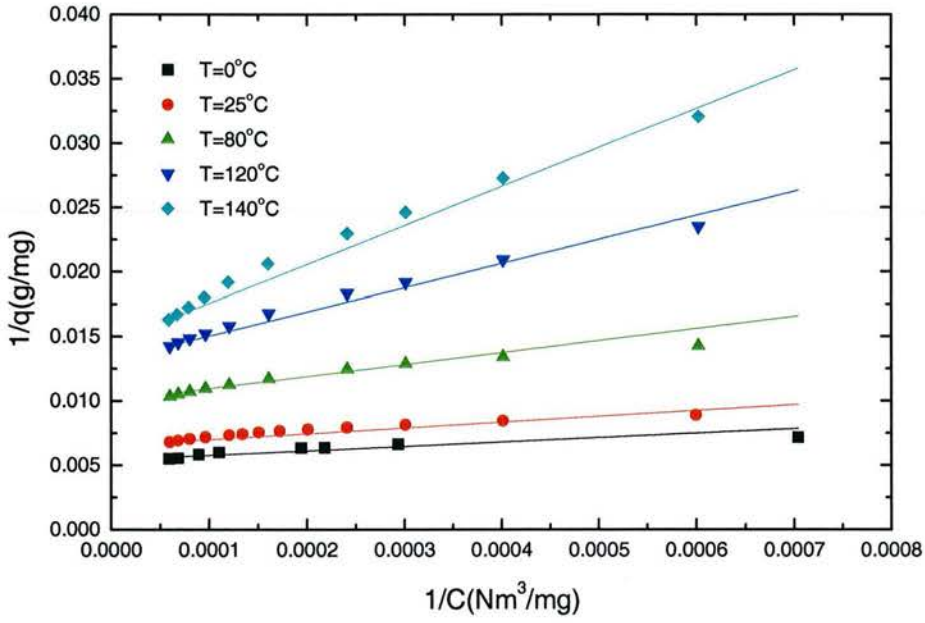

Fig. 2-5 Experimental data fitted with Langmuir Isotherm

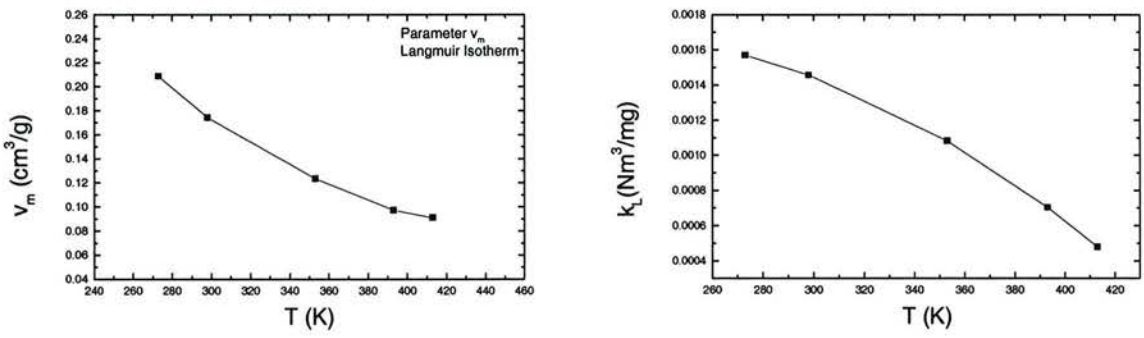

Fig. 2-6 Temperature Dependence of Langmuir Parameters v_m and k

The data fitting with Langmuir isotherm is also shown in Fig. 2-7 with normal coordinate. Relatively large deviations are observed between the experimental data and the calculated values, especially in the lower concentration and lower temperature range.

One of the possible reasons for the disagreement of experimental data with Langmuir isotherm is that, Langmuir isotherm is based on the adsorption phenomena of surface layering on the homogeneous surface and that is not the case for the Ambersorb 600/Toluene system.

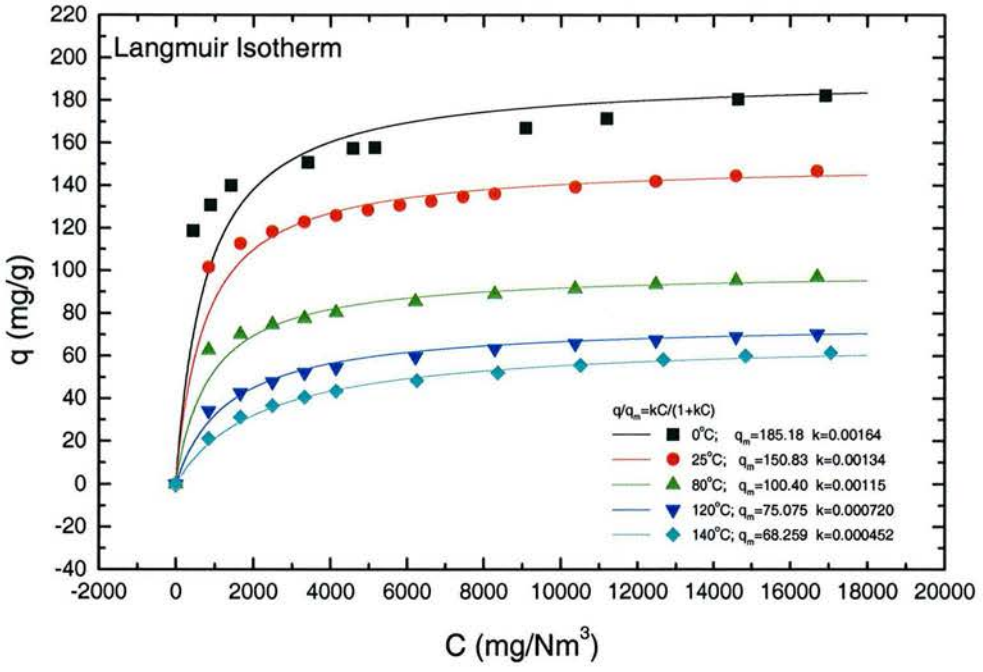

Fig. 2-7 Test Data Fitted With Langmuir Isotherm

To include the heterogeneity of the adsorbent surface, Freundlich isotherm was also used to fit the experimental data. We rewrite (2-2) as:

$$\ln(q) = \frac{1}{n}\ln(C) + \ln(k_F) \tag{2-10}$$

There is a linear relationship between *ln(q)* and *ln(C)* with the intercept of $ln(k_F)$ and slope of *1/n*. Table 2-5 and Fig. 2-8 gives the results from data fitting.

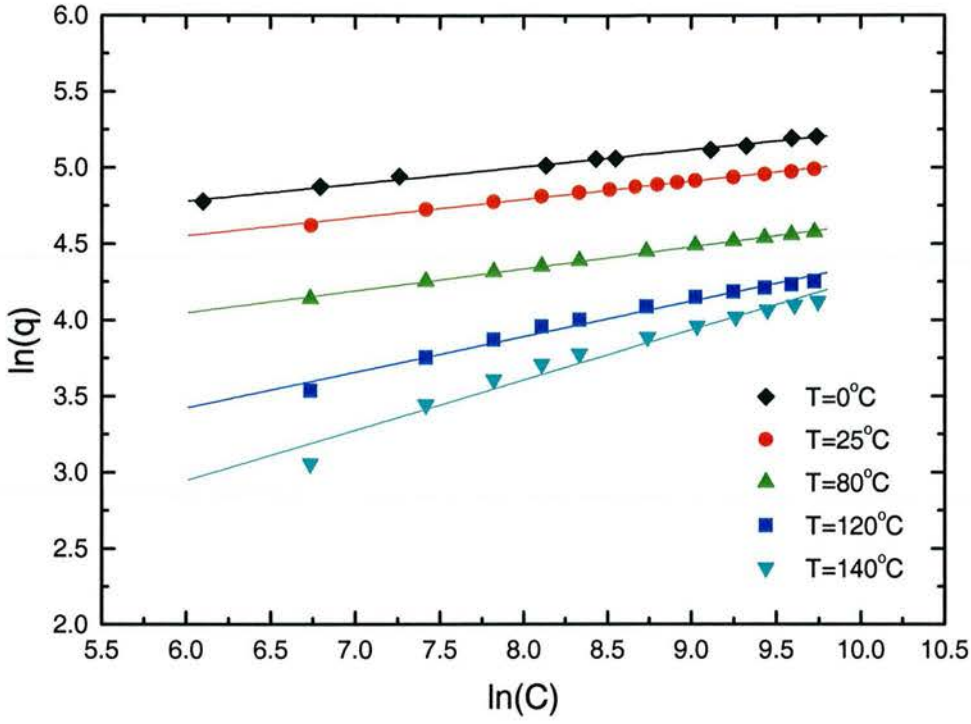

Fig. 2-8 Test Data Fitted with Freundlich Isotherm

Table 2-5. Linear Regression Results with Freundlich Isotherm

Temperature K	$Ln(k_F)$	1/n	R	SD
273.15	4.100	0.1131	0.99687	0.01176
298.15	3.837	0.1191	0.99739	0.00766
353.15	3.176	0.1447	0.99878	0.00728
393.15	2.019	0.2337	0.98983	0.0342
413.15	0.964	0.3300	0.98234	0.06448

The data fitting with Freundlich isotherm is also shown in Fig. 2-9 with normal coordinate. The agreement of experimental result with Freundlich isotherm is better than that of Langmuir isotherm.

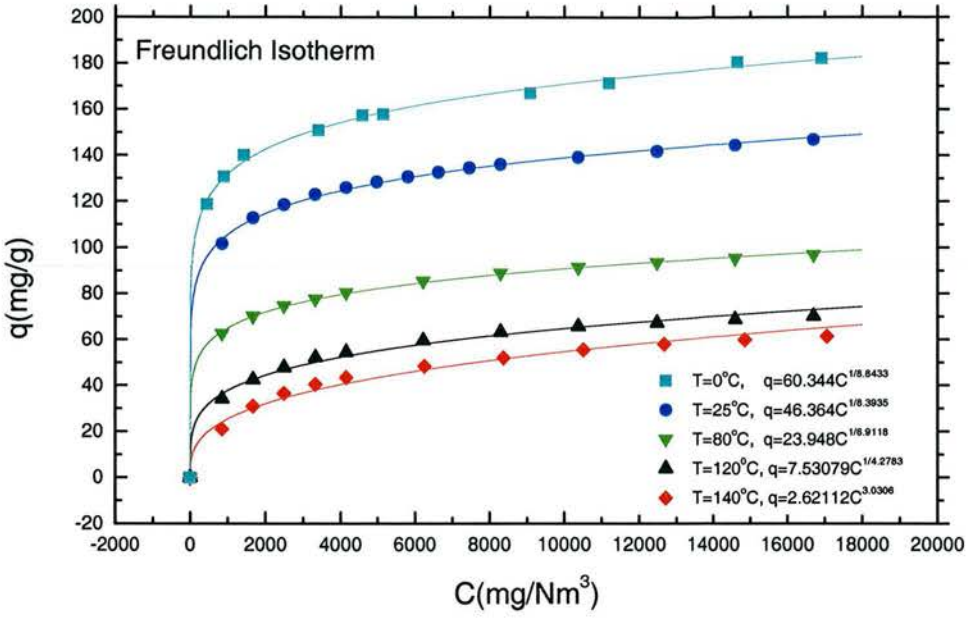

Fig. 2-9 Test Data Fitted with Freundlich Isotherm

Though the Freundlich isotherm describes the experimental data very well for each specific temperature, it is obvious that 1/n did not shown linear relationship with temperature and instead, k_F shows linear decrease with temperature. The temperature dependence of Freundlich parameters is shown in Fig. 2-10.

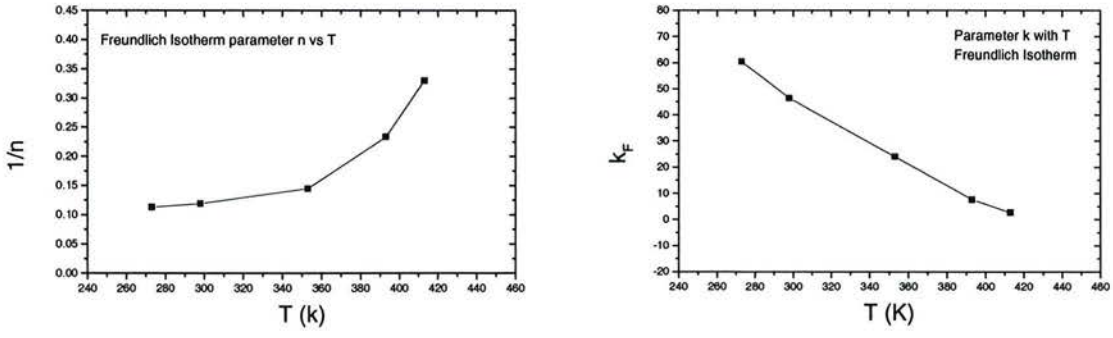

Fig. 2-10 Temperature Dependence of Freundlich Parameters 1/n and k

The third isotherm used for experimental data fitting is Dubinin-Astakhov equation. In D-A equation, W is the volume of the adsorbate. To express D-A equation in terms of q (weight of adsorbate per unit mass of adsorbent), mole weight (M=92.14 kg/kmole) and mole density of liquid toluene ρ_m are used.

$$q = M\rho_m W \quad \text{(kg/kg)} \tag{2-11}$$

The mole density of liquid Toluene ρ_m and the gas phase saturation concentration of Toluene at temperature T are estimated by the following formulations [22]:

$$\rho_m = 0.8488 \times 0.26655^{-[1+(1-T/591.8)^{0.02878}]} \quad (\text{kmole/m}^3) \tag{2-12}$$

$$C_{sat} = \frac{41.11}{1.013} EXP(80.877 - \frac{6902.4}{T} - 8.7761 \ln T + \frac{5.8034 T^2}{10^6}) \quad (\text{mg/Nm}^3) \tag{2-13}$$

Fig. 2-11 shows the data fitting of experimental results with Dubinin-Astakhov equation.

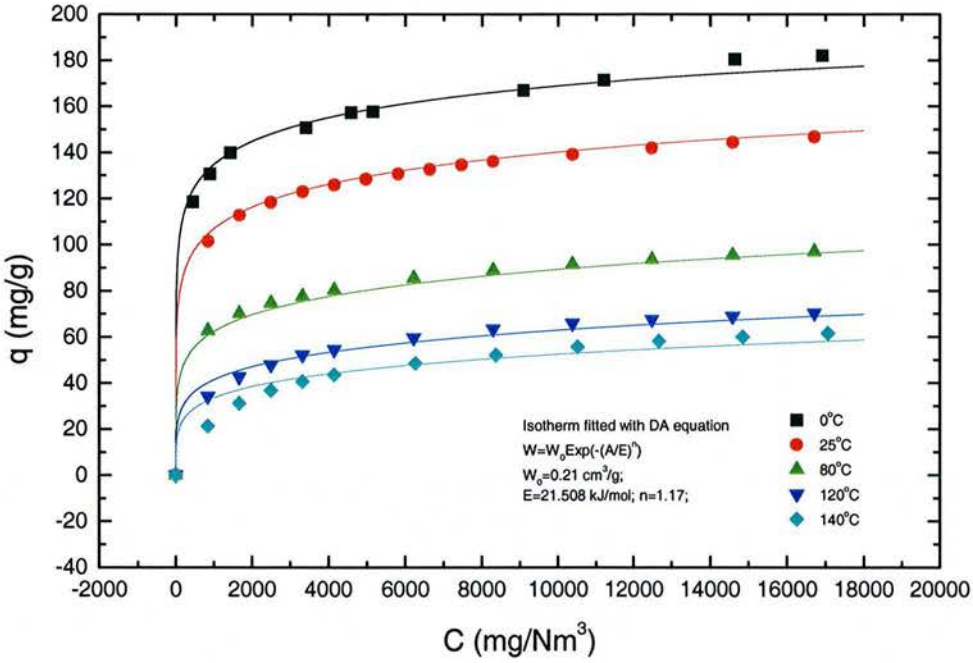

Fig. 2-11 Test Data Fitted with D-A Equation

The D-A equation describes the isotherm data very well within the experimental temperature and pressure range, except few points at the low-pressure range for high temperature (140°C) condition. Benzene is selected as the reference adsorbate substance and for toluene β is 1.25[25]. The fitting parameters obtained are W_0=0.21×10^{-3} m^3/kg, E_0=17.206 KJ/mol and m=1.17.

From the adsorbent pore size distribution measurement we know that the micropore volume of the adsorbent is 0.22×10^{-3} m^3/kg. This value is very close to the value of W_0 in D-A equation.

In order to compare the correlation results with experimental data, the averaged relative error of data fitting is defined as,

$$\Delta = \frac{1}{N}\sum_{i=1}^{N}\frac{q_{\exp}^{i} - q_{calc}^{i}}{q_{\exp}^{i}} \tag{2-14}$$

Table 2-6 gives the averaged relative error obtained with (2-14) for different isotherms at 25 °C. While three isotherms models can be used to describe the adsorption isotherm with acceptable accuracy, Freundlich Isotherm gives the best fit and Langmuir Isotherm gives the largest relatively error. If the temperature variation is also included, the Dubinin-Astakhov equation gives much more reasonable explanation for Ambersorb 600/Toluene adsorption.

Table 2-6. Averaged Relative Error with Different Isotherm

Model	Equations	Δ
Langmuir Isotherm	$q = \frac{q_m kC}{1+kC}$	3.318%
Freundlich Isotherm	$q = kC^{1/n}$	0.428%
Dubinin-Astakhov Isotherm	$q = q_m \exp\left[-\left(\frac{RT}{\beta E_0}\ln(\frac{C_{sat}}{C})\right)^m\right]$	1.111%

2.4.3. Isosteric Heat of Adsorption

One of the basic quantities in the adsorption study is the isosteric heat, which is the ratio of the infinitesimal change in the adsorption enthalpy to the infinitesimal change in the amount adsorbed. The Isosteric heat is considered as a measure of interaction between adsorbate molecules and adsorbent lattice atoms and may be used as an indication of energetic heterogeneity of the solid surface, it may or may not change with adsorbate loading. Isosteric heat of adsorption could be expressed as [16]:

$$\Delta H = A + \Delta H_{vap} + \frac{(\beta E_0)^n \delta T}{RT^2} \tag{2-15}$$

So the isosteric heat is the summation of three terms. The first is the adsorption potential, the second is the heat of vaporization and the third is due to the change of maximum capacity with temperature, where δ is the temperature dependence of relative saturation adsorption capacity and is defined as:

$$\delta = \frac{-1}{q_m}\frac{dq_m}{dT} = \frac{-1}{\rho_m W_0}\frac{d(\rho_m W_0)}{dT} \tag{2-16}$$

Assuming the temperature invariance of the adsorbent maximum specific volume W_0, the temperature dependence of adsorption capacity is that of liquid density. Substitute (2-12) into (2-16) we get:

$$\delta = \frac{-0.02878}{591.8}(1-\frac{T}{591.8})^{-0.97122}\ln(0.26655) \tag{2-17}$$

At 25 °C, the value of δ calculated from (2-17) is 0.00086K^{-1}. ΔH_{vap} is the heat of vaporization and it is 38 KJ/mol at 25 °C. To express the isosteric heat of adsorption in terms of surface loading q, we use the D-A equation and (2-15) could be expressed as:

$$\Delta H = \Delta H_{vap} + \beta E_0(\ln\frac{\rho_m W_0}{q})^{1/m} + \frac{(\beta E_0)\delta T}{m}(\ln\frac{\rho_m W_0}{q})^{-(n-1)/m} \tag{2-18}$$

The isosteric heat at 25 °C is calculated with (2-18), the result is shown in fig. 2-12. The averaged value of isosteric heat over the experimental concentration range is 65.15 KJ/mol. The isosteric heat can also be obtained directly from the experimental data with Clausius-Clapeyron equation for adsorption [26].

$$\frac{\Delta H}{RT_1T_2} = -\left[\frac{\ln P_1 - \ln P_2}{T_1 - T_2}\right]_N \tag{2-19}$$

With the experimental results of isotherm measurements at different temperatures indicated in Fig 2-3, the isosteric heat of adsorption for Ambersorb 600/Toluene system with different surface loading is calculated from equation (2-19) and plotted together with the results obtained from (2-18) in Fig. 2-12.

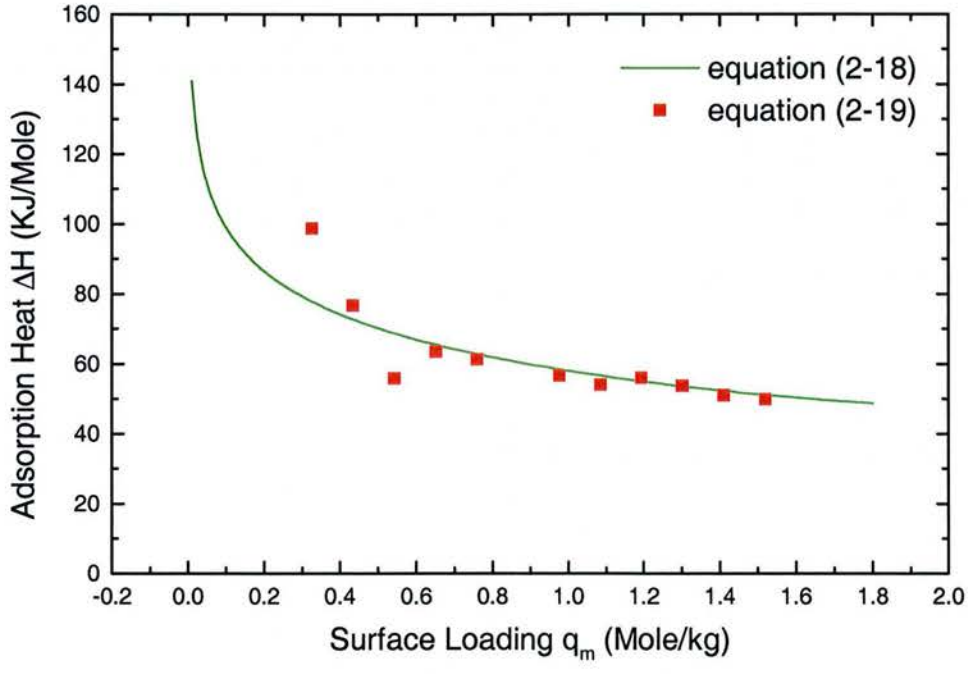

Fig. 2-12 Isosteric Heat vs Surface Loading

It is obvious that the isosteric heat decreases rapidly at first (low surface coverage)

followed by a slow decay with increasing surface coverage. This result indicates that adsorbent has an energetically heterogeneous surface. This also confirms that the micropore filling mechanism is much more suitable to describe the adsorption of Ambersorb 600/Toluene system.

2.5. Conclusions

- The isotherm measurement has been performed for Ambersorb 600/Toluene system at different temperatures (25, 80, 120 and 140 °C). The gas phase Toluene concentration is changed between 800 mg/Nm^3 and 16000 mg/Nm^3 (partial pressure between 20 Pa and 400 Pa).
- Freundlich, Langmuir and Dubinin-Astakhov equations can be used to describe the adsorption isotherm at tested temperatures with acceptable accuracy, while Dubinin-Astakhov equations gives much more reasonable explanation for Ambersorb 600/Toluene adsorption, or micropore filling mechanism is much more suitable to describe the adsorption behavior of Ambersorb 600/Toluene system.
- Dubinin-Astakhov equation (2-3), (2-4) could be used to describe the adsorption isotherm for Toluene concentration less than 16000 mg/Nm^3 and temperature between 0 °C and 140 °C. The parameters in D-A equation are W_0=0.21×10^{-3} m^3/kg, E_0=17.206 kJ/mol and m=1.17. This equation may also be used to predict the adsorption isotherm of other substances on Ambersorb 600 with the corresponding similarity coefficient.
- The isosteric heat of adsorption decreases rapidly at first, followed by a slow decay with increasing surface coverage. The averaged value over the experimental concentration range is 65.15 KJ/mol.

3. CFB ADSORPTION EXPERIMENTS

The Circulating Fluidized Bed (CFB) adsorption process will certainly be designed as a stable and continuous operation process. That is, the regenerated adsorbent will be introduced into the bed and the used adsorbent will be removed and fed into a desorber for regeneration continuously. The gas phase adsorbate concentration profile along the bed height is stable. But for the continuous adsorption process with a desorber, the stable operation condition will take long time to establish and this becomes a difficult issue for the experimental study where frequent change of operation conditions is required.

To avoid this difficulty, a batch operation CFB adsorption experimental unit has been constructed and used for the experimental study. That is, the adsorption process will start with fresh or regenerated adsorbent until all adsorbent in the CFB system becomes saturated. Fig. 3-1 is the schematic diagram of the experimental setup for the CFB adsorption. The details of gas supplying system, solid circulation system and the CFB unit will be introduced in this section. For a batch operation adsorption process, the adsorbate concentration distribution along the bed height is no longer stable, but changing with operation time.

16 CFB adsorption experiments with different superficial gas velocity, solid adsorbent circulating rate and inlet gas phase adsorbate concentrations have been conducted. The details of experimental setup and operation conditions are presented.

3.1. Experimental Setup

3.1.1. CFB Unit

Fig. 3-2 is the detailed design of the CFB unit. The CFB unit is basically composed of a riser, a downer and two-stage gas-solid separator. The CFB riser, act as an adsorber, is a 2.88m high tube with the inner diameter of 29mm. On the top of the riser, a large container is installed acting as the primary gas-solid separator. This special design eliminates the influence of exit geometry on the solid distribution in the CFB riser, which is often observed when the typical strong or weak restrictive exit design for CFB was employed. The other purpose of this design is to reduce the abrasion of the adsorbents. The secondary separator is a cyclone to catch up the very fines. The CFB downer is a 33mm inside diameter tube, acting as both the solid re-circulation loop and container.

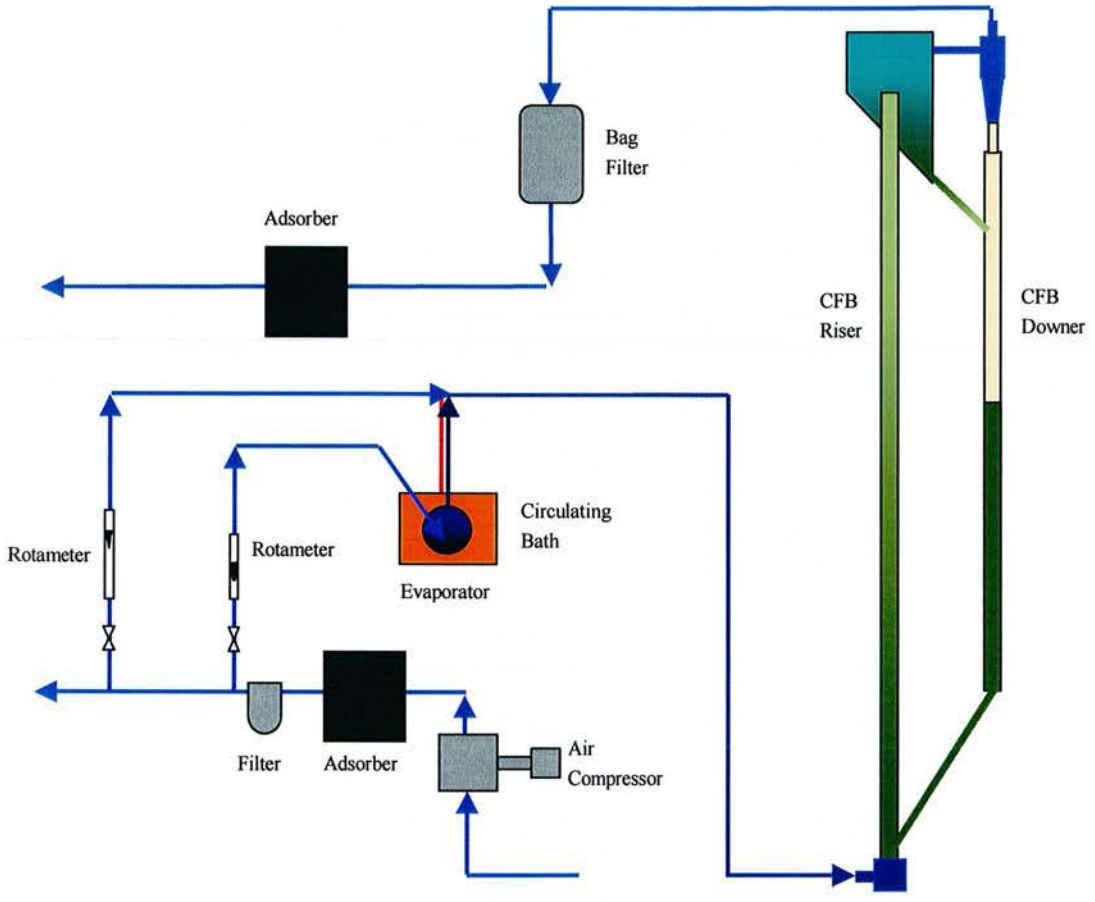

Fig. 3-1 Schematic Diagram of CFB Adsorption experimental setup

3.1.2. The Gas Supply System

Compressed air is used as the fluidizing gas and an activated carbon bed is installed after the air compressor to eliminate the possible oil vapor. Two rotameters are used to control the gas flow rate of primary fluidizing air and VOCs evaporation air with the full-scale range of 15 m^3/h and 0.15 m^3/h respectively. The evaporation air flowing through the VOCs evaporator first, which is immersed inside a circulating bath to maintain a stable temperature. The evaporation air is then directed to a mixer via a heated line to mix with the primary air. The desired VOCs concentration is obtained by adjusting the air flow rate to the evaporator or the temperature of circulating bath.

The fluidizing air with stable VOCs concentration is then directed into the CFB riser through the air distributor. It flows through the bed with the entrained solid adsorbents while adsorption is taking place. The gas and adsorbent are separated by a two-stage gas-solid separator at the top of the riser. The gas is then vented out via a bag filter to remove the dust and another activated carbon bed to remove the residual VOCs substance.

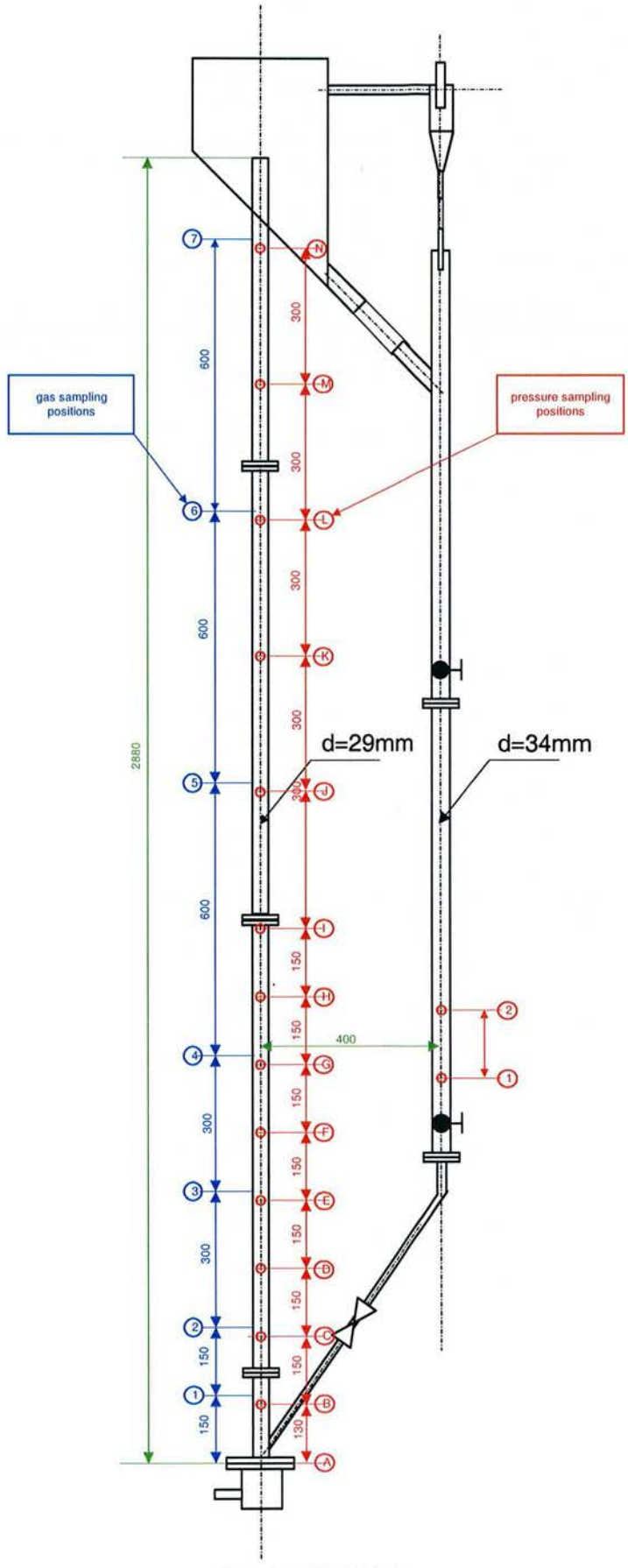

Fig. 3-2 CFB Unit

3.1.3. The Solid Circulating System

The adsorbent is stored inside the CFB downer and re-circulation loop. It is fed into the CFB riser nearby the air distributor and fluidized by air. Almost all the adsorbent particles are separated from air in the primary gas-solid separator, as the particle size of the adsorbent is uniform and relatively large (0.65mm). The adsorbent is then fed back to the re-circulation loop. The rate of solid re-circulation is controlled by a valve that is mounted on the inclined tube connecting the riser and downer.

In this simple design of solid re-circulation loop, the solid is actually fed back to the riser by gravity and the adjusting of re-circulation rate is limited. The air driven feed back valve was initially installed, which is widely used for CFB system with much larger flexibility for solid re-circulation rate control. The main problem associated with the air driven valve is: too much driving air is needed and it is difficult to measure how much goes into the CFB riser. In the present design, no additional air will come into the CFB riser with the re-circulation solid. Instead, some air will bypass via the CFB downer.

In order to measure the quantity of air bypass, two pressure sampling probes are installed along the CFB downer. The calibration experiment shows a linear relationship between the airflow rate and pressure drop across the 150mm adsorbent bed. The pressure drop is between 3 to 36 mm H_2O for all the experiment operations. The corresponding gas bypass flow rate is 0.006 to 0.072 m^3/h, which is 0.1% to 1% of the total gas flow rate. Therefore the gas bypass is omitted in the experimental data processing.

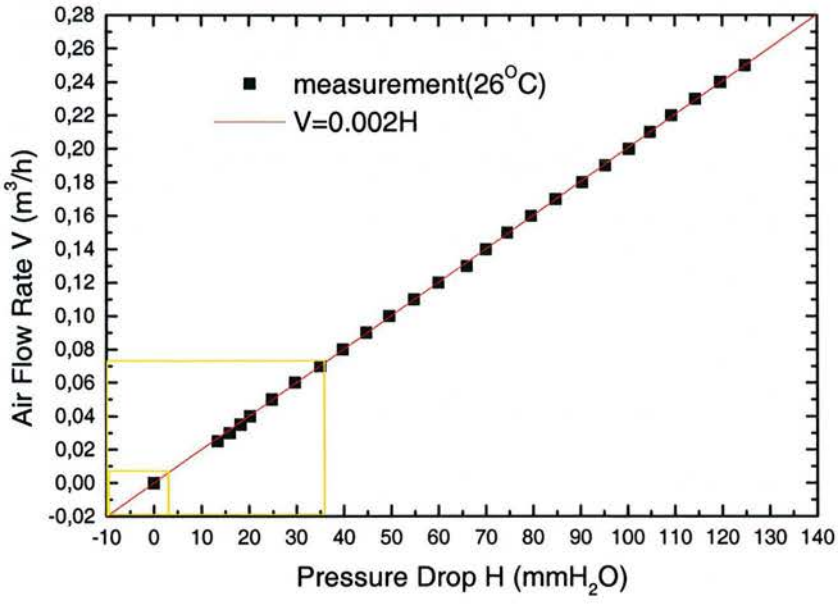

Fig. 3-3 Calibration of Bypass Flow Rate and Pressure Drop

Two special valves are installed on the CFB downer that could stop the solid but let the air pass through when they are closed. The solid re-circulation rate is measured by

closing the upper valve and accounting the time with a stopwatch for the bed surface traveling through 100mm space in the CFB downer. With the calibrated value of adsorbent weight and bed height in the CFB downer, the solid re-circulation rate is obtained.

3.1.4. Gas Sampling and Pressure Sampling

7 gas-sampling probes with an outside diameter of 3mm are installed along the CFB riser to measure the gas phase concentration inside the bed. The space between the sampling points is (starting from the gas distributor plate) increased from 150mm to 300mm and 600mm, as shown in Fig. 3-2. Though a small cross section is adopted for the CFB riser, a concentration distribution along the radial direction is observed by preliminary experiments with a single hole prob. In order to get the average concentration of the cross-section of the bed, the sampling probe is designed with six 1mm holes stuffed with porous metal to eliminate the solids. The 6 holes are symmetrically positioned from the center with the radius r=0.408R, 0.707R and 0.913R. The idea is to divide the cross section into 6 concentric circles with identical area and r is the radii of 1st, 3rd and 5th circles. The probes are moveable at the position outside the bed and only pushed inside the bed when sampling is taking place.

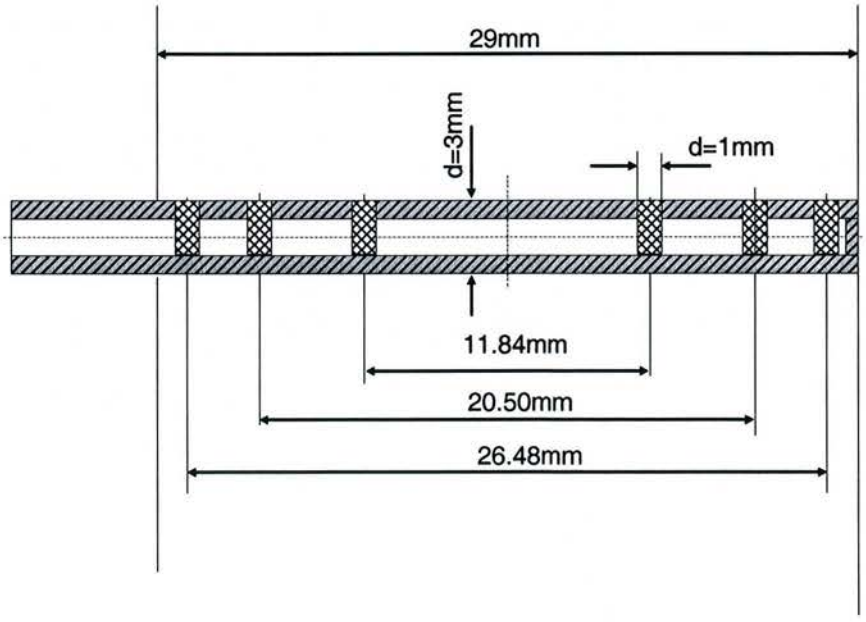

Fig. 3-4 Gas Sampling Probe

14 pressure-sampling probes are installed along the CFB riser. The space between sampling points is 150 mm or 300mm, as shown in Fig. 3-2. To avoid the influence of gas sampling probes and pressure sampling probes, the space between the first two pressure sampling position is 130mm. 14 manometers are connected to the probes to get the pressure drop readings between two neighboring sampling positions and the overall

pressure drop across the CFB riser.

3.1.5. Measurement of Gas Phase Concentration

A PGM-7600 VOCs Analyzer, a product of RAE Systems Inc., is purchased for the measurement of Toluene concentration in air. PGM-7600 uses photo-ionization detector to analyze the VOCs concentrations.

A Photo Ionization Detector (PID) uses an Ultraviolet (UV) light source ("Photo") to "Ionize" a gas sample and "Detect" its concentration. Ionization occurs when a molecule absorbs the high energy UV light, which excites the molecule and results in the temporary loss of a negatively charged electron and the formation of positively charged ion. The gas becomes electrically charged. These charged particles produce a current that is easily measured. The ions quickly recombine after the electrodes to "reform" their original molecule. Therefore, PIDs are a non-destructive measurement and PID samples can be bagged and used for further analysis.

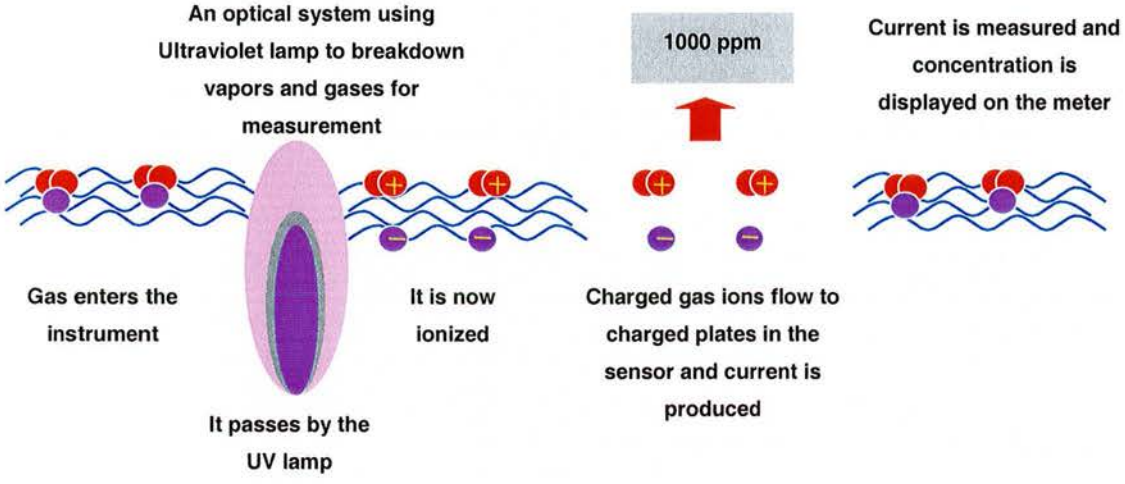

Fig. 3-5 Principle of PID Measurement

All elements and chemicals can be ionized, but they differ in the amount of energy they require. The energy required to displace an electron and "ionize" a compound is called its Ionization Potential (IP), measured in electron volts (eV). The light energy emitted by a UV lamp is also measured in eV. If the IP of the sample gas is less than the eV output of the lamp, then the sample gas will be ionized. Benzene has an IP of 9.24 eV and can be seen by a "standard" 10.6 eV lamp. Acetic acid has an IP of 10.66 eV and can only be seen by our 11.7 eV lamp. Carbon monoxide has an IP of 14.01 eV and cannot be ionized by a PID lamp.

The PID can be used to measure many organic substances, like benzene, toluene, xylene, acetaldehyde, trichloroethylene (TCE), mercaptans, diethyl amine, DMF, butadiene, ethanol, isopropanol, butane, and hexane. It can also be used to measure some inorganic

substances like ammonia and chlorine. PID does not detect air (N_2, O_2, CO_2, H_2O), natural gas and common toxics (CO, HCN, SO_2).

PGM-7600 has been equipped with a standard 10.6 eV lamp and is suitable to measure most VOCs substances. It has also equipped with a sampling pump and a memory of 15000 readings. One can directly get the numerical readings with the response time of less than 3 seconds. The accuracy of measurement and other technical specifications are listed in Table 3-1.

Table 3-1. Technical Specifications of PGM-7600

RANGE	RESOLUTION	RESPONSE TIME	ACCURACY
0 to 999 ppm	0.1 ppm	< 3 seconds	± 2 ppm or 10% of reading, <2000 ppm
100 to 10,000 ppm	1 ppm	< 3 seconds	± 20% of reading > 2000 ppm Calibrated to 100 ppm isobutylene
Sampling Pump	Internal integrated flow rate 400 cc/min Sample from horizontally or vertically		
Datalogging	15,000 points with time/date, header information		
Approvals	UL, cUL Class I, Division 1, Groups A, B, C and D EEx ia IIL C T4		
Battery	Rechargeable, field changeable NiMH battery pack, 10 hours operation		

3.1.6. Measurement of Axial Voidage Distribution

There are two ways to measure the axial voidage distribution in CFB riser. The direct measurement is to stop the gas and solid flow in a normally operated CFB riser with a set of parallel plates along the bed height. Then measure the weight of collected particles between plates and figure out the voidage in this space. The indirect measurement is to measure the pressure drop along the bed height and calculate the voidage from that. The indirect measurement is much simple with reasonable accuracy. So the pressure drop method is used in this study.

The pressure drop method is based on the assumption that the particles are suspended or moving with constant velocity in the bed, thus the forces exerted on the particle equals the weight of it. In fact, after entering the CFB riser the particles will be speeded up first by the gas. Pressure drop method considering the influence of acceleration on the voidage calculation could be omitted

If the solid particles in the CFB riser are moving at constant velocity, the weight of the solid particle equals the pressure drop minus the buoyancy of gas, that is:

$$\Delta p \cdot F = (\rho_p - \rho_g) F \Delta L (1 - \varepsilon) g \tag{3-1}$$

When $\rho_p >> \rho_g$, $$\varepsilon = 1 - \frac{\Delta p}{g \cdot \Delta L \cdot \rho_p} \quad (3\text{-}2)$$

ρ_p and ρ_g are the solid and gas density. ΔL is the distance between two pressure sampling position and F is the cross sectional area of the bed.

14 pressure sampling probes are installed along the CFB riser. The distance between two sampling position is either 150mm or 300mm, as showing in Fig. 3-2. To avoid the influence of gas sampling on the pressure measurement, two types of sampling probes are positioned at different height. 14 pressure gauges are used to measure the pressure drop between two neighbouring positions and across the whole bed.

3.2. Experimental Procedures

3.2.1. Preparatory Operation

In order to get stabilized experimental conditions, the circulating bath and gas supply system is put in operation 4 hours before the experiment. One hour before the test, the adsorbent is re-circulated in the CFB system with air at rated flow rate. The solid re-circulation rate is then measured and adjusted to the desired value. The VOCs evaporation gas is also in operation, and vented out directly via a bypass.

Before the experiments, the adsorbent is dried in an air-blown oven at 180 °C for several days and kept in the airtight bottles. 500.00g adsorbent is weighted and added into the CFB system for each experimental operation. The bulk density of the adsorbent is also measured before and after the adsorption experiments.

3.2.2. Experimental Operations and Measurements

The experiment starts when the VOCs stream is mixed with the primary fluidizing gas. The PGM-7600 is set to record the concentration readings every 6 seconds (the averaged value during 6 seconds). The inlet VOCs concentration is first measured under the air distributor plate. Then PGM-7600 is connected to the 7 gas sampling probes in turn from bottom to the top of the CFB riser to measure the gas phase concentrations at the corresponding position. The gas-sampling probe is pushed inside the bed only when it is connected with the gas analyzer and the measurement at this point is finished when the VOCs concentration reading is stabilized for about one minute. This measurement process is repeated every half hour and the gas analyzer is connected to the coming stream to measure the inlet VOCs concentrations in the meantime.

Fig. 3-6 is the typical recorded measurement results of VOCs concentrations along the CFB riser during the experiment. Ten concentration values (one minute) at each sampling position are then averaged and taken as the concentration value at the corresponding time.

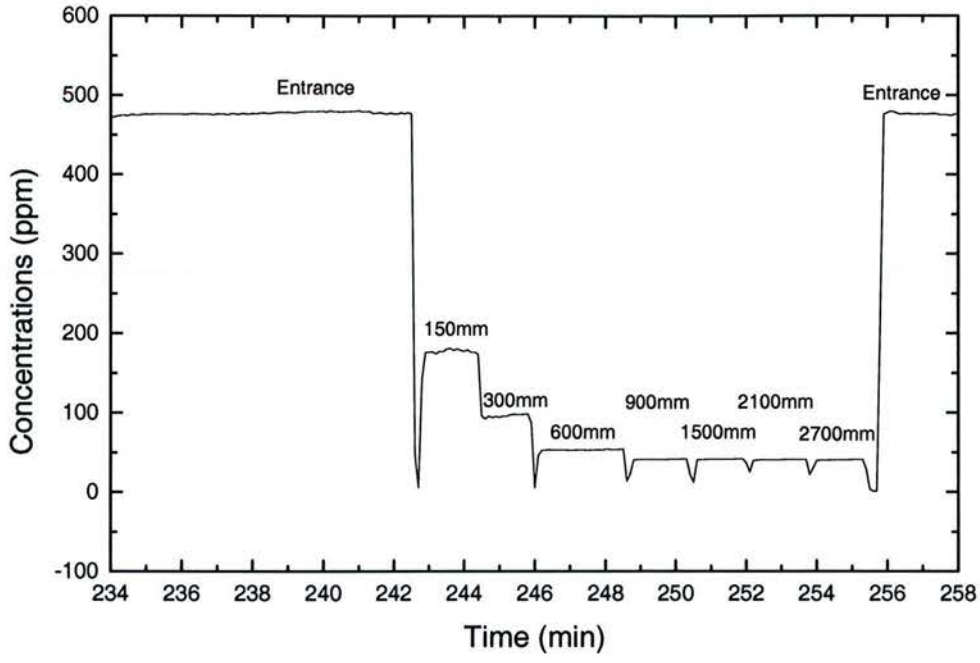

Fig. 3-6 Concentration Records of PGM-7600 During Experiment

The pressure drop between the neighboring pressure-sampling probes and the solid re-circulation rate are also measured during the experiments. The voidage distribution along the CFB riser and the solid inventory inside the CFB riser are obtained from the pressure drop readings. The test operation is terminated when the gas phase concentration at the entrance and exit are almost the same.

Two RHLOG thermometers are fixed inside the CFB to measure the gas temperature, one at entrance and the other at the exit of the CFB riser. The temperature readings are automatically recorded by the thermometer and the time interval between the records could be set from 1 second to 8 hours. The technical specifications of RHLOG thermometer are listed in Table 3-2.

Table 3-2. Technical Specifications

RANGE	RESOLUTION	RESPONSE TIME	ACCURACY
-20 to 75 °C	0.01 °C	< 2 minutes	±0.3 °C
Datalogging	1624 points with time/date	**Battery**	3.6V

The thermometers are set to take the temperature record every minute during the experiments. The typical temperature history during the experiment is shown in Fig. 3-6. The averaged value of these records is taken as the mean temperature of the experiment. The temperature at CFB riser exit is 1 °C to 3 °C higher than that at entrance. From the

adsorption isotherm discussion we know that the averaged adsorption heat of Ambersorb 600/Toluene system is 65.15 KJ/mol. Assuming all the adsorption heat is used to heating up the gas and solid particles (adiabatic condition), then the corresponding maximum gas temperature increase due to adsorption is only 0.15 °C ~ 0.36 °C. So the temperature difference between the entrance and exit of the CFB riser should not be mainly induced by the adsorption, but the other reasons. The temperature fluctuation during the experiments is between 2-3 °C due to the temperature change of ambient atmosphere.

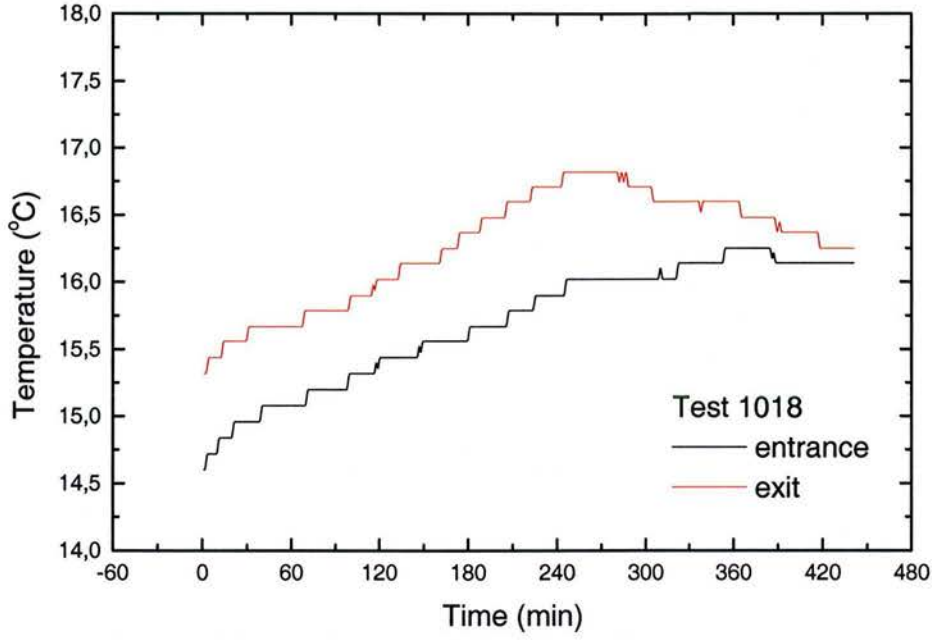

Fig. 3-7 Temperature History of Experiments

3.2.3. Operation Conditions and Experimental Results

16 CFB adsorption experiments have been conducted with different superficial gas velocity, solid circulating rate, gas phase concentration, fresh and regenerated adsorbent. Experimental conditions are listed in Table 3-3.

The superficial gas velocity and solid circulating rate will greatly change the voidage distribution and solid inventory in the CFB riser. Higher superficial gas velocity and lower solid circulating rate will result in higher bed voidage and lower solid inventory in CFB riser. In the experiments, the superficial gas velocity, U_g, ranged from 2.23 m/s to 2.74 m/s. The solid circulation rate ranged from 6.58 kg/m^{2}s to 19.83 kg/m^{2}s. The corresponding solid inventory in the CFB riser is 38g to 116g under different operation conditions.

Table 3-3: Experimental Conditions

Tests No	Superficial Gas Velocity U_g (m/s)	Solid Recirculating Rate G_s (kg/m^{2}s)	VOCs Concentration C_{in} (mg/m^3)	Adsorbent Regeneration Cycles	Temperature K
108	2.23	6.70	1911(465ppm)	Fresh	290.1
111	2.58	19.0	1915(466ppm)	Fresh	291.3
118	2.74	19.28	1956(476ppm)	Fresh	288.0
320	2.56	19.83	4676(1140ppm)	Fresh	286.2
131	2.56	19.78	4185(1018ppm)	Fresh	286.7
220	2.56	19.61	3780(920ppm)	Fresh	287.9
206	2.57	19.44	2978(720ppm)	Fresh	289.0
1022	2.40	6.58	1941(472ppm)	1	291.4
1011	2.40	9.7	1904(463ppm)	1	291.5
1018	2.39	12.33	1949(474ppm)	1	288.6
1016	2.40	19.26	1941(472ppm)	1	288.6
1121	2.41	12.58	1924(468ppm)	2	293.8
1031	2.39	9.89	1940(472ppm)	2	288.2
1108	2.40	9.91	1957(476ppm)	2	290.5
1114	2.39	6.98	1932(470ppm)	2	289.4
1122	2.42	12.58	1919(467ppm)	3	293.2

Fig. 3-8 and Fig. 3-9 are the typical voidage distribution and gas phase VOCs concentration along the bed height. The VOCs concentration measurements at different bed height for a typical adsorption test are shown in Fig. 3-10.

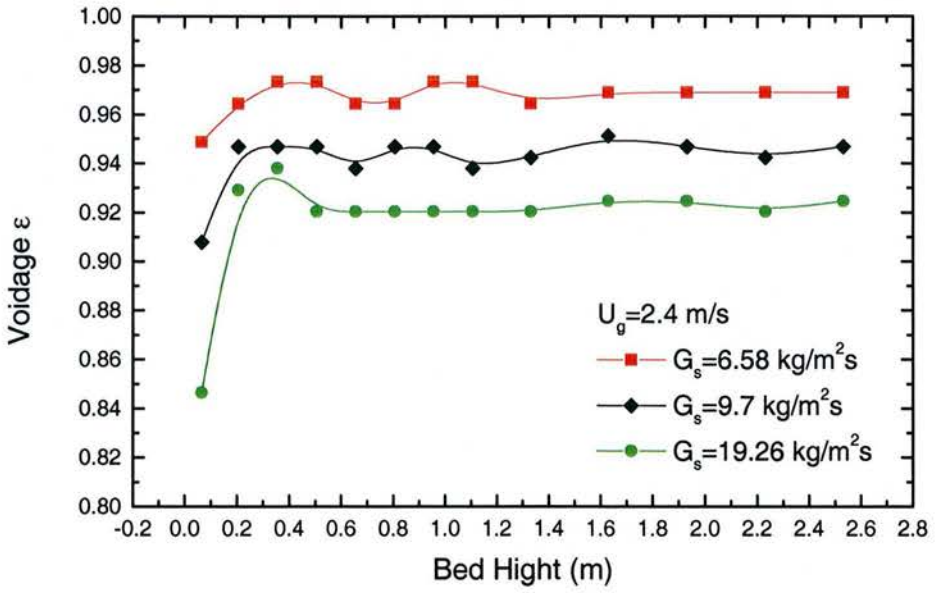

Fig. 3-8 Voidage Distribution Along CFB Riser

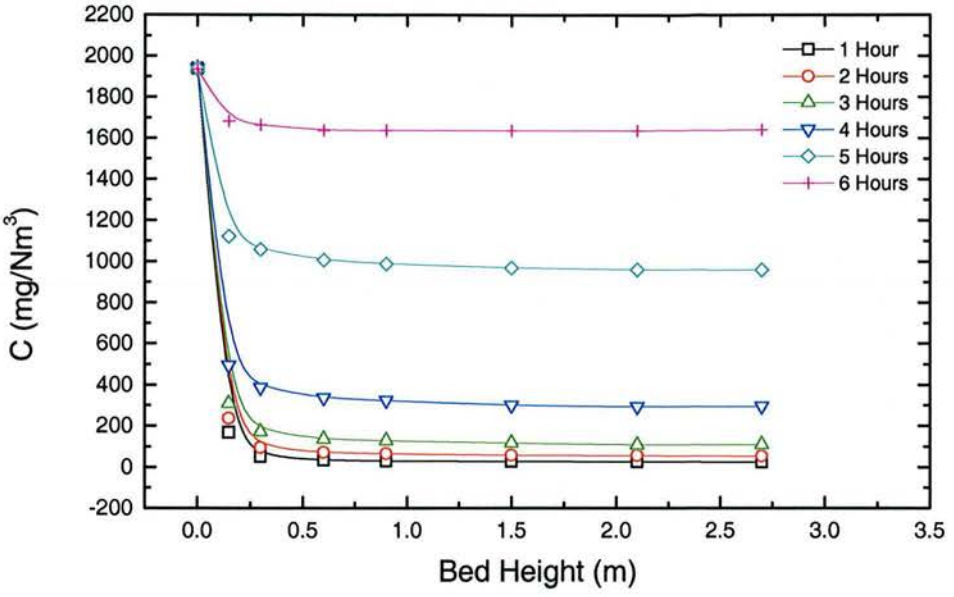

Fig. 3-9 VOCs Concentration Distribution Along CFB Riser

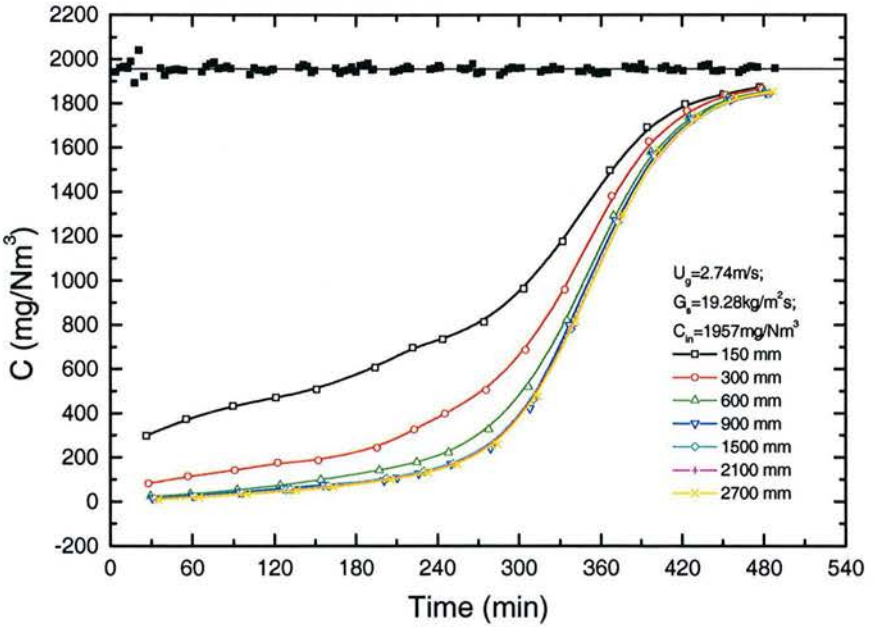

Fig. 3-10 VOCs Concentration Measurements at Different Bed Height

4. BREAKTHROUGH CURVE

For a batch operation CFB adsorption system, the gas phase concentration of adsorbate is decreasing along the CFB riser and increasing with the operation time under stable inlet concentration, until saturation capacity of adsorbent is reached. Like fixed bed adsorber, a breakthrough curve at the exit of CFB riser will be obtained. Here the breakthrough curve is estimated with an equilibrium model.

4.1. Mathematical Model

Considering a batch operation CFB adsorption system, as illustrated in Fig. 4- 1. The gas stream comes into the bottom of the CFB with constant VOCs concentration C_{in} (mg/Nm^3) and superficial velocity U_g (Nm^3/m^{2}h). The gas phase concentration of adsorbate at the exit of CFB system is C_{out} (mg/Nm^3). The inventory of adsorbent in the CFB system, including the adsorbent inside the re-circulating loop, is G (kg). The height of CFB riser is H and the cross section area is F. Assuming that the adsorbent particles are well mixed within the CFB system due to the high circulating rate, then the quantity of VOCs adsorbed by the adsorbent is the same for all adsorbent particles inside the CFB system and is varied with time only. Assuming the gas phase concentration at the exit of CFB system is in equilibrium with the adsorbent (this is the case when the CFB riser is long enough) and neglecting the influence of adsorption on the gas flow rate, solid density and temperature (as the adsorbate concentration is very low), the mass balance of adsorbate in CFB system at any time gives:

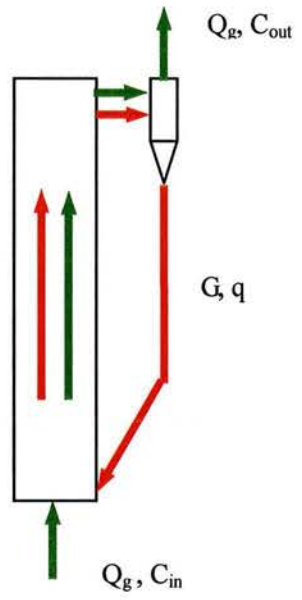

Fig. 4-1 CFB Adsorption System

$$U_g F(C_{in} - C_{out})dt = Gdq + \varepsilon_b FHdC_{out} \tag{4-1}$$

From the isotherm discussion we know that the relation between q and C_{out} can be described by Dubinin-Astakhov equation:

$$q = \rho_{ad} W_0 \exp\left[-\left(\frac{A}{E}\right)^m\right] \tag{4-2}$$

and

$$A = RT\ln(\frac{P_{sat}}{P}) = RT\ln(\frac{C_{sat}}{C}) \tag{4-3}$$

The dynamic change of gas phase concentration is much easier to detect than the solid phase concentration during the experiments. So we substitute solid phase adsorbate concentration q with gas phase concentration C_{out} and get the relation between C_{out} and time t. From equation (4-2) and (4-3), we can get:

$$\frac{dq}{dC} = \frac{\rho_{ad}W_0}{C} mB(B\ln\frac{C_{sat}}{C})^{m-1} EXP[-(B\ln\frac{C_{sat}}{C})^m] \tag{4-4}$$

Here $B = \frac{RT}{E}$

Substitute (4-4) into (4-1) we get the differential equation of C_{out}:

$$\frac{dC_{out}}{dt} = U_g F(C_{in} - C_{out})/[\frac{\rho_{ad}W_0 mGB}{C_{out}}(B\ln\frac{C_{sat}}{C_{out}})^{m-1} e^{-(B\ln\frac{C_{sat}}{C_{out}})^m} + \varepsilon_b FH] \tag{4-5}$$

Here C_{sat} is the saturation concentration of adsorbate at T. C_{sat} is estimated with (2-13). P_{ad} is the liquid density and can be calculated with (4-6). For Toluene, M=92.14 kg/kmol; ρ_m is the mole density and is calculated with (2-12)

$$\rho_{ad}(T) = M\rho_m \quad (kg/m^3) \tag{4-6}$$

4.2. The Validation of Assumptions

4.2.1. Influence of Inlet VOCs Concentrations

The differential equation (4-5) has been solved numerically using the Runge-Kutta method with all the parameters in accordance with the experimental conditions. The first set of experiments is conducted with different initial gas phase concentrations C_{in}, while the gas flow rate Q_g and solid re-circulating rate G_s are kept about the same. The experimental conditions are listed in table 4-1.

Table 4-1: Experimental Conditions for Different Gas Phase Concentration

Tests No.	C_{in} (mg/Nm^3)	Q_g (Nm^3/h)	U_g (m/s)	G_s (kg/m^{2}s)	Temperature K
320	4676(1140ppm)	5.80	2.56	19.83	286.2
131	4185(1018ppm)	5.79	2.56	19.78	286.7
220	3780(920ppm)	5.78	2.56	19.61	287.9
206	2978(720ppm)	5.77	2.57	19.44	289.0
111	1915(466ppm)	5.74	2.58	19.01	291.3

Fig. 4-2 shows the calculated and experimental results of gas phase concentration at exit of CFB riser with operation time. The predicted values of exit VOCs concentration agreed well with experimental results for low inlet gas phase concentration conditions. Large deviations exist for predicted and experimental results when the inlet VOCs concentration is higher(4676mg/Nm^3).

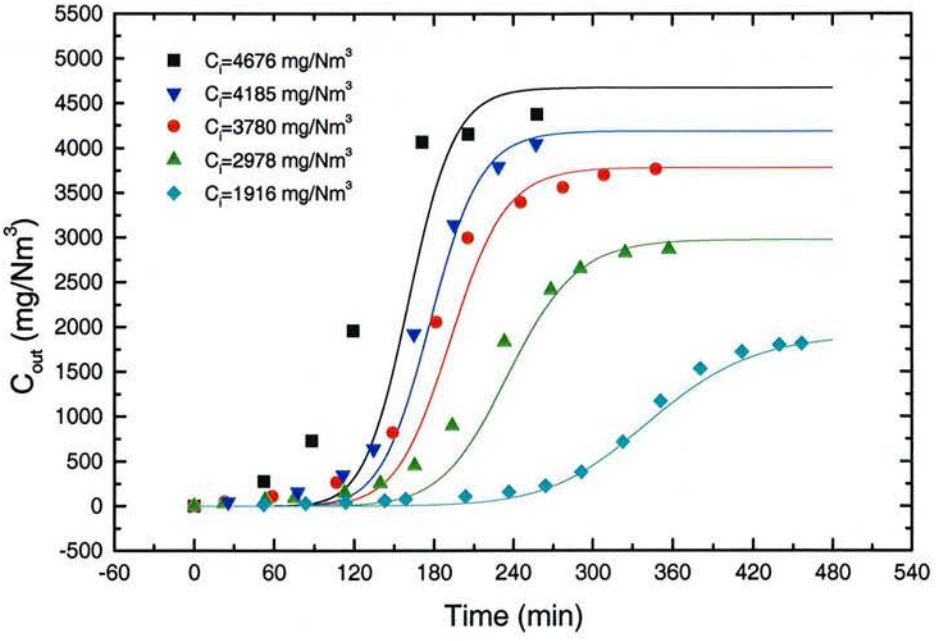

Fig. 4-2 Exit Gas Phase Concentrations with Different Inlet VOCs Concentrations

One of the fundamental assumptions for this model is that the gas and solid are in equilibrium at the exit of the CFB riser. Under experimental conditions, the nearly equilibrium between gas and solids was obtained when the inlet VOCs concentration was lower, as the measured concentration values wewe almost the same for the last 3 sampling positions nearby the exit. But under higher inlet VOCs concentration conditions, relatively large concentration difference existed for the last few sampling positions, indicating more time was needed for the gas and solid to reach equilibrium. In the other word, the height of CFB riser is not long enough and the equilibrium assumption is far from satisfaction.

So with this CFB test unit, the equilibrium model is valid only when the inlet gas phase concentration is less than 4100 mg/Nm^3(1000ppm).

4.2.2. Influence of Solid Circulation Rate

Another fundamental assumption of the model is that the solids are well mixed within the whole CFB system. The validation of this assumption should depend on the solid circulation rate. The higher the solid circulation rate is, the better the solid mixing

within the CFB system. The CFB adsorption experiments have also been conducted with different solid circulation rate. The experimental conditions are listed in table 4-2. Fig. 4-3 shows the experimental results of exit gas phase VOCs concentration with different solid circulation rate. No obvious difference has been found from the experimental results.

Table 4-2: Experimental Conditions for Different Solid Circulation Rate

Tests No	C_{in} (mg/Nm^3)	Q_g (Nm^3/h)	U_g (m/s)	G_s (kg/m^{2}s)	G_1 (kg)	Temperature (K)
1114	1932(470ppm)	5.36	2.39	6.98	58.13×10^{-3}	288.6
1031	1940(472ppm)	5.38	2.39	9.89	71.34×10^{-3}	291.4
1108	1956(476ppm)	5.35	2.40	9.91	76.62×10^{-3}	291.5
1121	1923(468ppm)	5.33	2.41	12.58	80.58×10^{-3}	288.6

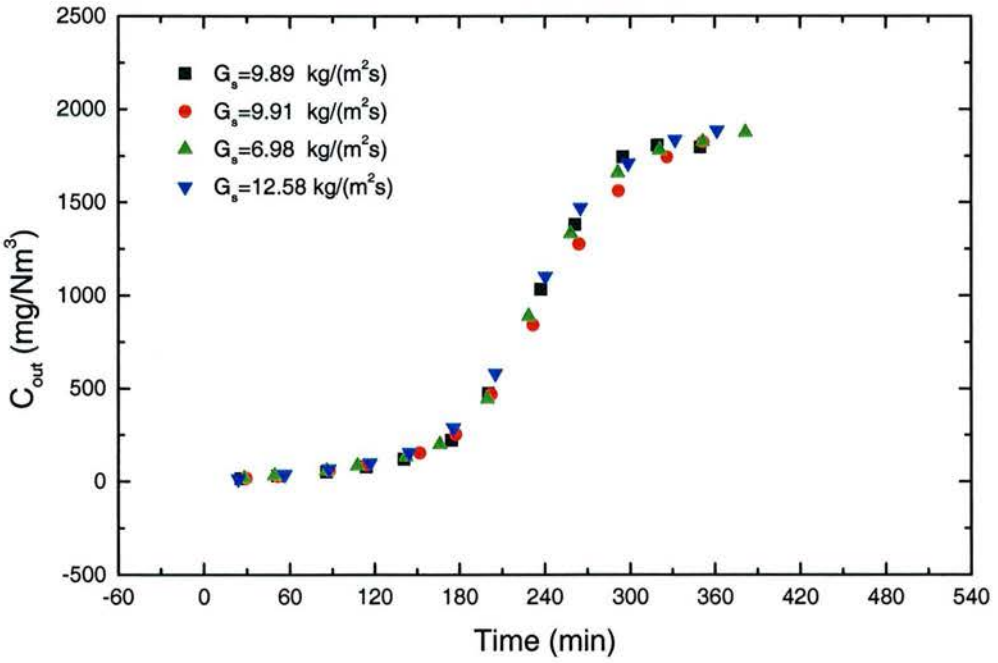

Fig. 4-3 Exit VOCs Concentrations with Different Solid Circulation Rate

To consider the influence of solid circulation rate on the performance of adsorption in CFB riser, another model is proposed. Here the solids are assumed to be well mixed within the CFB riser only. In the re-circulation loop plug flow is assumed for solid. The inventory of adsorbent in the CFB riser and in the re-circulating loop is G_1(kg) and G_2(kg) respectively. The solid adsorbent circulating rate is G_s(kg/m^{2}h). The other assumptions are the same as those used in the first model. The material balance of adsorbate at any given time gives:

$$U_g F(C_{in} - C_{out})dt + G_s(q_{in} - q_{out})dt = G_1 dq_{out} + FH\varepsilon_b dC_{out} \tag{4-7}$$

or: $$G_1 \frac{dq_{out}}{dt} + HF\varepsilon_b \frac{dC_{out}}{dt} = U_g F(C_{in} - C_{out}) + G_s(q_{in} - q_{out}) \tag{4-8}$$

Here:
$$\begin{aligned} & q_{in} = q_0; && t \le t_0 \\ & q_{in}\big|_t = q_{out}\big|_{t-t_0}; && t > t_0 \\ & t_0 = G_2 / G_s \end{aligned} \tag{4 - 9}$$

From the isotherm discussion we know that the relation between q_{out} and C_{out} can be described by Dubinin-Astakhov equation. Substitute (4-2), (4-3) and (4-4) into (4-8), and indicate the gas phase concentration in equilibrium with the inlet solid phase concentration q_{in} as C_{in}^* we get:

$$\frac{dC_{out}}{dt} = \frac{U_g F(C_{in} - C_{out}) + \rho_{ad} W_0 G_s \{e^{-[B\ln(C_{sat}/C_{in}^*)]^m} - e^{-[B\ln(C_{sat}/C_{out})]^m}\}}{\rho_{ad} W_0 G_1 \frac{mB}{C_{out}} [B\ln(C_{sat}/C_{out})]^{m-1} e^{-[B\ln(C_{sat}/C_{out}]^m} + \varepsilon_b HF} \tag{4-10}$$

and
$$\begin{aligned} & C_{in}^* = C_0^*; && t \le t_0 \\ & C_{in}^*\big|_t = C_{out}\big|_{(t-t_0)}; && t > t_0 \\ & t_0 = G_2 / G_s \end{aligned} \tag{4-11}$$

Here C_{sat} is the saturation concentration of adsorbate at T. ρ_{ad} is the liquid density of toluene. The solid circulation rate is changed from 6.6 to 19.4 kg/m^{2}s in the experiments with 5.1 Nm^3/h gas flow rate, the corresponding solid inventory in the CFB riser is between 38g to 116g. The gas phase exit concentration is calculated with this model for the two extreme situations, while the other parameters remain the same. The maximum concentration (4670 mg/Nm^3) in the experiments is used as the inlet gas phase concentration. Table 4-3 gives the parameters used in the calculation. The results show that the maximum calculated concentration difference ΔC with (4-12) is 21.96 mg/Nm^3, as shown in Fig 4-4 and that is 1.72% of the corresponding concentration value.

$$\Delta C = C_{(Gs=6.6kg/m^2s)} - C_{(Gs=19.8kg/m^2s)} \tag{4-12}$$

Table 4-3: Conditions for Calculation

No	C_{in} (mg/Nm^3)	G_s (kg/m^{2}s)	G (kg)	G_1 (kg)	Q_g (Nm^3/h)	Temperature (K)
1	4674(1140ppm)*	6.58**	0.5	38x10^{-3}**	5.34**	291**
2	4674(1140ppm)*	19.36***	0.5	116x10^{-3}***	5.34**	291**

* Value from test 0320

** Value from test 1022

*** Value from test 1122

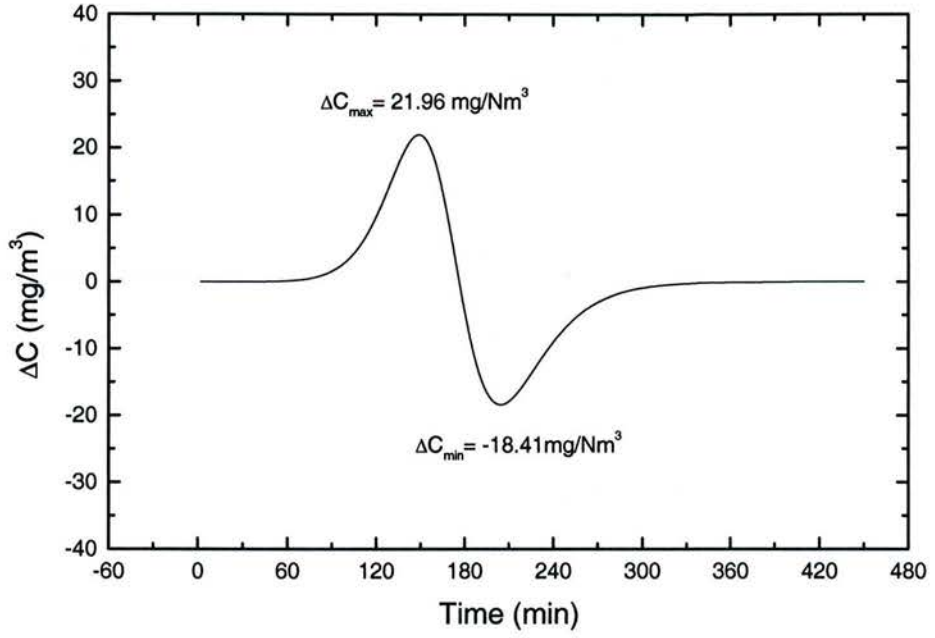

Fig. 4-4 Influence of Solid Circulation Rate

This is to say that the influence of solid circulation rate on the exit concentration is negligible within the range of experimental conditions, or the well mixed assumption for the solids is reasonable. The first model is used in the preceding discussions to avoid the complexity of calculation.

The above conclusion did not means that the solid re-circulation rate has no influence on the adsorption process inside the CFB riser. In fact, the solid re-circulation rate will greatly change the voidage distribution along the bed height and the solid inventory in the CFB riser. So it will certainly influence the VOCs concentration distribution along the bed height, though the concentration at exit has not been affected under experimental conditions.

4.2.3. The Influence of Regeneration on Adsorbent.

After each experiment, the adsorbents are regenerated for reuse. As the regeneration is simple carried out in an air blown oven under 180 degree C, the adsorbate did not completely removed by the desorption process. The adsorption capacity of the adsorbent is reduced with the repeated adsorption/desorption cycles. To consider the influence of regeneration cycles on the adsorption capacity, a set of CFB adsorption experiments have been conducted under approximately the same conditions with the fresh and regenerated adsorbents, as indicated in table 4-4.

Table 4-4 Experimental Conditions

Tests No	C_{in} (mg/Nm^3)	G_s (kg/m^{2}s)	Q_g (Nm^3/h)	U_g (m/s)	Temperature K	Adsorbent
0111	1916	19.01	5.74	2.58	291.3	Fresh
1011	1903	9.70	5.35	2.40	291.5	After 1 Cycle
1016	1940	19.27	5.39	2.40	288.6	After 1 Cycle
1114	1932	6.98	5.36	2.39	289.4	After 2 Cycle
1121	1924	12.58	5.33	2.41	293.8	After 2 Cycle
1122	1920	19.36	5.35	2.42	293.2	After 3Cycles

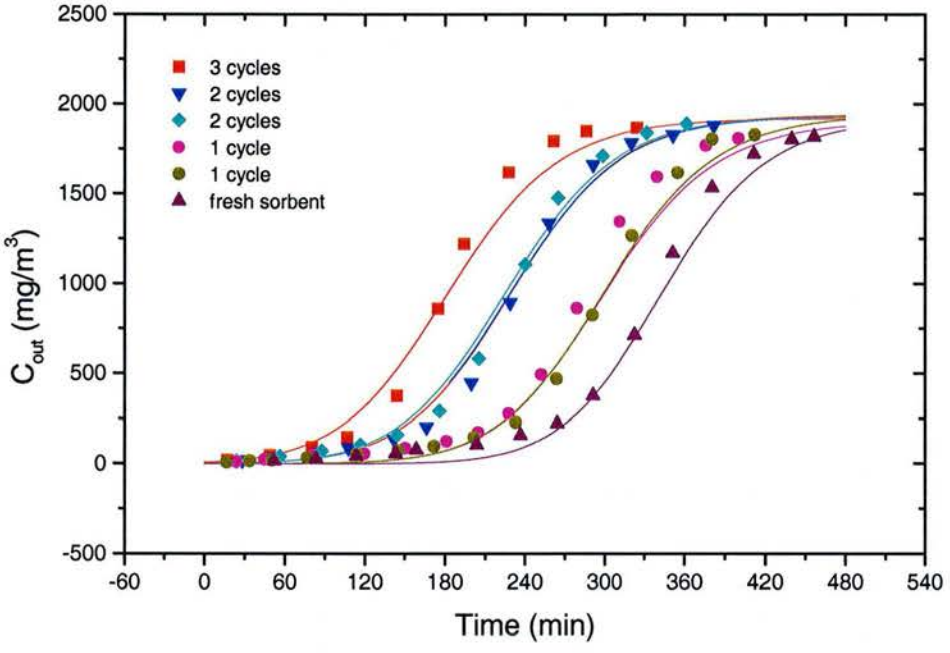

Fig. 4-5 Exit VOCs Concentrations with Different Fresh and Regenerated Adsorbent

The experimental results show steady decrease of breakthrough time with repeated adsorption/desorption cycles of adsorbents. The experimental results are used to determine the initial solid phase concentration of adsorbents q_{in} for different regeneration cycles. Table 4-5 shows the results of q_{in} from date fitting. Fig. 4-5 shows the experimental results and calculated values with q_{in}.

Table 4-5 Initial Solid Phase Concentrations

	Fresh sorbent	After 1 cycle	After 2 cycles	After 3 cycles
q_{in} (g/kg)	0	25	46	60
C^*_{in} (mg/Nm^3)	0	0.01	1	8

4.3. Discussion and Conclusions

4.3.1. Dimensionless Analysis

If the dimensionless form of gas and solid phase concentration is used, then (4-5) could be expressed as:

$$\frac{dY}{d\theta}=\frac{(1-Y)(e^{-(B\ln Y_{sat})^m}-e^{-(B\ln\frac{Y_{sat}}{Y_{in}^*})^m})}{\frac{mB}{Y}(B\ln\frac{Y_{sat}}{Y})^{m-1}e^{-(B\ln\frac{Y_{sat}}{Y})}+\frac{\varepsilon_b FHC_{in}}{G\rho_{ad}W_0}} \tag{4-13}$$

here the dimensionless gas phase concentration $Y=C/C_{in}$; $Y^*_{in}=C^*_{in}/C_{in}$, C^*_{in} is the gas phase concentration in equilibrium with initial solid phase concentration q_{in}; dimensionless solid phase concentration $X=q/q^*$. q^* is the solid phase concentration in equilibrium with C_{in} at corresponding temperature and can be obtained from the adsorption isotherm:

$$q^*=\rho_{ad}W_0\exp\left[-\left(\frac{RT}{E}\ln(\frac{C_{sat}}{C_{in}})\right)^m\right] \tag{4-14}$$

Dimensionless time $\theta=t/t^*$, t^* is the stoichiometric breakthrough time and defined as: $t^*=G(q^*-q_{in})/Q_gC_{in}$. It is obvious that the change of superficial gas velocity U_g and solid circulation rate G_s has no influence on the dimensionless concentration distribution with dimensionless time. In addition, the secondary term of the denominator in (4-13) is the ratio of gas phase adsorbate in the riser to the solid phase adsorbate in the CFB system when saturation is reached, and it's value is very small ($\sim10^{-4}$). So the dimensionless gas and solid phase concentration profile calculated with (4-13) is almost unchanged for different inlet gas phase concentrations.

Fig. 4-6 is the calculated dimensionless gas and solid phase concentration with dimensionless time θ. Six experimental results, representing different gas flow rate, solid circulation rate and inlet VOCs concentrations, have also been plotted. The experimental conditions are listed in table 4-6.

Table 4-6. Experimental Conditions

Tests No	0108	1022	1011	1016	0131	0111
U_g (m/s)	2.23	2.40	2.40	2.40	2.56	2.58
G_s (kg/m^{2}s)	6.70	6.58	9.70	19.27	19.78	19.01
C_{in} (mg/Nm^3)	1911	1940	1903	1940	4184	1916

With the dimensionless parameters, the VOCs concentrations at exit of CFB riser with

different gas flow rate, solid circulating rate and inlet VOCs concentrations could be described by the same curve. The calculated results shows that the solid phase concentration q shows liner increase with time first (θ<0.7) and then slow down to it's saturation capacity. The predicted gas phase concentration agreed well with experimental values, while slight smaller values are predicted for the earlier period of operation. The gas and solid phase concentration reaches $0.52C_{in}$ and $0.93q^*$ respectively when stoichiometric time is reached.

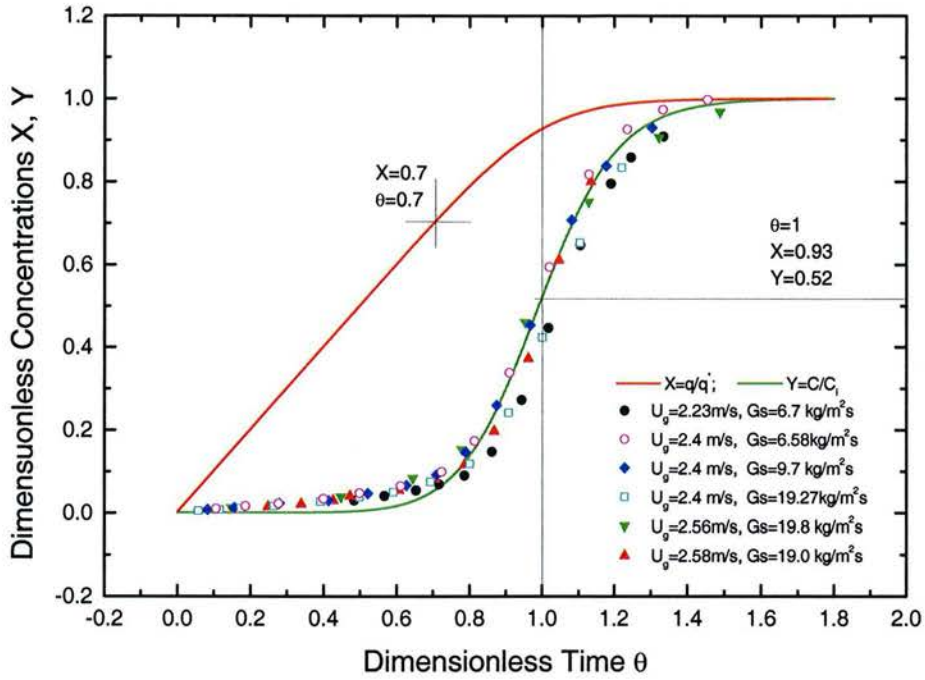

Fig. 4-6 Dimensionless Gas and Solid Phase Concentration

4.3.2. Conclusions:

- The dynamic change of gas phase exit concentration and solid phase concentration of adsorbent for the batch operation CFB adsorption unit could be estimated with the equilibrium model. The predicted and experimental values agreed well for inlet gas phase concentration less than 4100 mg/Nm^3 (1000 ppm) and solid re-circulation rate in the experimental range.
- The decrease of adsorption capacity with repeated adsorption/desorption cycles could be explained as the result of uncompleted desorption. The residual adsorbate after each cycle is estimated by fitting it with the experimental results.
- The gas phase concentration at exit is described by differential equation (4-13). It reaches 52% of inlet concentration when stoichiometric time is reached.

- Solid phase concentration is estimated by (4-13) and Dubinin-Astakhov equation (2-4). It shows liner increase with time first ($\theta<0.7$) and then slows down to the saturation capacity. q reaches 93% of its saturation capacity when $\theta=1$.

5. HYDRODYNAMICS OF CFB RISER

The purpose of the present chapter is to develop a relatively detailed flow model for gas-solid two phases flow in Circulating Fluidized Bed (CFB), which will be used later to describe mass transfer between gas and solid. The starting point is the so-called EMMS model (Energy-Minimization Multi-Scale model) of Li[34],[35]. This model divides the heterogeneous gas-solid system in the CFB into two homogeneous gas-solid systems: on one hand a dilute phase consisting of gas and discrete individual particles and on the other hand a dense phase or clusters of particles, which behaves like large highly porous particles. The constitutive equations are based on force balances and an assumption relating cluster size to energy. The unknown variables are the local volume fraction of different phases and the relative local gas and solid velocities of these phases, including velocities inside the clusters, and the cluster size.

The EMMS approach normally determines the unknowns by minimizing the total energy dissipated. It is therefore a numerical search on several variables. We shall use here an additional assumption and some modifications of the original model, which allow a straightforward semi-analytical solution, reducing the numerical search to just one variable.

In the following, we first describe the various patterns of phase distribution in fast fluidization. Then we introduce the EMMS model and its relations, and the modifications we proposed. As it is a local model, we shell also introduce an overall model of gas voidage distribution in the bed. This model needs to be combined in the EMMS approach to yield a complete description of the phases distribution along the bed.

Calculated examples are presented and discussed based on our experimental conditions in adsorption.

5.1 Characteristics of Circulating Fluidized Bed

5.1.1. Introduction

The CFB process has been used for Fluid Catalytic Cracking (FCC) in oil industry since the 1930's. But most research were mainly concerned with the low velocity bubble fluidized bed in the early years because of the widespread applications of bubble fluidized bed coal combustion process in industry[27]. It was not until Reh [28] termed the ***Circulating Fluidized Bed*** for high gas and solid throughput fluidization operation, and Yerushalmi et al. [29] gave the concept of ***Fast Fluidization,*** that the CFB process was

recognized as a unique process different from bubble fluidized bed and pneumatic conveying.

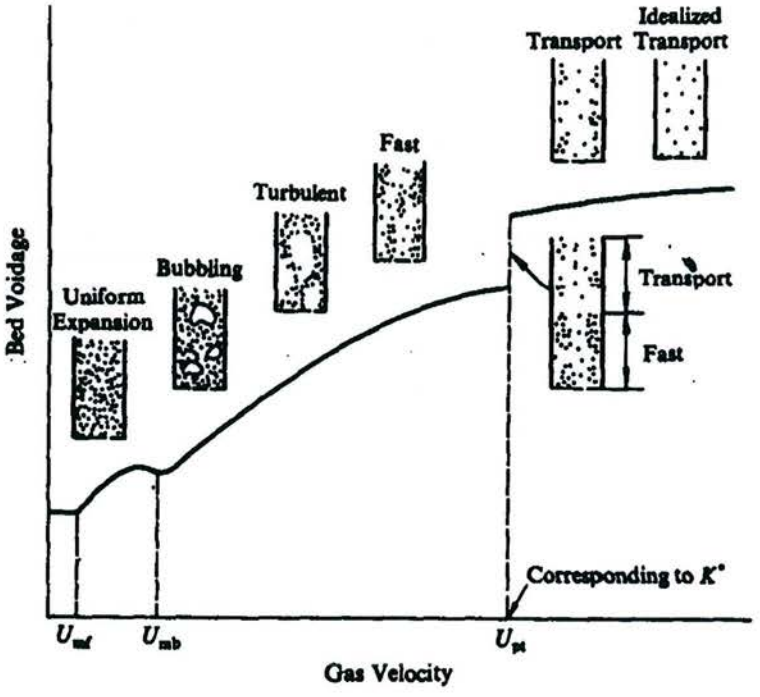

Fig. 5-1 Fluidization Regimes of Gas/solid System

For a given gas-solid system, with increasing gas velocity, the system will experience different operating conditions: fixed bed, particulate fluidized bed (Geldart A particles[30]), bubble fluidized bed, turbulent fluidized bed, circulating fluidized bed (fast fluidization) and pneumatic transport. In the fast fluidization regime, the superficial gas velocity is much higher than the terminal gas velocity of a single solid particle. The superficial gas velocity is normally in the range of 3-28 m/s, compared with less than 1m/s for conventional bubble fluidized bed. At this gas velocity, there will be significant solids carryover at the riser exit. Solids exiting the riser are separated from the gas stream and returned to the riser through a vertical standpipe. So CFB is a high intensity, bubble-less gas-solid reactor. The inherent features of CFB are:

- High gas velocity;
- High solids throughput;
- High heat and mass transfer rate between gas and particles;
- High heat transfer between bed and immersed surface;
- Separate control of gas and solids flow rate;

An important practical aspect of CFB from the point of view of mass transfer is that, since there is solids carryover, a continuous process of gas treatment is possible, while at the same time, the average residence time of the particle may be large, because there is internal re-circulation. CFB has been widely used in many industrial operations due to these inherent features, like Fluid Catalytic Cracking (FCC) for oil refinery, Circulating

Fluidized Bed Combustion (CFBC) for coal power generation, city waste incineration and material drying. Serggren et al. [31] reviewed potential applications of CFB for different chemical and physical operations. Kajiyama, et al. [13], also reported the test on CFB adsorption for bulk gas separation. Table 5-1 is the characteristics of typical CFB reactors.

Table 5-1 Characteristics of Typical CFB Reactors

Operating Conditions	FCC	CFBC
Particle Density (kg/m^3)	1100 ~ 1700	1800 ~ 2600
Particle Diameter (μm)	40 ~ 80	100 ~ 300
Superficial Gas Velocity (m/s)	6 ~ 28	5 ~ 9
Solid Circulating Rate (kg/m^2s)	400 ~ 1200	10 ~ 100
Height/Diameter Ratio	>20	< 5 ~ 10
Diameter of CFB Riser (m)	0.7 ~ 1.5	4 ~ 8
Solid Inventory	Higher	Lower

5.1.2. Characteristics of CFB Riser

Investigations of CFB hydrodynamics have demonstrated that the riser can be divided into several regions with respect to their solids volume concentrations.

The bottom zone, where the acceleration of return particle takes place, is characterized by a cross-sectional average voidage of typically 0.8 - 0.9. The dense bottom zone shows hydrodynamic behavior similar to turbulent or bubble fluidized bed, with fluidization gas passing through the bottom zone mostly in the form of voids. When the voids reach the surface of the bottom zone, they break and eject solids into the transition zone.

The transition zone is where the transition occurs from the dense bottom zone to the dilute zone with its low solids volume concentrations. In this region the frequency and size of clusters diminish with height. A large amount of solids is ejected by bursting voids from the bottom zone into the transition zone. Down falling clusters carry solids from the dilute zone back into the transition zone. Hence, the transition zone is a region of high intensity solids mixing. However, gas and solids mixing in the transition zone has not yet been investigated separately.

The dilute zone, which occupies most of the CFB riser height, is characterized by low solids volume fractions (bed voidage >0.9 for CFB combustor and < 0.9 for FCC riser) and the variation of value is much smaller than that in the transition zone. Two phases are co-existing in the dilute zone: the lean phase consists of upward flowing dilute suspension, whereas the dense phase is formed by particle clusters and shows solids concentrations at least an order of magnitude higher than the lean phase. The other character in the dilute zone is the core-annulus structure, that is, near the wall of the riser exists a dense layer of particles which may traveling upward or downwards, depending on the solids circulation rate and operation velocity. Considerable researches have been

carried out to describe the hydrodynamic behavior, as well as the gas and solids mixing for this region, as it dominates the overall behavior of the CFB riser.

The exit Zone is located at the top of the riser. The particle concentration in exit zone may be increased or not, depending on the geometry of the riser exit. Two major types of exit have been distinguished in the literature, i.e. an abrupt exit and a smooth exit. The latter is a smooth bend from the riser to the cyclone entrance, exhibiting negligible influence on the flow regime below. A more compact exit geometry is the abrupt exit, where the solids exit through a sharp 90 degree take-off just below the riser top, and this brings the increasingly solids concentration towards the top of the CFB riser and the intensified solids mixing there.

5.2. Local Hydrodynamics – the EMMS Model

5.2.1. Introduction

Two distinct fluidization phenomena are possible for a gas/solid system: particulate fluidization and aggregative fluidization, depending on the gas/solid properties and operating conditions. In particulate fluidization system, the solid particles are discretely distributed in the gas stream, there is no direct interaction between the solid particles. For such homogeneous gas/solid system, the traditional methodology of mass and momentum analysis could be used to describe the gas/solid flow in CFB riser. In aggregative system, the gas phase appears as gas bubbles in the emulsion phase for bubble fluidized bed or, the solid phase appears as clusters in the gas phase. In this heterogeneous gas/solid system, the dilute and dense phase co-exits. The hydrodynamic behavior of the system is complex and the traditional methodology of mass and momentum analyses are not sufficient to describe the gas/solid flow in the CFB riser.

Li [34],[35] proposed the Energy-Minimization Multi-Scale model (EMMS Model) to account for the intrinsic characteristics of particle-fluid two-phase flow in fast fluidization. In EMMS model, the particles and fluid are considered to interact with each other on three different scales: the Micro-scale for single particle, the Meso-scale for clusters and the Macro scale for the whole system. With the analysis of interaction of multi-scale system (the mass and momentum conservation and the interaction between the different scales) and the constraints of system stability (the energy consumption for transporting and suspending solid particles is extremum), the EMMS model is able to describe heterogeneous structure of gas/solid system in CFB riser.

5.2.2. The Three Scales and Interactions

The aggregative gas/solid system consists of a dense or concentrated phase and a dilute phase, no matter whether it is gas aggregation (bubbles) or solid aggregation (clusters). So in the gas/solid system, the interactions are on three different scales: micro scale

(single particle scale), meso scale (cluster scale) and macro scale (equipment scale). To describe this multi scale gas/solid system, eight variables are used, including voidage (the volumetric fraction of fluid) in dense and dilute phase, solid superficial velocity, gas superficial velocity, cluster diameter and volumetric fraction. It could be expressed as:

$$\boldsymbol{X}=\left(\varepsilon_d,\varepsilon_c,f,U_{gd},U_{gc},U_{pd},U_{pc},d_{cl}\right)$$

The subscript "*d*" denotes dilute phase, "*c*" denote dense or concentrated phase, "*g*" means gas and "*p*" means particle. Symbol "ε" is the voidage and "*U*" is superficial velocity□ "d_{cl}" and "*f*" denote cluster diameter and cluster phase volumetric fraction respectively. It is obvious that U_{gd}, U_{pd} and ε_d are associated with dilute phase, while U_{gc}, U_{pc}, ε_c, f and d_{cl} with the dense phase.

In our notation, the superficial velocities are defined with respect to the respective phases. U_g and U_p are the gas and solid velocities superficial to the whole bed, U_{gc}, U_{gd} and U_{pc}, U_{pd} are the gas and solid velocities superficial only to the cluster and dilute phases, not the whole bed. So the actual gas and solid velocities in the clusters are:

$$\frac{U_{gc}}{\varepsilon_c},\qquad \frac{U_{pc}}{1-\varepsilon_c};$$

And the real gas and solid velocities in the dilute phase are:

$$\frac{U_{gd}}{\varepsilon_d},\qquad \frac{U_{pd}}{1-\varepsilon_d};$$

Three superficial slip velocities have been defined. The superficial slip velocity between gas and solid particles in the cluster phase U_{sc} is defined as (U_{sc} is superficial to the cluster phase):

$$U_{sc}=U_{gc}-\frac{\varepsilon_c U_{pc}}{1-\varepsilon_c} \tag{5-1}$$

The superficial slip velocity between gas and solid particles in the dilute phases U_{sd} is defined as (U_{sd} is superficial to the dilute phase):

$$U_{sd}=U_{gd}-\frac{\varepsilon_d U_{pd}}{1-\varepsilon_d} \tag{5-2}$$

The superficial slip velocity between dilute gas and cluster particle U_{si} is defined as (U_{si} is superficial to the whole bed):

$$U_{si}=U_{gd}-\frac{\varepsilon_d U_{pc}}{1-\varepsilon_c}(1-f) \tag{5-3}$$

Fig. 5-2 shows the multi-scale structure and the defined parameters to describe this heterogeneous gas/solid structure in CFB.

8 Variables

Between Phases□ f, d_{cl}

Dilute Phase□ U_{gd}, U_{pd}, ε_d

Dense Phase□ U_{pc}, U_{gc}, ε_c

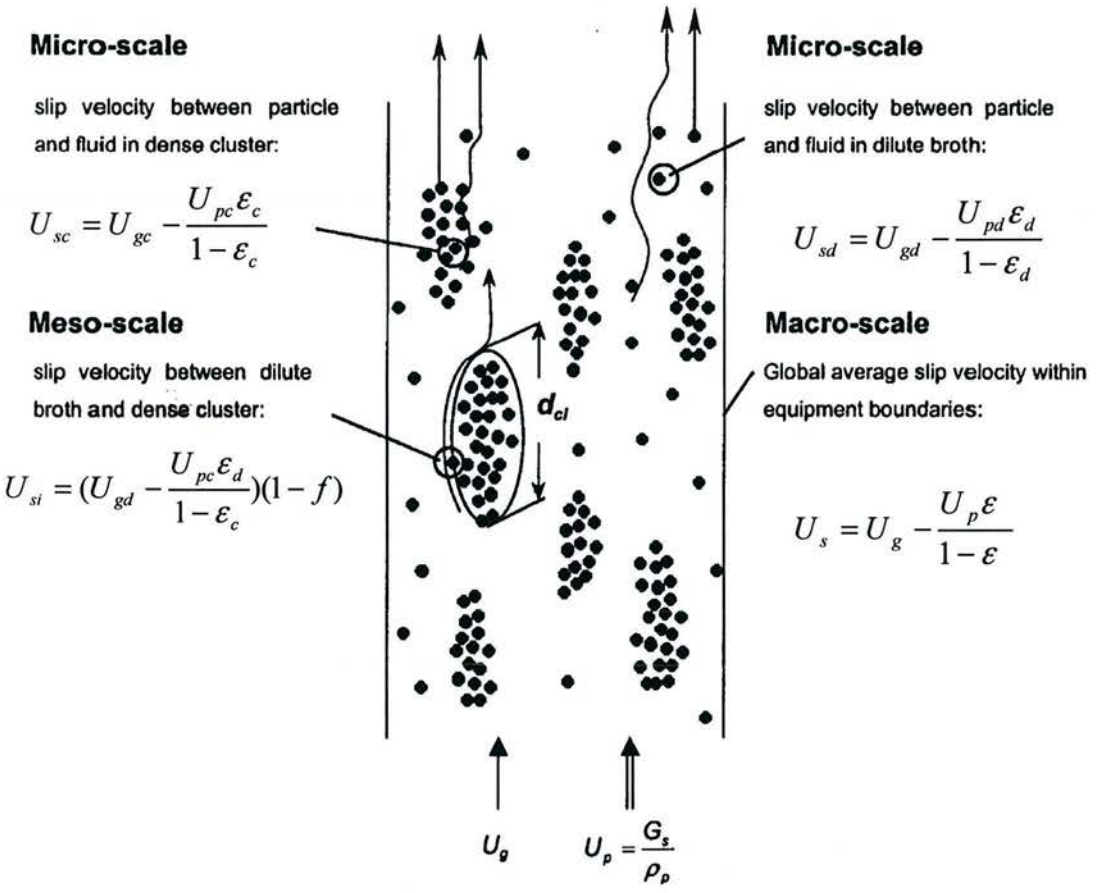

Fig.5-2 Three Scales of Interactions in Heterogeneous Gas/Solid Systems

Micro Scale

Micro scale interaction is the force that the fluid exerts on a single particle, it exists in both dense and dilute phase. In the dense phase, this micro scale force can be expressed as:

$$F_c = C_{Dc}\frac{\pi d_p^2}{4}\frac{\rho_g}{2}U_{sc}^2 \tag{5-4}$$

In the dilute phase, it is:

$$F_d = C_{D_d}\frac{\pi d_p^2}{4}\frac{\rho_g}{2}U_{sd}^2 \tag{5-5}$$

Where C_D are drag coefficient, the expression of which is summarized in table 5-2.

Table5-2 Summary of Notations and Expressions of Variables in EMMS Model

Parameters	Dense Phase	Dilute Phase	Inter Phase	
			Gas/Particle	Particle/Particle
Real Slip Velocity	$\frac{U_{gc}}{\varepsilon_c}-\frac{U_{pc}}{(1-\varepsilon_c)}$	$\frac{U_{gd}}{\varepsilon_d}-\frac{U_{pd}}{(1-\varepsilon_d)}$	$(\frac{U_{gd}}{\varepsilon_d}-\frac{U_{pc}}{1-\varepsilon_c})$	$(\frac{U_{pd}}{1-\varepsilon_d}-\frac{U_{pc}}{1-\varepsilon_c})$
Superficial Slip Velocity	$U_{sc}=U_{gc}-\frac{\varepsilon_c U_{pc}}{1-\varepsilon_c}$	$U_{sd}=U_{gd}-\frac{\varepsilon_d U_{pd}}{1-\varepsilon_d}$	$U_{si}=(U_{gd}-\frac{\varepsilon_d U_{pc}}{1-\varepsilon_c})(1-f)$	
Characteristic Reynods Number	$\mathrm{Re}_c=\frac{\rho_g d_p U_{sc}}{\mu_g}$	$\mathrm{Re}_d=\frac{\rho_g d_p U_{sd}}{\mu_g}$	$\mathrm{Re}_i=\frac{\rho_g d_{cl} U_{si}}{\mu_g}$	
Number of Particles or Clusters in Unit Volume	$m_c=(1-\varepsilon_c)\Big/\frac{\pi d_p^3}{6}$	$m_d=(1-\varepsilon_d)\Big/\frac{\pi d_p^3}{6}$	$m_i=f\Big/\frac{\pi d_{cl}^3}{6}$	
Drag Coefficient for Single Particle/Cluster[32]	$C_{DO_c}=\frac{24}{\mathrm{Re}_c}+\frac{3.6}{\mathrm{Re}_c^{0.313}}$	$C_{DOd}=\frac{24}{\mathrm{Re}_d}+\frac{3.6}{\mathrm{Re}_d^{0.313}}$	$C_{DO_i}=\frac{24}{\mathrm{Re}_i}+\frac{3.6}{\mathrm{Re}_i^{0.313}}$	
Drag Coefficient for Fluidized Particles[33,36]	$C_{D_c}=C_{DO_c}\varepsilon_c^{-4.7}$	$C_{D_d}=C_{DO_d}\varepsilon_d^{-4.7}$	$C_{D_i}=C_{DO_i}(1-f)^{-4.7}$	$C_p=0.7d_p^{-0.146}$
Pressure Drop Cross Unit Bed Height	$\Delta P_c=m_c F_c$	$\Delta P_d=m_d F_d$	$\Delta P_i=m_i F_i/(1-f)$	

Meso Scale: a modified model

Meso scale interaction is the force that the dilute phase exerts on the dense phase clusters. The original EMMS model considered this as the interaction between the fluid of dilute phase and the whole cluster:

$$F_i=C_{D_i}\frac{\pi d_{cl}^2}{4}\frac{\rho_g}{2}U_{si}^2 \tag{5-6}$$

The calculated results with the original EMMS model gave too high negative values for the cluster gas and particle velocities: the clusters are moving downward in the bed with an actual velocity ranging from 8m/s to 24m/s. This is certainly not in accordance with the experimental observations. So a modification to the original assumption of EMMS model has been made as follows:

We assume the force that the dilute phase exerts on the dense phase clusters has two components, one is the drag force by the gas acting on the clusters, and the other is the force by discrete particles in the dilute phase acting on the clusters as a particle-particle interactive force.

$$F_i=F_{ig}+F_{ip} \tag{5-7}$$

F_{ig} is actually the F_i in the original EMMS model:

$$F_{ig} = C_{D_i} \frac{\pi d_{cl}^2}{4} \frac{\rho_g}{2} U_{si}^2 \tag{5-8}$$

According to Arastoopour et. al. [36], the particle-particle interaction force that the finer particles exert on a coarse particle in a dilute gas-solid system can be estimated from the slip velocity between fine particles and the coarse particles:

$$F_{ip} = C_{Dp} \frac{\pi d_{cl}^2}{4} \frac{\rho_p (1-\varepsilon_d)}{2} \left[\frac{U_{pd}}{1-\varepsilon_d} - \frac{U_{pc}}{1-\varepsilon_c} \right]^2 \tag{5-9}$$

The dimensionless coefficient C_{Dp} is a function of the coarse particle diameter (d_{cl} is in meters):

$$C_{Dp} = \frac{4}{3} \times 0.7 d_{cl}^{-0.146} \tag{5-10}$$

We use (5-9) and (5-10) here to estimate the interactions between dilute particles and dense clusters, the latter representing the coarse particles of Arastoopour's relation.

Macro Scale

Macro scale interaction is the boundary conditions of the system, including the geometry of entrance and exit, equipment wall and the pressure of the system. This interaction is omitted in the local hydrodynamic analysis.

5.2.3. Force and Mass Balance

As shown in Fig.5-2□the gas/solid system can be divided into three sub-systems: the dilute phase, the dense phase and their interface. The number of clusters in a unit bed volume is m_i and the number of particles in the dense phase in this volume is $m_c f$. For the dense phase clusters, the effective weight of solid particles $f(1-\varepsilon_c)(\rho_p-\rho_g)$ is considered to be jointly balanced by the force of the gas acting on the particles in the dense phase $m_c F_c f$ and the force of the dilute phase acting on the dense phase clusters $m_i F_i$.

$$F_1(\boldsymbol{X}) = m_c F_c f + m_i F_i - f(1-\varepsilon_c)(\rho_p - \rho_g)g = 0 \tag{5-11}$$

The particles in the dilute phase are considered not affected by the gas or solid in the dense phase. So the effective weight of particle $(1-f)(1-\varepsilon_d)(\rho_p-\rho_g)$ is supported by the force that the gas in the dilute phase exerts on the particles $m_d F_d(1-f)$.

$$F_2(\boldsymbol{X}) = m_d F_d - (1-\varepsilon_d)(\rho_p - \rho_g)g = 0 \tag{5-12}$$

The condition for the co-existence of dense and dilute phase in the fluidized bed is that, the pressure drop produced by the fluid flow through the two phases is equal. The total pressure drop for the fluid in the dilute phase consists of two parts; one is the pressure drop of the gas flow through the particles in the dilute phase ΔP_d, the other is the pressure drop of the gas passing between the dense clusters ΔP_i. The pressure drop that the gas

flow through the dense phase is ΔP_c. Thus $\Delta P_d + \Delta P_i - \Delta P_c = 0$, or

$$F_3(\boldsymbol{X}) = m_d F_d + m_i F_i/(1-f) - m_c F_c = 0 \tag{5-13}$$

The mass balance for gas and particle gives:

$$F_4(\boldsymbol{X}) = U_g - U_{gd}(1-f) - U_{gc} f = 0 \tag{5-14}$$

$$F_5(\boldsymbol{X}) = U_p - U_{pd}(1-f) - U_{pc} f = 0 \tag{5-15}$$

The relation between average voidage ε and volume fraction of dense phase f is defined as:

$$F_6(\boldsymbol{X}) = \varepsilon - f\varepsilon_c - (1-f)\varepsilon_d = 0 \tag{5-16}$$

The EMMS model assumes the cluster diameter is inversely proportional to the energy required for suspending and transporting a unit mass of particles N_{st}, that is

$$d_{cl} = \frac{K}{energy\ \ input}$$

The input energy refers to that which is responsible for breaking up the dense phase into clusters. At minimum fluidization, $d_{cl} \rightarrow \infty$. Therefore, the energy input $(N_{st})_{mf}$ at minimum fluidization should be subtracted from the total input N_{st}, thus the energy input is N_{st}-$(N_{st})_{mf}$. As Matsen[37] mentioned for very fine particles, when the voidage reaches 0.9997, all particles are discretely distributed in the fluid, that is, clusters disappear or $d_{cl}=0$, the slip velocity between gas and solid u_s reaches the terminal velocity of single particle u_t. Therefore this value is used in the determination of K and the calculation for maximum voidage (ε_{max}=0.9997). The final relation is expressed in (5-17). One may refer to LI's article [34] for the detailed discussion.

$$F_7(\boldsymbol{X}) = d_{cl} - d_p \frac{[U_p/(1-\varepsilon_{\max}) - (U_{mf} + U_p\varepsilon_{mf}/(1-\varepsilon_{mf}))]g}{N_{st}\rho_p/(\rho_p-\rho_g) - (U_{mf} + U_p\varepsilon_{mf}/(1-\varepsilon_{mf}))g} = 0 \tag{5-17}$$

In 5-17, ε_{mf} and U_{mf} are the voidage and superficial velocity at minimum fluidization. N_{st} is the energy required for suspending and transporting unit mass of particles, the expression of which is established in the next section. ρ_p and ρ_g are the particle and gas densities and d_p is the particle diameter. The notations and expressions of other parameters in (5-11) ~ (5-17) are listed in table 5-2.

It is obvious that the seven equations (5-11) ~ (5-17) are not enough to determine the eight variables that describe the hydrodynamic state of a heterogeneous gas/solid system. An additional condition is needed to define this solution.

5.2.4. Energy Resolution and System Stability Conditions

In gas/solid system, the total energy consumption per unit mass of solids N_T (J/kg s) consists of two parts: one is used in suspending and transporting the particles N_{st}, the other is purely dissipated in particle collision, N_d.

$$N_T = N_{st} + N_d \tag{5-18}$$

For a given gas/solid system with gas and particle densities ρ_p and ρ_g, N_T is only associated with superficial gas velocity U_g, the relation is:

$$N_T = \frac{\rho_p - \rho_g}{\rho_p} g U_g \tag{5-19}$$

The suspending and transporting energy N_{st} (J/kg s) could be further split into that in dense phase $(N_{st})_c$, in dilute phase $(N_{st})_d$ and between the phases $(N_{st})_i$

$$N_{st} = (N_{st})_c + (N_{st})_d + (N_{st})_i \tag{5-20}$$

$(N_{st})_d$ and $(N_{st})_c$ are the products of force between gas and solid times the superficial gas velocity in dense and dilute phases, while $(N_{st})_i$ is the products of force between the dense and dilute phases times the superficial gas velocity in the dilute phase. That is:

$$N_{st} = \frac{1}{(1-\varepsilon)\rho_p}\left[m_c F_c U_{gc} f + m_d F_d U_{gd}(1-f) + m_i F_i U_{gd}(1-f)\right] \tag{5-21}$$

If the superficial gas velocity is less than the minimum fluidization velocity U_{mf}, that is the case of fixed bed, the gas/solid system is fully particle dependent, or *Particle-Dominating, PD*. The theory of single-phase flow can be used.

If the superficial gas velocity is higher than minimum fluidization velocity, with the increasing gas velocity, the dominating position of gas/particle will change. At very high gas velocities, the behavior of the system will be dominated by fluid, or *Fluid Dominating (FD),* like the case in pneumatic transport. Otherwise the system is in the state of *Particle Fluid Compromising (PFC),* like fast fluidization, turbulent fluidization and bubble fluidization.

In *PFC* regime, the fluid flows through the system with minimal resistance and the particles tend to keep the minimal potential energy and the result is N_{st}=*min.* In *FD* regime, the movement of solid particle is dominated by fluid. The collision between the solid particles is significantly reduced, so the dissipated energy N_d is correspondingly reduced. As the total energy consumption is unchanged, the suspending and transporting energy N_{st} reaches maximum value, N_{st}=*max.* This could be expressed as:

$$\textbf{Model PFC} \quad \left\{ \begin{array}{l} N_{st} = min \\ F_i(\boldsymbol{X}) = 0 (i = 1,2,\cdots,7) \\ U_{sc} \geq 0, U_{sd} \geq 0, U_{si} \geq 0 \end{array} \right\} \text{ Fluidization}$$

$$\textbf{Model FD} \quad \left\{ \begin{array}{l} N_{st} = max|_{f=0} \\ F_i(\boldsymbol{X}) = 0 (i = 1,2,\cdots,7) \\ U_{sc} \geq 0, U_{sd} \geq 0, U_{si} \geq 0 \end{array} \right\} \text{ Pneumatic Transport}$$

5.2.5. Analytical Solution of EMMS Model

EMMS model is a nonlinear optimization problem involving eight variables and eleven constraints consisting of both equalities and inequalities. It could be solved by using the so-called GRG-2 algorithm, developed by Lasdon et al [38] for coding the "Generalized Reduced Gradient" method. The use of algorithm is not convenient as the model is not always convergent. Cheng [39] proved that, the voidage of dense and dilute phase could be determined by the conditions for characteristic energy N_{st} extrema, that is:

(1) $\varepsilon_c = \varepsilon_{mf}$□ when $N_{st} = min$;

(2) $\varepsilon_d = \varepsilon_{uni}$□ *when* $N_{st} = max|_{f=0}$;

ε_{uni} is voidage of homogeneous suspension system under the same operation conditions and it is determined by the superficial gas and solid velocities U_g and U_p. In the homogeneous suspension system, the real slip velocity between gas and solid particle approchs the terminal velocity of single particle u_t. So

$$u_t = \frac{U_g}{\varepsilon_{uni}} - \frac{U_p}{1-\varepsilon_{uni}} \tag{5-22}$$

From (5-22) we get:

$$\varepsilon_{uni} = [(U_g + U_p + u_t) - \sqrt{(U_g + U_p + u_t)^2 - 4U_g u_t}\,]/2u_t \tag{5-23}$$

As CFB is normally operated under fast fluidization regime, not pneumatic transport, the first extrema, N_{st}=*min* is used.

Now, the nonlinear optimization problem has been simplified to a problem of solving a set of nonlinear algebraic equations. With the variable ε_c determined from the extrema conditions of characteristic energy, the other seven variables can be obtained with equations (5-11) to (5-17). The full analytical solutions are summarized in Table 5-3.

Table 5-3 The Analytical Solution of PFC Model

$$\varepsilon_c = \varepsilon_{mf} \tag{5-24}$$

$$\varepsilon = f\varepsilon_c + (1-f)\varepsilon_d \tag{5-25}$$

$$0.15\left(\frac{\rho_g d_p}{\mu_g}\right)^{0.687} U_{sc}^{1.687} + U_{sc} - \varepsilon_c^{4.7}\frac{1-\varepsilon}{1-\varepsilon_c}\frac{(\rho_p-\rho_g)gd_p^2}{18\mu_g} = 0 \tag{5-26}$$

$$0.15\left(\frac{\rho_g d_p}{\mu_g}\right)^{0.687} U_{sd}^{1.687} + U_{sd} - \varepsilon_d^{4.7}\frac{(\rho_p-\rho_g)gd_p^2}{18\mu_g} = 0 \tag{5-27}$$

$$U_{pd} = \frac{(1-\varepsilon_d)(1-\varepsilon_c)}{\varepsilon-\varepsilon_c}[U_g - \frac{\varepsilon_c}{1-\varepsilon_c}U_p - (1-f)U_{sd} - fU_{sc}] \tag{5-28}$$

$$U_{pc} = [U_p - (1-f)U_{pd}]/f \tag{5-29}$$

$$U_{gc} = U_{sc} + \frac{\varepsilon_c}{1-\varepsilon_c}U_{pc} \tag{5-30}$$

$$U_{gd} = U_{sd} + \frac{\varepsilon_d}{1-\varepsilon_d}U_{pd} \tag{5-31}$$

$$N_{st} = \frac{\rho_p-\rho_g}{\rho_p}g[U_g + (fU_{gc} - U_g)f^2\frac{\varepsilon_d-\varepsilon_c}{1-\varepsilon}] \tag{5-32}$$

$$d_{cl} = d_p\frac{[U_p/(1-\varepsilon_{\max}) - (U_{mf} + U_p\varepsilon_{mf}/(1-\varepsilon_{mf}))]g}{N_{st}\rho_p/(\rho_p-\rho_g) - (U_{mf} + U_p\varepsilon_{mf}/(1-\varepsilon_{mf}))g} \tag{5-33}$$

$$0.15\left(\frac{\rho_g d_{cl}}{\mu_g}\right)^{0.687} U_{si}^{1.687} + U_{si} + 0.7(1-f)^{4.7}(1-\varepsilon_d)\frac{\rho_p d_{cl}^{0.854}}{18\mu_g}$$
$$(\frac{U_{pd}}{1-\varepsilon_d} - \frac{U_{pc}}{1-\varepsilon_c})^2 - (1-f)^{4.7}(\varepsilon-\varepsilon_c)\frac{(\rho_p-\rho_g)gd_{cl}^2}{18\mu_g} = 0 \tag{5-34}$$

Fig. 5-3 is the calculation procedure of PFD model, based on a search on the value of variable f.

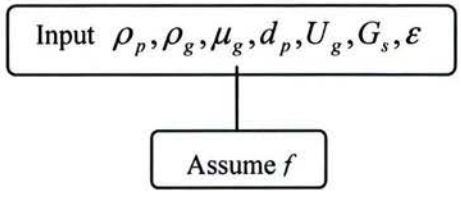

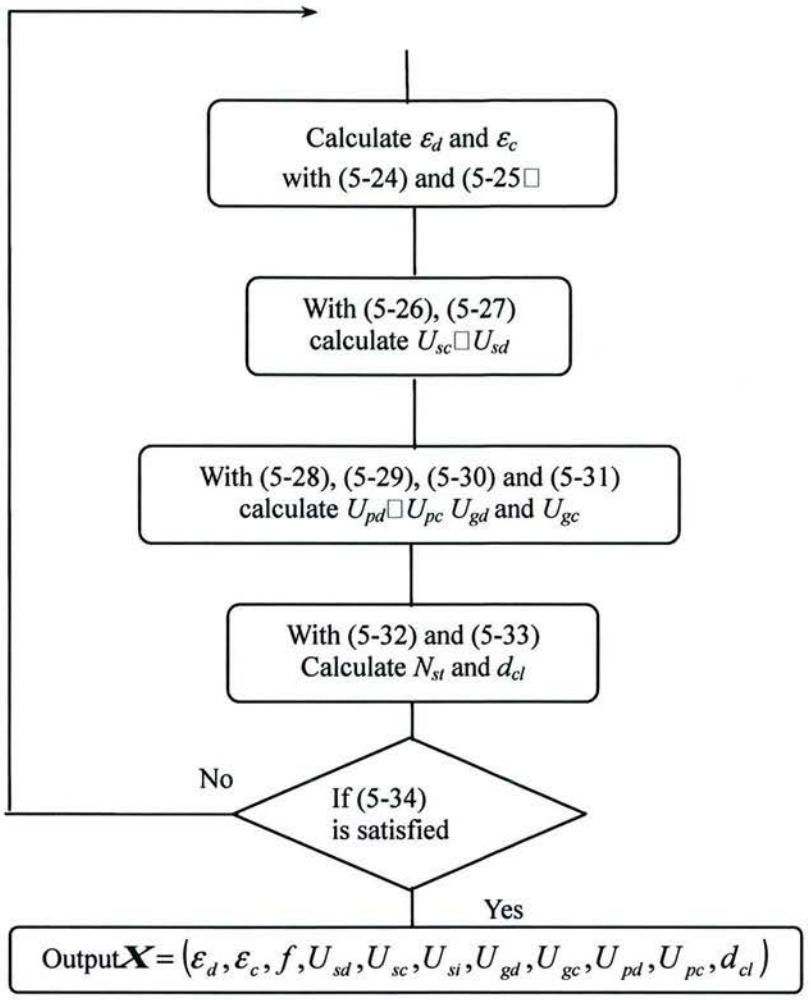

Fig. 5-3 Calculation Procedure of PFD Model.

The EMMS model is solved according to the experimental conditions for VOCs adsorption, that is the operation parameters (superficial gas velocity U_g, solid circulation rate G_s), gas and solids physical properties, and the cross-sectional averaged voidage corresponding to the values of experiments. Interesting results have been obtained, as it shows detailed information inside the fluidized bed.

Parameters concerning the dilute phase

Parameters concerning the dilute phase including the dilute phase voidage ε_d, gas and solid superficial velocities in the dilute phase (U_{gd}, U_{pd}) and the superficial slip velocity between them (U_{sd}).

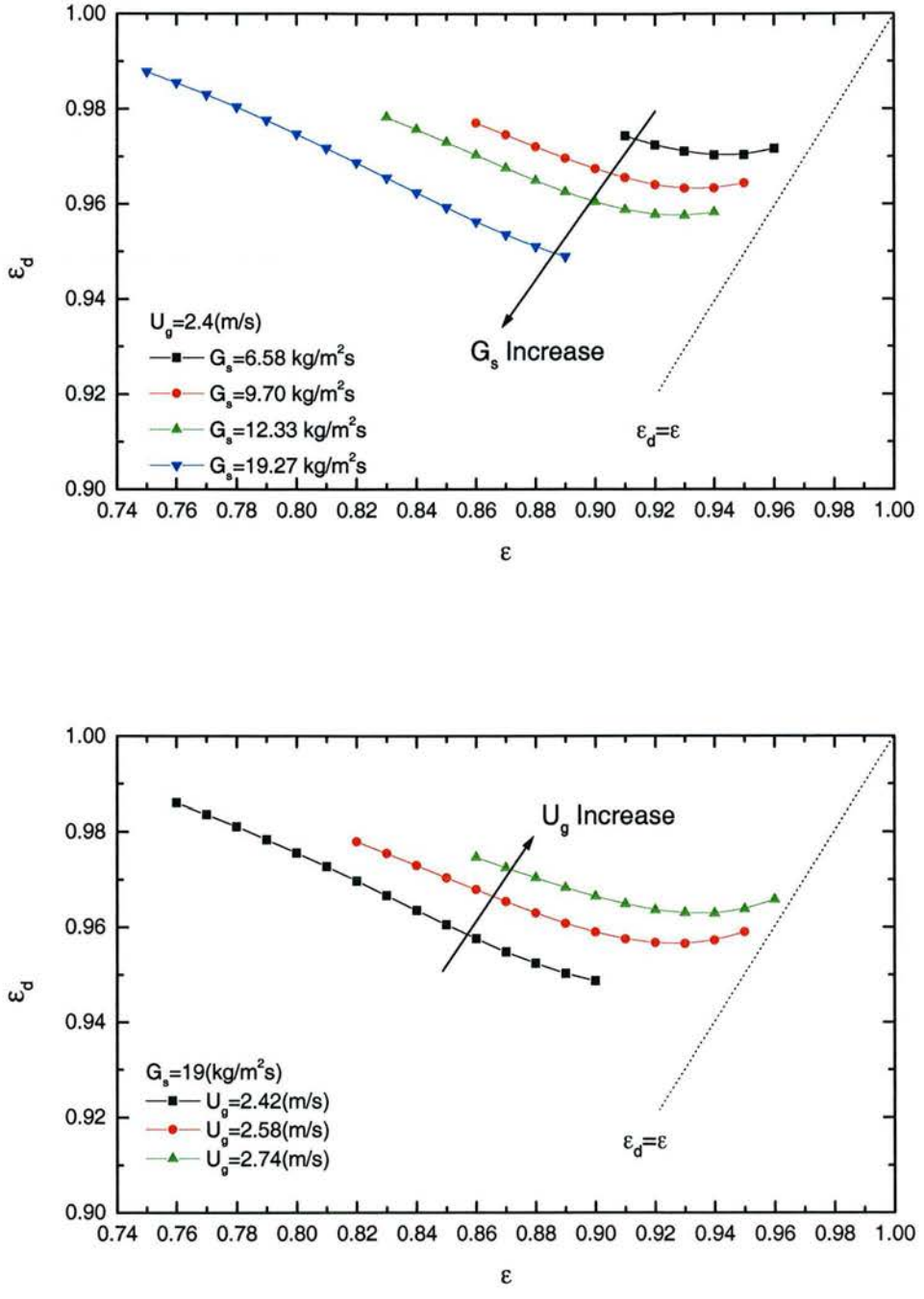

Fig. 5-4 Relation Between ε_d and ε at Different U_g and G_s

Fig. 5-4 shows the relation between ε_d and ε at different U_g and G_s. The value of ε_d is between 0.95 and 0.99 in all the experiments and it is decreasing with ε first, and then increases towards the averaged value for the whole bed ε ($\varepsilon_d = \varepsilon$ when $f=0$, or clusters disappear). The decrease of G_s and increase of U_g will increase the voidage in the dilute phase ε_d.

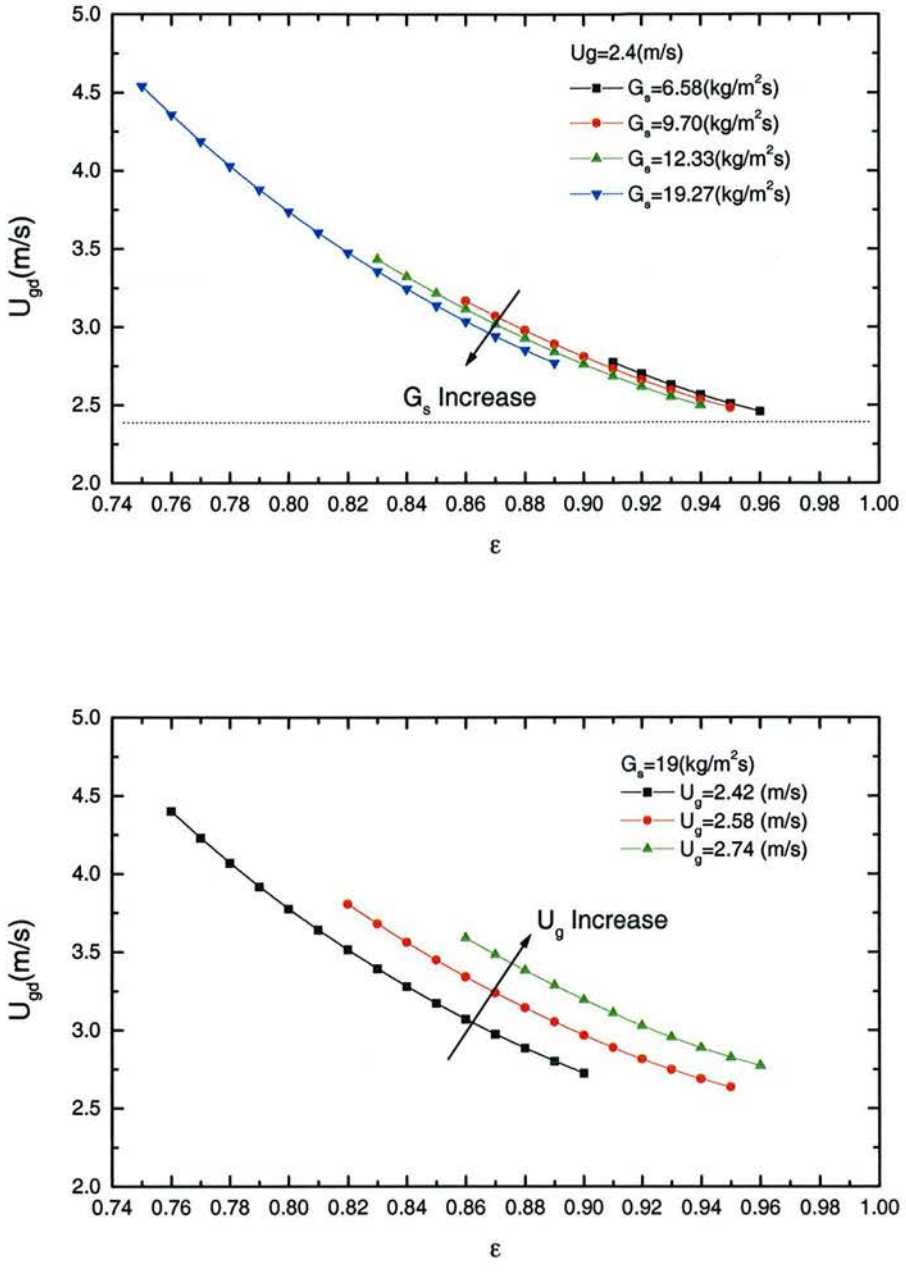

Fig. 5-5 Relation Between U_{gd} and ε at Different U_g and G_s

Fig. 5-5 shows the relation between U_{gd} and ε at different U_g and G_s. The value of U_{gd} is decreasing with the increasing ε. A small increase of U_g will significantly increase the value of U_{gd}, while the change of G_s has little influence on it. The limiting value of U_{gd} is U_g when $f=0$.

Fig. 5-6 shows the change of U_{pd} with ε at different U_g and G_s. The value of U_{pd} is increasing first, and then decreases with increasing ε. The increase of G_s and decrease of U_g will increase the value of superficial particle velocity in the dilute phase U_{pd}.

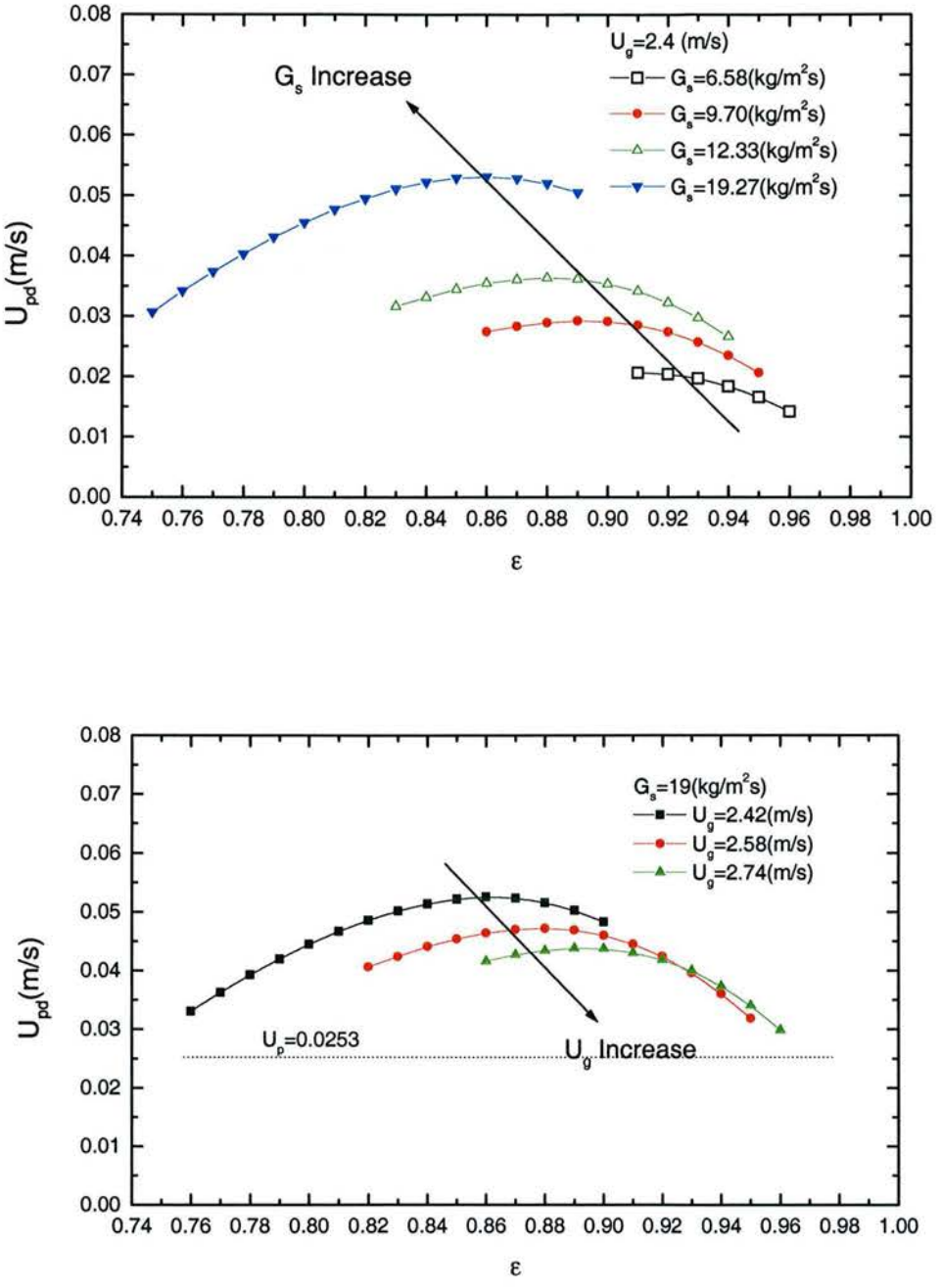

Fig. 5-6 Relation Between U_{pd} and ε at Different U_g and G_s

It is not intuitive that the superficial particle velocity in the dilute phase decreases with increasing superficial gas velocity. To understand this, one must consider that the increase of gas velocity increases the volume fraction and the solid velocity of the cluster phase, and therefore also its particle mass flow rate. At specified total solid circulating rate, the particle mass flow rate of the dilute pseudo-phase therefore decreases, entailing the decrease of both its volume fraction and its solid velocity.

The slip velocity between the gas and solid particle is of interest as it determines the rate of heat and mass transfer between the gas and solid particles in the CFB riser. Fig.5-7 shows that the superficial slip velocity in the dilute phase U_{sd} is decreasing first, then increasing with bed voidage ε. The increase of superficial gas velocity U_g and the decrease of solid circulation rate G_s will increase the slip velocity.

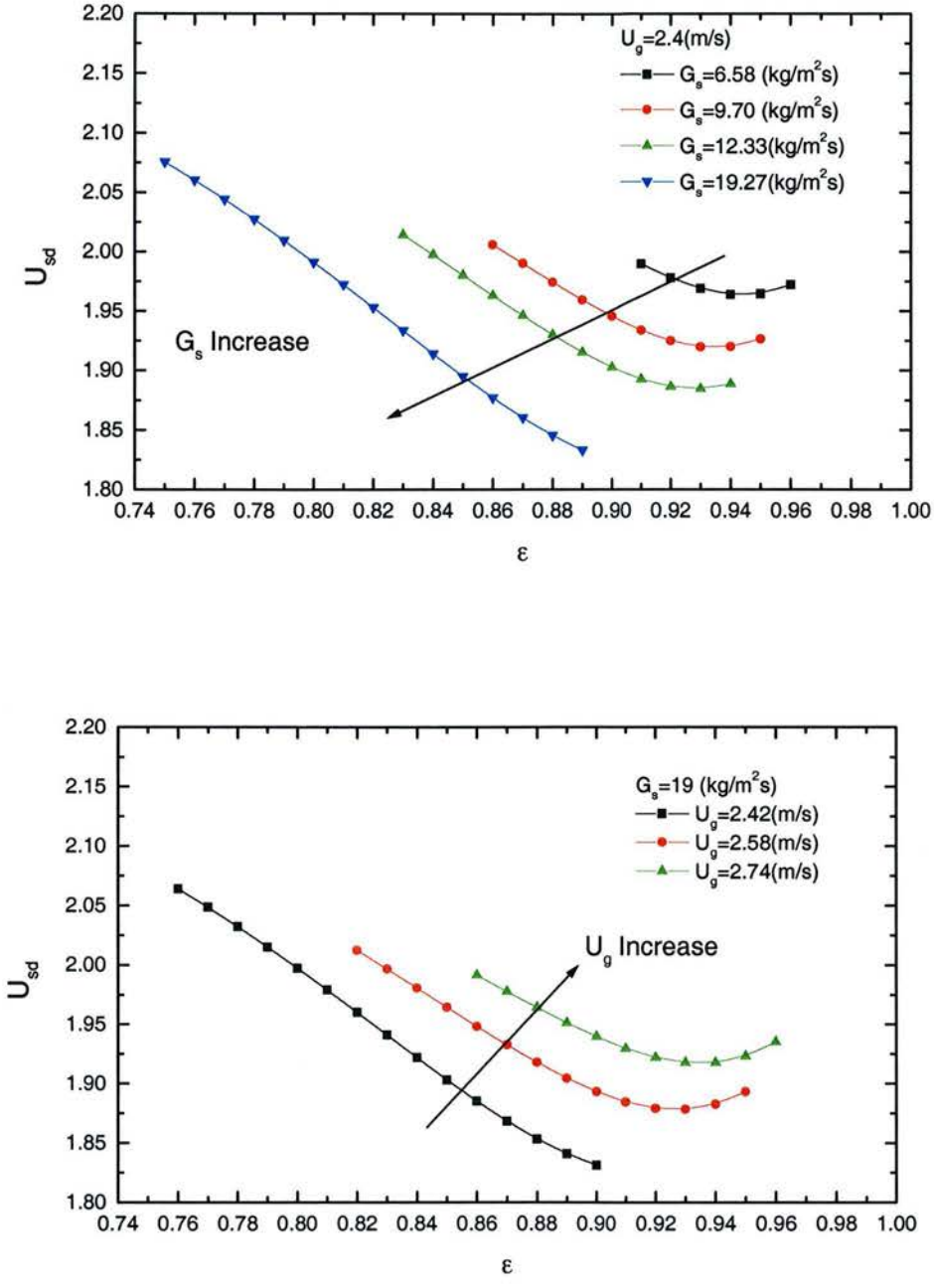

Fig. 5-7 Relation Between U_{sd} and ε at Different U_g and G_s

Fig. 5-8 shows the change of real slip velocity with ε. It can been seen that the real slip velocity is between 1.9m/s and 2.1m/s, less than the terminal velocity of the particle.

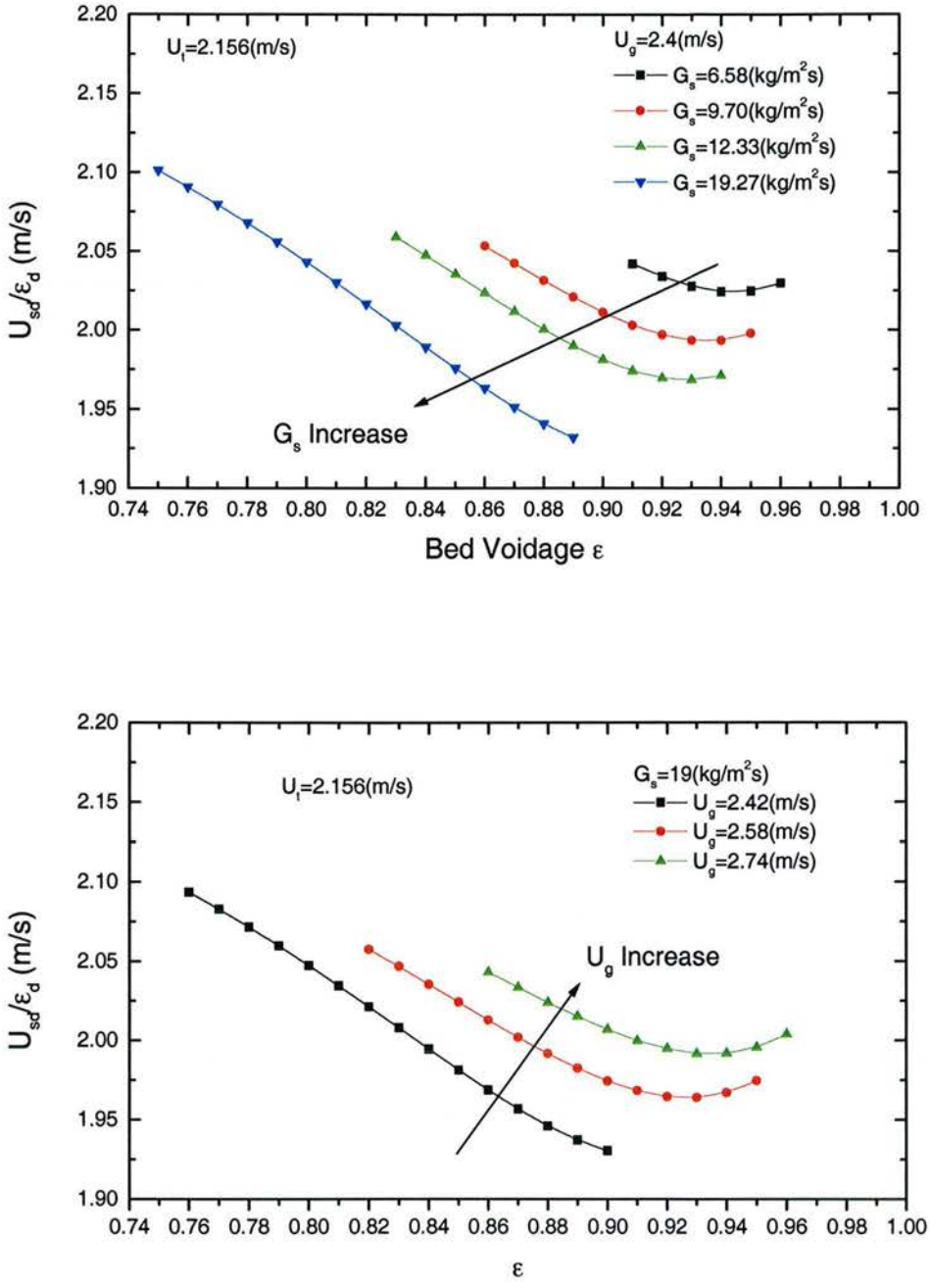

Fig. 5-8 Real Slip Velocity in Dilute Phase at Different U_g and G_s

Parameters concerning the dense phase

Parameters concerning the dense phase, or cluster phase include the cluster phase voidage ε_c, gas and solid superficial velocities in the clusters (U_{gc}, U_{pc}) and the superficial slip velocity between them (U_{sc}). The value of ε_c is determined from the stability condition and it is considered as the same as the bed voidage at minimum fluidization ε_{mf}. The rest of the parameters will be discussed.

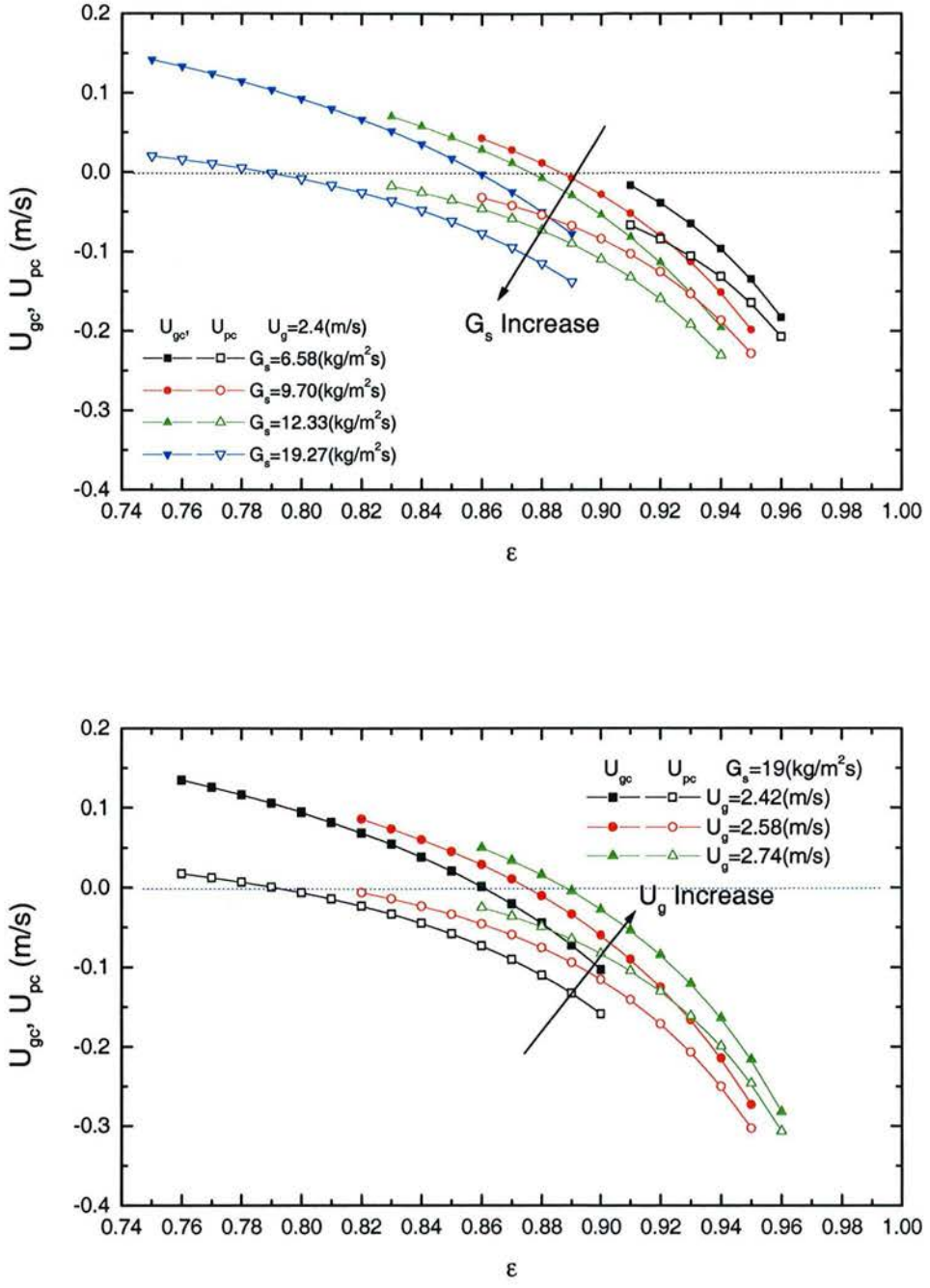

Fig. 5-9 Relation Between U_{gc}, U_{pc} and ε at Different U_g and G_s

Fig. 5-9 shows the relation between U_{gc}, U_{pc} and ε at different U_g and G_s. It can been seen that the influence of ε on U_{gc} and U_{pc} are the same: with the increasing ε, the superficial velocities in the cluster phase is decreasing. Both U_{gc} and U_{pc} could be positive or negative, depending on operation conditions. This means that the particle clusters and the gas in the clusters may be moving upward or downward in the bed. This phenomenon has been observed by many investigators in the CFB experiments.

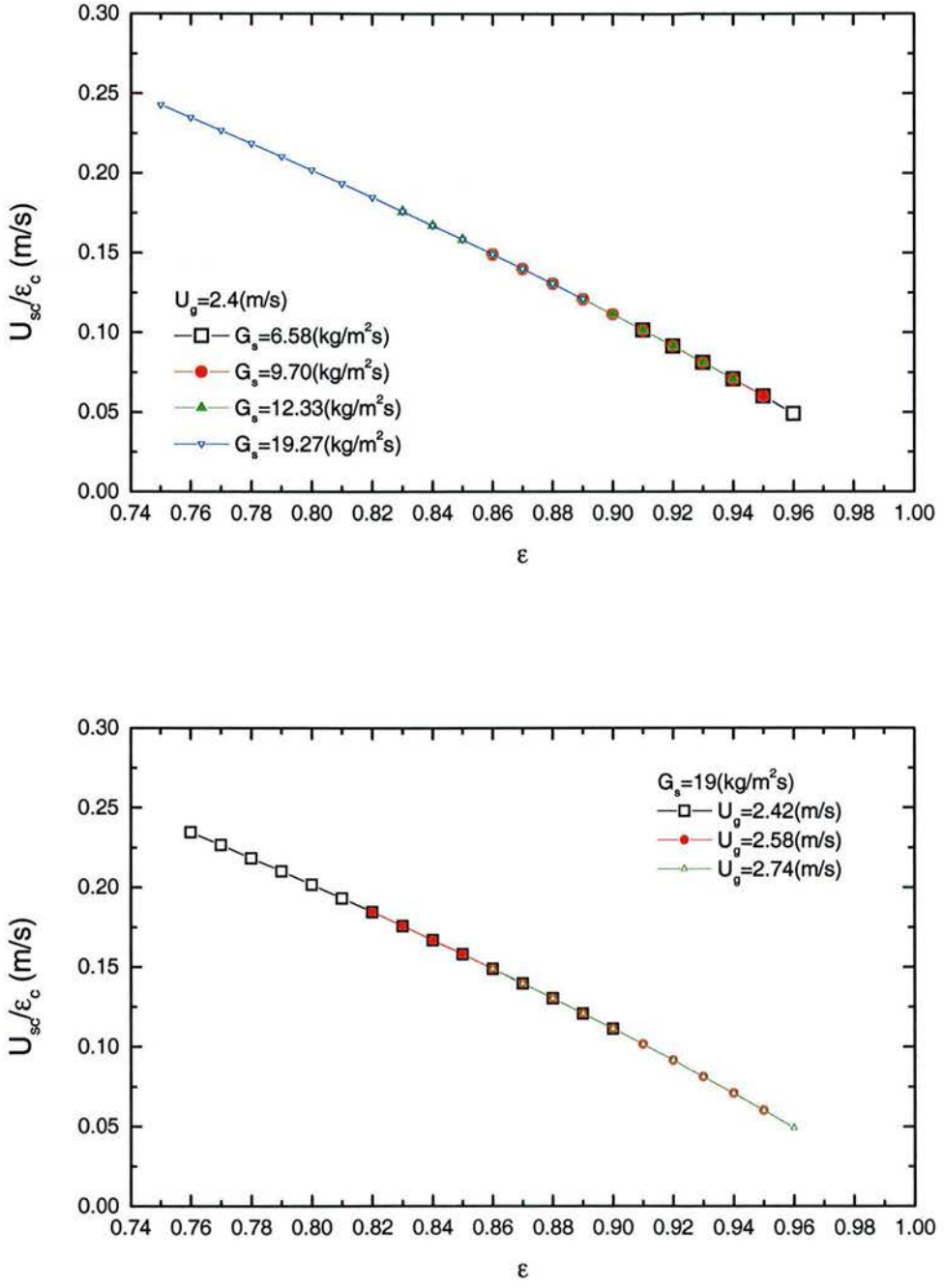

Fig. 5-10 Real Slip Velocity in the Cluster Phase at Different U_g and G_s

Fig. 5-10 shows that the real slip velocity between gas and solid in the clusters decreasing as ε is increased and that the dependence is close to linearity. The value of real slip velocity is around 0.05~0.25 m/s under experimental conditions, and this value is much small than the terminal velocity of the particle (2.156 m/s). The changes of U_g and G_s have no influence on the real slip velocity between the gas and solid particles inside the clusters.

Parameters concerning the relation between phases

Parameters concerning the relation between the phases include: volume fraction of cluster phase f, the cluster size d_{cl} and the slip velocity between the dilute and cluster phase U_{si}.

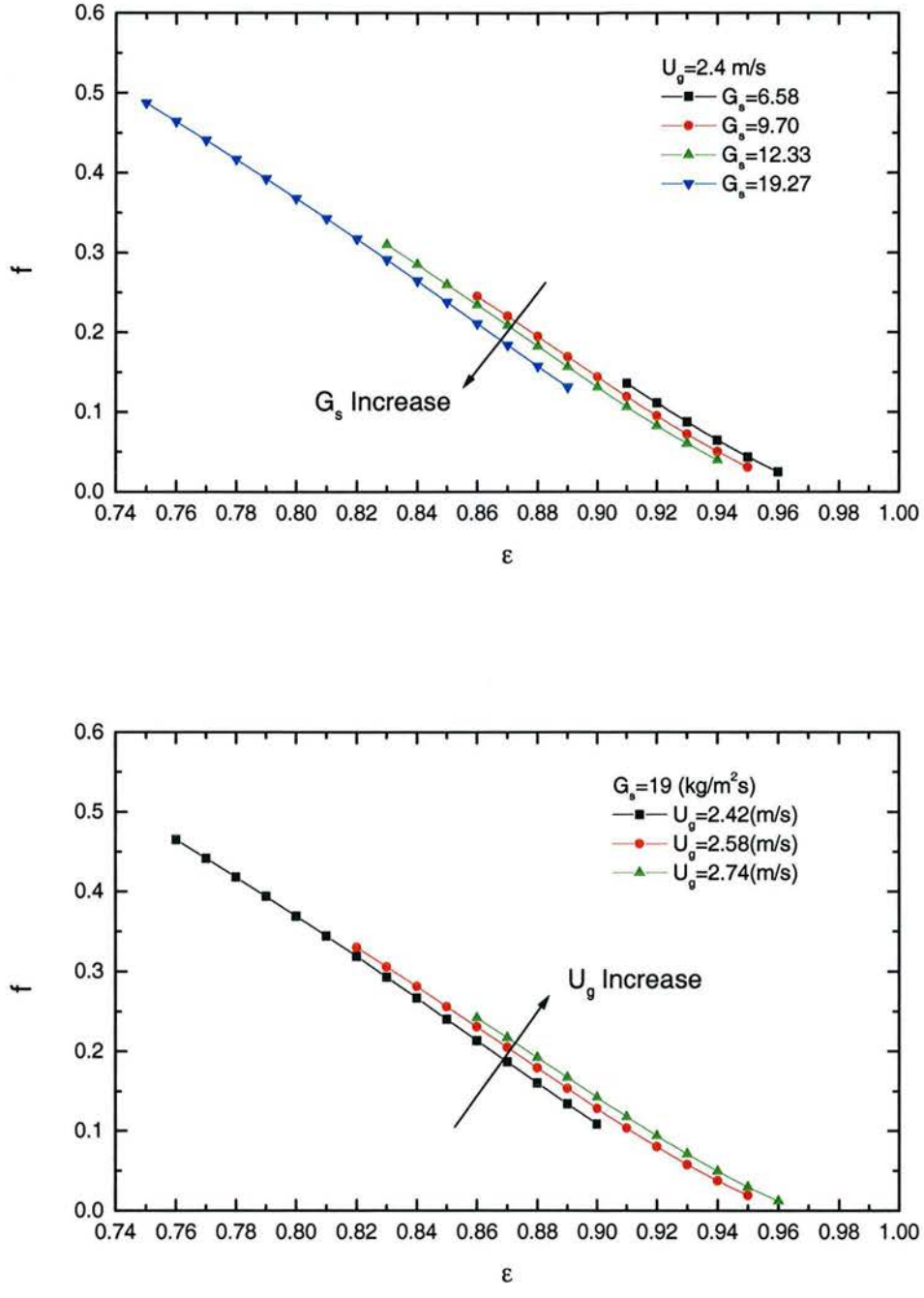

Fig. 5-11 Relation Between f and ε at Different U_g and G_s

Fig. 5-11 and Fig. 5-12 shows the relation between f, d_{cl} and ε at different U_g and G_s.

With the increase of ε, the volume fraction of clusters f shows a practically linear decrease. The influence of U_g and G_s are relatively small: the cluster phase volume fraction will decrease with increasing G_s or decreasing U_g for the same value of ε. Cluster size is mainly determined by the operation conditions U_g and G_s. The change of d_{cl} with ε is relatively small, especial when ε is large, or the bed is dilute. Higher G_s and lower U_g will result in bigger cluster size. These results are interesting as no one has mentioned this in the literature before, and these need to be verified with experiments in the future.

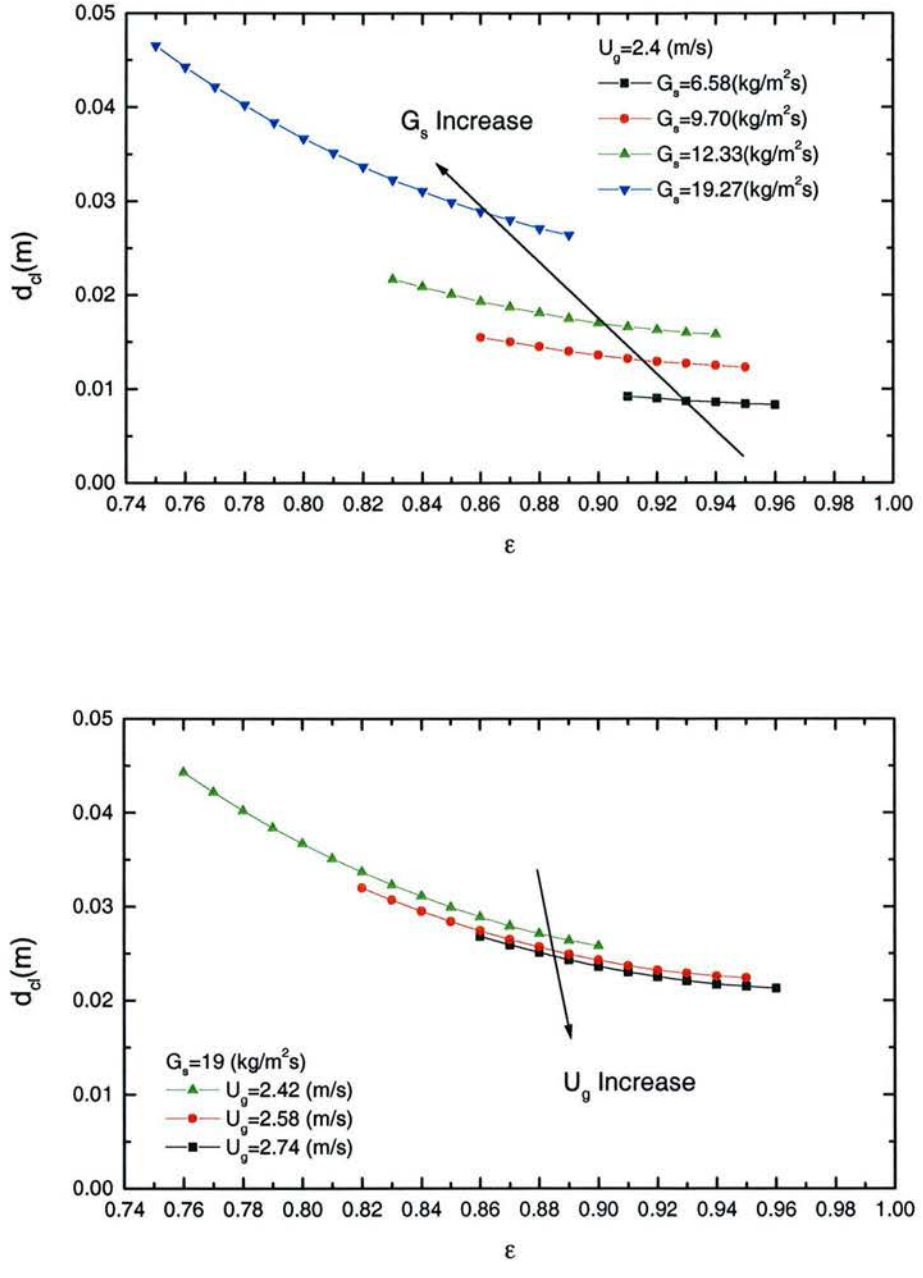

Fig. 5-12 Relation Between d_{cl} and ε at Different U_g and G_s

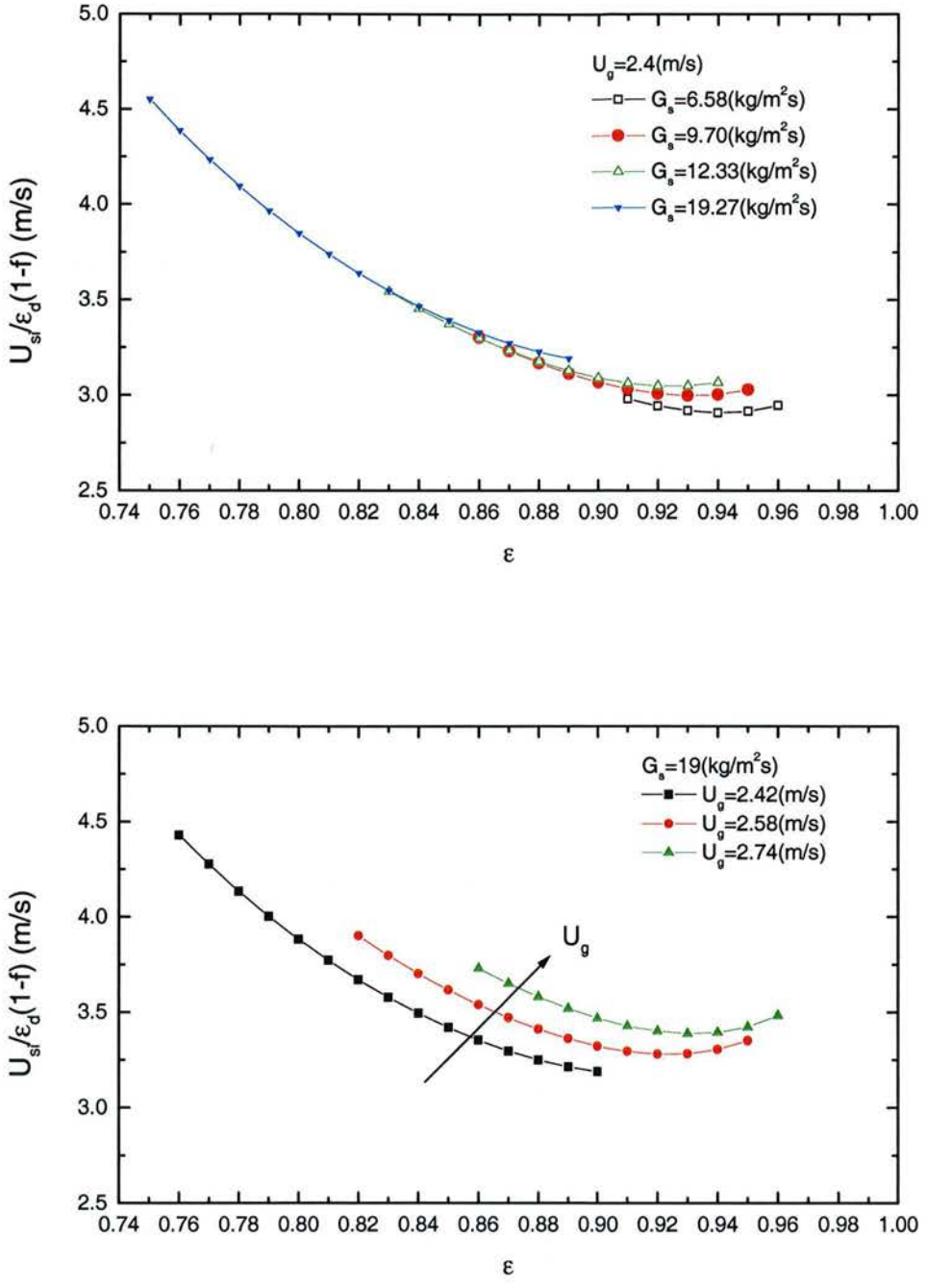

Fig. 5-13 Real Slip Velocity Between Dilute Gas and Clusters at Different U_g and G_s

Fig 5-13 shows that the real slip velocity between dilute gas and cluster solids is much higher (between 2.8 ~ 4.5 m/s), especial when the bed is dense. It decreases with increasing ε when the bed is dense, then increase after a minimum value reached. This slip velocity and the minimum value will increase with increasing superficial gas velocity and solid circulation rate, while the influence of solid circulation rate is relatively small.

5.3. Axial Hydrodynamics - Voidage Distribution

5.3.1. Two Types of Axial Voidage Distribution

In CFB riser, the axial voidage distribution is heterogeneous. Li and Kwauk's[40] experimental results show that the voidage is higher at top and lower at bottom. The superficial gas velocity and solid circulating rate will affect the voidage distribution along the bed height. The typical voidage axial distribution is *S* shaped, that is: a dense region with average voidage of ε_a at bottom and a dilute region with average voidage of ε^* at top are bridged by a transition region, where an inflexion point is located. But many other investigator's experimental results show that the voidage axial distribution is not always S shaped, but exponential [41], [42]. Jing [43] found the C type axial voidage distribution for the CFB riser with a strong restrictive exit, that is the voidage is higher in the middle and lower at the two ends of the bed. Fig. 5-14 is the experimental results of axial voidage distribution of Li and Kwauk [40]. One may recognize both S type and exponential type voidage distribution in it.

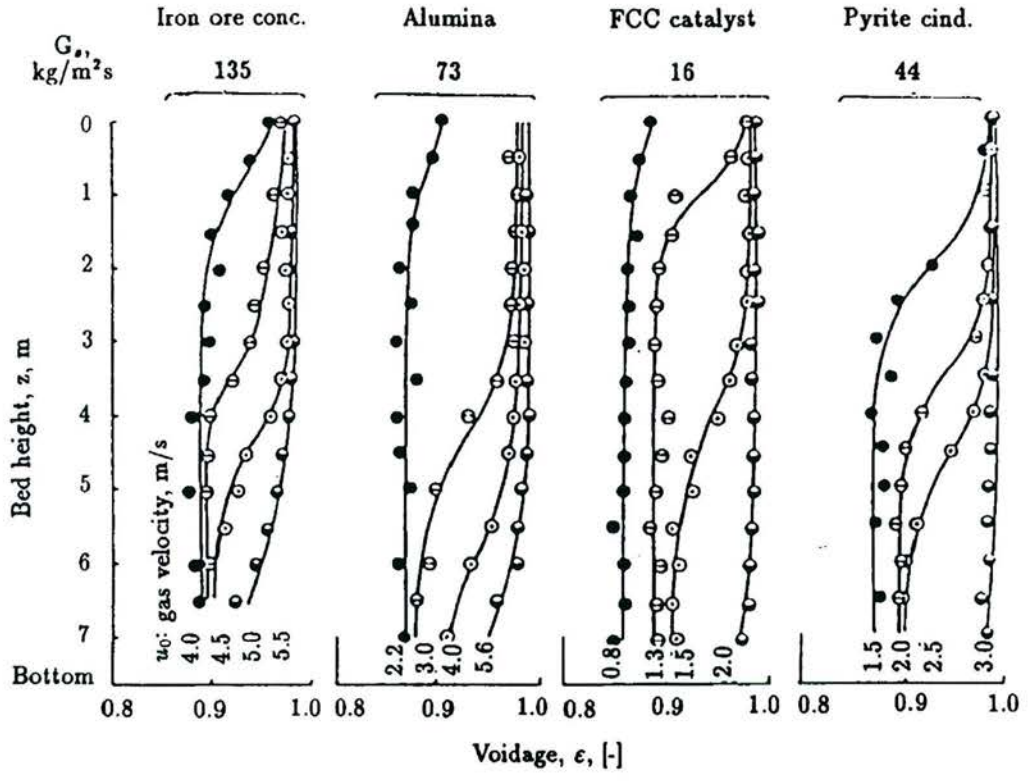

Fig. 5-14 Axial Voidage Distribution

Excluding the influence of exit geometry, the type of voidage axial distribution (S or exponential) in CFB riser is most probably determined by the solid circulation rate and the saturation carrying capacity of the system. The saturation carrying capacity G_s^* of gas is the maximum solid flow rate that the gas can transport at a given superficial gas

velocity. G_s^* is determined only by the superficial gas velocity and the gas/solid physical properties, and is independent of solid circulating rate, solid inventory in the system and the geometry of CFB riser.

In a CFB riser, when the solid circulating rate is increased by increasing the solid inventory or adjusting the solid circulating controlling valve while keeping the superficial gas velocities constant, the axial voidage distribution is exponential at first, with dilute bed at the top and dense bed at the bottom. The cross sectional voidage at the bottom ε_a will decrease with increasing solid circulating rate. If the solid circulating rate is higher than the saturation carrying capacity G_s^*, the axial voidage distribution will be S type and the increase of lower voidage bed height at the bottom will reduce the solid circulating rate and make it equal to G_s^*. At this condition, the voidage at bottom ε_a reaches it's saturation value. The temporary increase of solid circulating rate can only increase the height of dense bottom zone of the bed and the bottom voidage ε_a will not be affected.

Weinstein et al. [44] and Li[45] studied the influence of solid inventory on the axial voidage distribution. They found that when the axial voidage distribution is S shaped, the increase of solid inventory in the system will only make the inflexion point of the S shape move upward in the bed, while the voidage at bottom and exit of the bed remains unchanged. This has also been confirmed by many other investigators (Gao[46]□Li and Kwauk[40]□Yang and Sun[47]□Bai et al.[42]). Li [34] pointed out that the S type voidage distribution appears only when the solid circulating rate equal the saturation carrying capacity G_s^*.

The saturation carrying capacity G_s^* can be estimated with the correlation proposed by Bai and Kato [48]:

$$\frac{G_s^* d_p}{\mu} = 0.125 F_r^{1.85} A_r^{0.63} \left(\frac{\rho_p - \rho_g}{\rho_g}\right)^{-0.44} \tag{5-35}$$

The dimensionless parameters in the above equation are the Froude Number F_r and Archimedes Number A_r defined as:

$$F_r = \frac{U_g}{\sqrt{g d_p}} \tag{5-36}$$

$$A_r = \frac{d_p^3 \rho_g (\rho_p - \rho_g) g}{\mu^2} \tag{5-37}$$

The superficial gas velocity in our experiments is between 2.23 m/s ~ 2.74 m/s, the corresponding saturation carrying capacity for Ambersorb 600/air system calculated with (5-35) is between 25.7 kg/m^{2}s ~ 37.7 kg/m^{2}s.

5.3.2. Estimation of Bed Voidage at Bottom

Two different conditions should be considered for estimating the voidage at the bottom of CFB riser ε_a. When the solid circulating rate is less than G_s^*, or the axial voidage distribution is exponential, the voidage at bottom ε_a will decrease with the increasing solid circulating rate G_s. When the solid circulating rate is equal to G_s^*, or the axial voidage distribution is S shaped, the voidage at bottom ε_a is only determined by the gas velocity and gas/solid physical properties. Bai and Kato [48] reviewed the published experimental results and proposed the following correlation for estimating ε_a.

$$\frac{1-\varepsilon_a}{1-\varepsilon^*}=1+6.14\times10^{-3}\left(\frac{U_g}{U_p}\right)^{-0.23}\left(\frac{\rho_p-\rho_g}{\rho_g}\right)^{1.21}\left(\frac{U_g}{\sqrt{gd_b}}\right)^{-0.383} \qquad G_s<G_s^* \qquad (5\text{-}38)$$

$$\frac{1-\varepsilon_a}{1-\varepsilon^*}=1+0.103\left(\frac{U_g}{U_p}\right)^{1.13}\left(\frac{\rho_p-\rho_g}{\rho_g}\right)^{-0.013} \qquad G_s=G_s^* \qquad (5\text{-}39)$$

In the above equations, U_p is the superficial solid velocity $U_p=G_s/\rho_p$. d_b is the diameter of CFB riser. ε^* is the voidage when the slip velocity between gas and solid particle equal the terminal velocity of the solid particle u_t and it is defined as,

$$\varepsilon^*=[U_g+U_p+u_t-\sqrt{(U_g+U_p+u_t)^2-4U_gu_t}\,]/(2u_t) \qquad (5\text{-}40)$$

The terminal velocity of the particle is the maximum velocity that a single particle eventually reaches when falling down freely in a still unlimited fluid. The value of u_t can be obtained from a force balance between the gravity of a particle and the drag force exerted by the fluid, that is,

$$u_t=\left[\frac{4}{3}\frac{gd_p(\rho_p-\rho_g)}{\rho_gC_D}\right]^{\frac{1}{2}} \qquad (5\text{-}41)$$

The drag coefficient C_D for a single particle is calculated with Flemmer and Banks's correlations [49]:

$$\begin{aligned} C_D&=\frac{24}{R_e}+\frac{3.6}{R_e^{0.313}} && R_e\le 2000\\ C_D&=0.44 && R_e>2000 \end{aligned} \qquad (5\text{-}42)$$

The Reynolds Number in the above equations is defined as:

$$R_e=\frac{d_pu_t\rho_g}{\mu_g} \qquad (5\text{-}43)$$

5.3.3. Estimation of Axial Voidage Distribution

When the solid circulating rate is less than G_s^*, or the axial voidage distribution is exponential, Kunii and Levenspiel's entrainment model [27] is used to describe the axial voidage distribution in CFB riser:

$$\frac{\varepsilon^* - \varepsilon}{\varepsilon^* - \varepsilon_a} = e^{-\alpha z} \tag{5-44}$$

The decay constant in the above equation is estimated with the relation proposed by Adanze et al [50] for Geldart B particles.

$$a = \frac{0.88 - 420 d_p}{(U_g - u_t)^2 d_b^{0.6}} \tag{5-45}$$

When the solid circulating rate is equal to G_s^*, or the axial voidage distribution is S shaped, Li and Kwauk's diffusion model [40] is used for estimating the axial voidage in CFB Riser:

$$\frac{\varepsilon^* - \varepsilon}{\varepsilon - \varepsilon_a} = \exp[-\frac{1}{Z_0}(Z - Z_i)] \tag{5-46}$$

Z_0 is the characteristic length, which governs how quickly the top and bottom regions merge into each other, and is related to operation conditions and physical properties of the gas and solids.

$$Z_0 = 500 \exp[-69(\varepsilon^* - \varepsilon_a)] \tag{5-47}$$

The inflection point Z_i varies with solids inventory in the CFB system G. From the mass balance and pressure balance for the solid circulating loop, the averaged bed voidage in the CFB riser could be estimated as (when the solid particles are also fluidized in the CFB downer):

$$\bar{\varepsilon} = 1 - \frac{Gg + F_{downer} \sum \Delta p_i}{\rho_p g (F + F_{downer}) H} \tag{5-48}$$

Δp_i are the pressure drops across the gas-solid separators, the feed back valve and other parts of the solid circulating system. F and F_{downer} are the cross sectional area of CFB riser and downer respectively. This averaged voidage for CFB riser should be equal to that obtained from integrating (5-46) along the bed height:

$$\frac{\bar{\varepsilon} - \varepsilon_a}{\varepsilon^* - \varepsilon_a} = \frac{Z_0}{H} \ln\{\frac{1 + \exp(Z_i / Z_0)}{1 + \exp[(Z_i - H)/Z_0]}\} \tag{5-49}$$

Z_i is then obtained from (5-48) and (5-49).

5.3.4. One Dimensional Hydrodynamics in CFB Riser

One-dimensional hydrodynamics of gas and solid in CFB riser could be simulated by combining the local EMMS model (5-24) ~ (5-34) and the correlations for axial voidage distribution (5-44) ~ (5-47).

As mentioned before, the feedback of solid particles is by gravity and the adjusting of solid circulating rate is limited for this CFB test system. The saturation carrying capacity calculated with (5-35) is between 26 ~ 38 kg/m^{2}s, while the solid circulating rate is between 7 ~ 20 kg/m^{2}s in the experiments. So the axial voidage distribution is exponential in all the experiments and Kunii and Levenspiel's equation (5-44) is used to estimate the voidage in CFB riser.

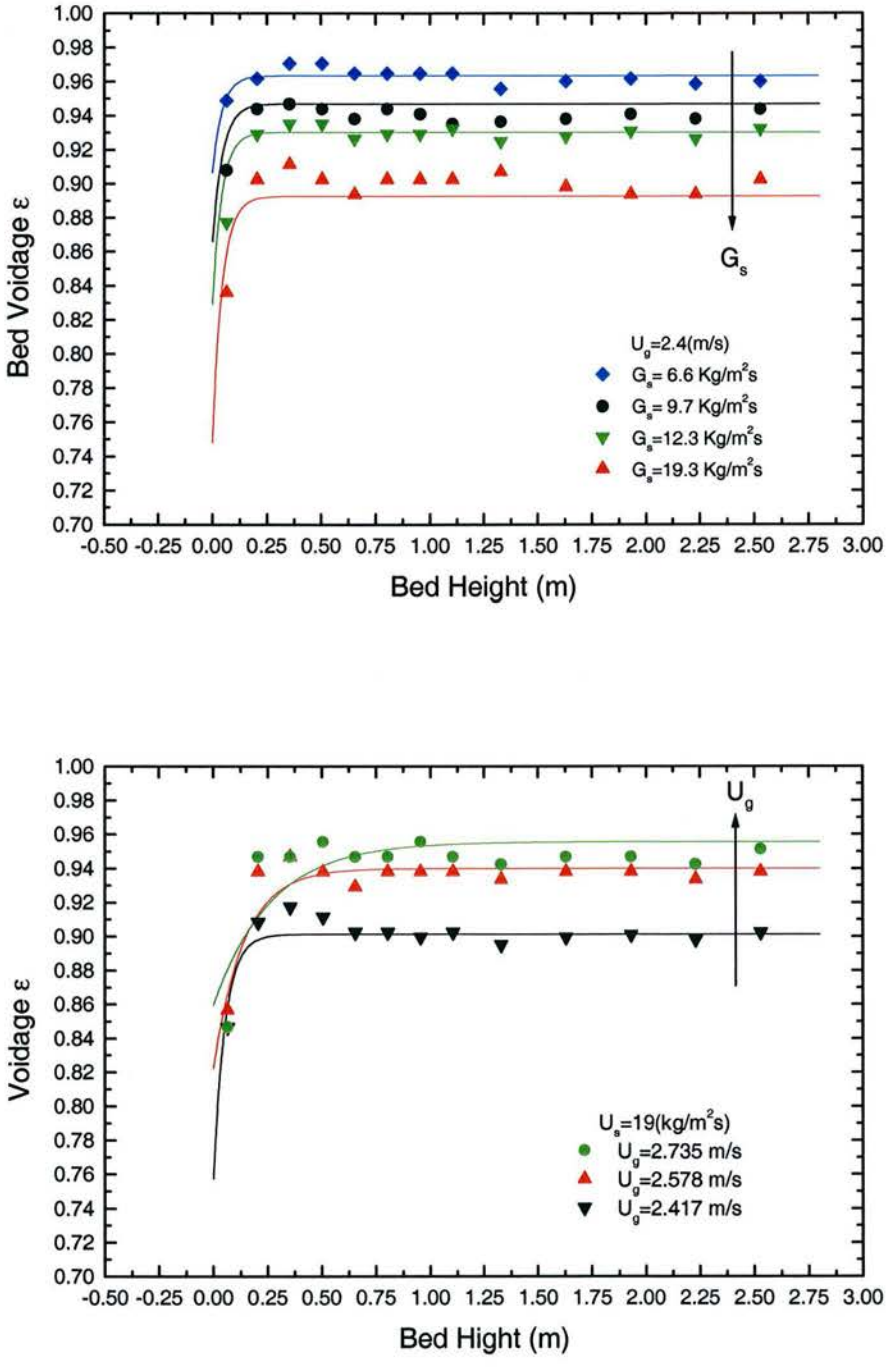

Fig. 5-15 Axial Voidage Distribution for Different G_s and U_g

Fig. 5-15 shows the estimated and experimental results of axial voidage distributions at different solid circulation rates and superficial gas velocities. It shows that the decay constant estimated with (5-45) are smaller for the higher superficial gas velocity conditions leading to large deviations between experimental and predicted values for bed height less than 0.5 m. Considering the fact that these results are obtained from the literature correlation and no fitting parameter is used, the agreement between experimental and the predicted values are reasonable.

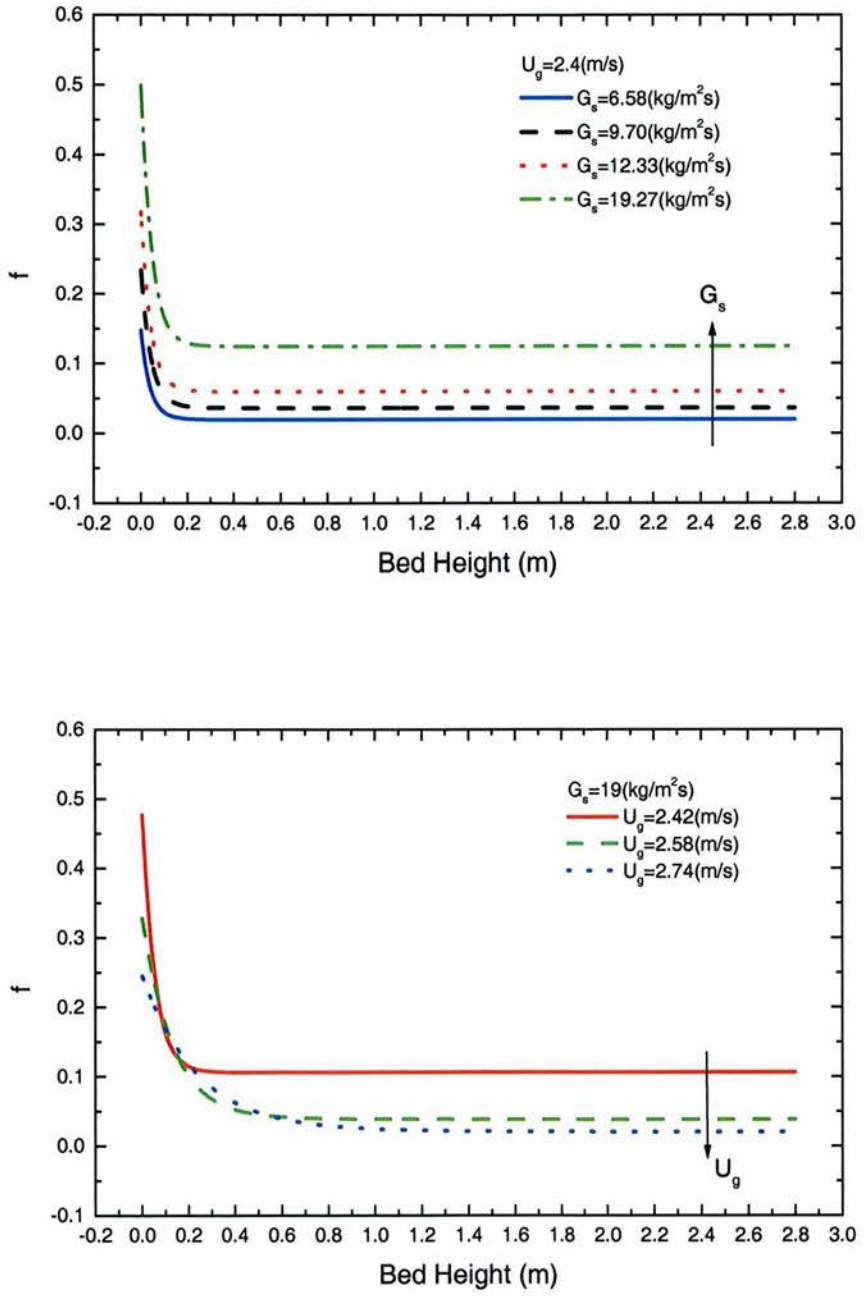

Fig. 5-16 f Distribution Along CFB Riser at Different U_g and G_s

Fig. 5-16 shows the change of cluster phase volume fraction f along the CFB riser. It is clear that f is almost a constant for most part of the riser and the value is small, except at the very bottom of the bed, where f decreases rapidly with the change of bed height.

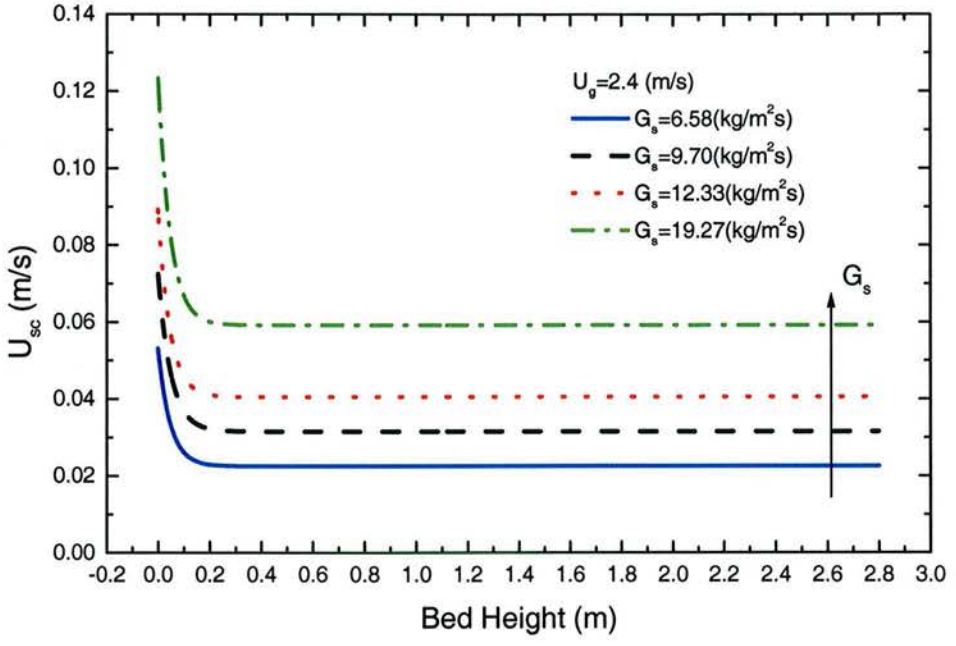

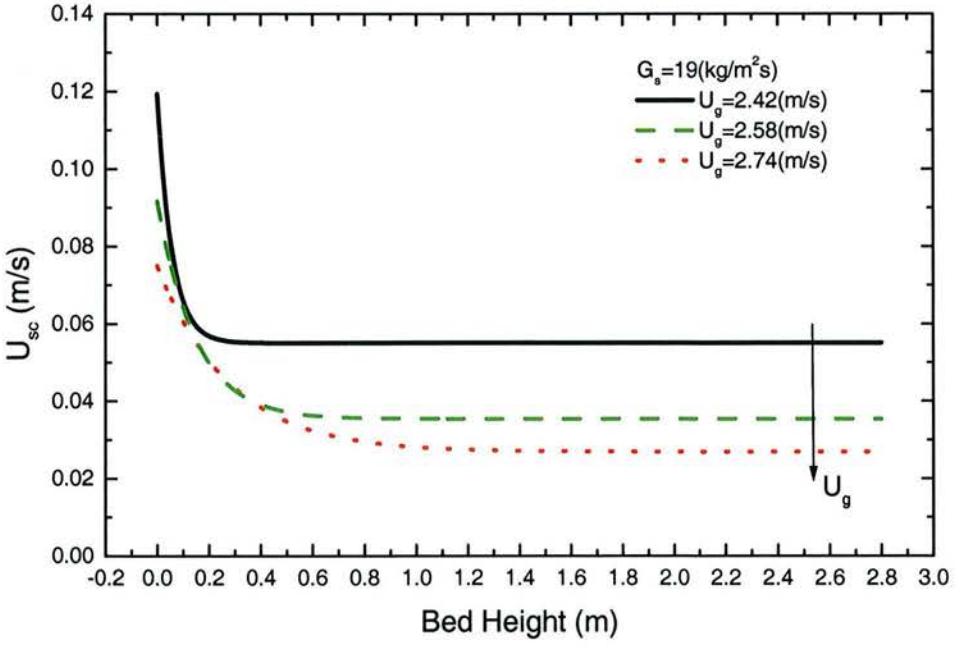

Fig. 5-17 U_{sc} Distribution Along CFB Riser at Different U_g and G_s

Fig. 5-17 and Fig. 5-18 are the superficial slip velocity between gas and particle within the cluster and dilute phases respectively. The calculated results show that, the superficial slip velocity increases in the dilute phase, but decreases in the cluster phase when the superficial gas velocity is increased, or solid circulation rate is decreased. All the parameters are almost constant for most part of the CFB riser, except at the bottom of the bed. The slip velocity in the dilute phase is much higher (1.8 ~ 2m/s), than that in the cluster phase (0.02 ~ 0.06m/s), implying a better gas and solid contacting in the dilute phase.

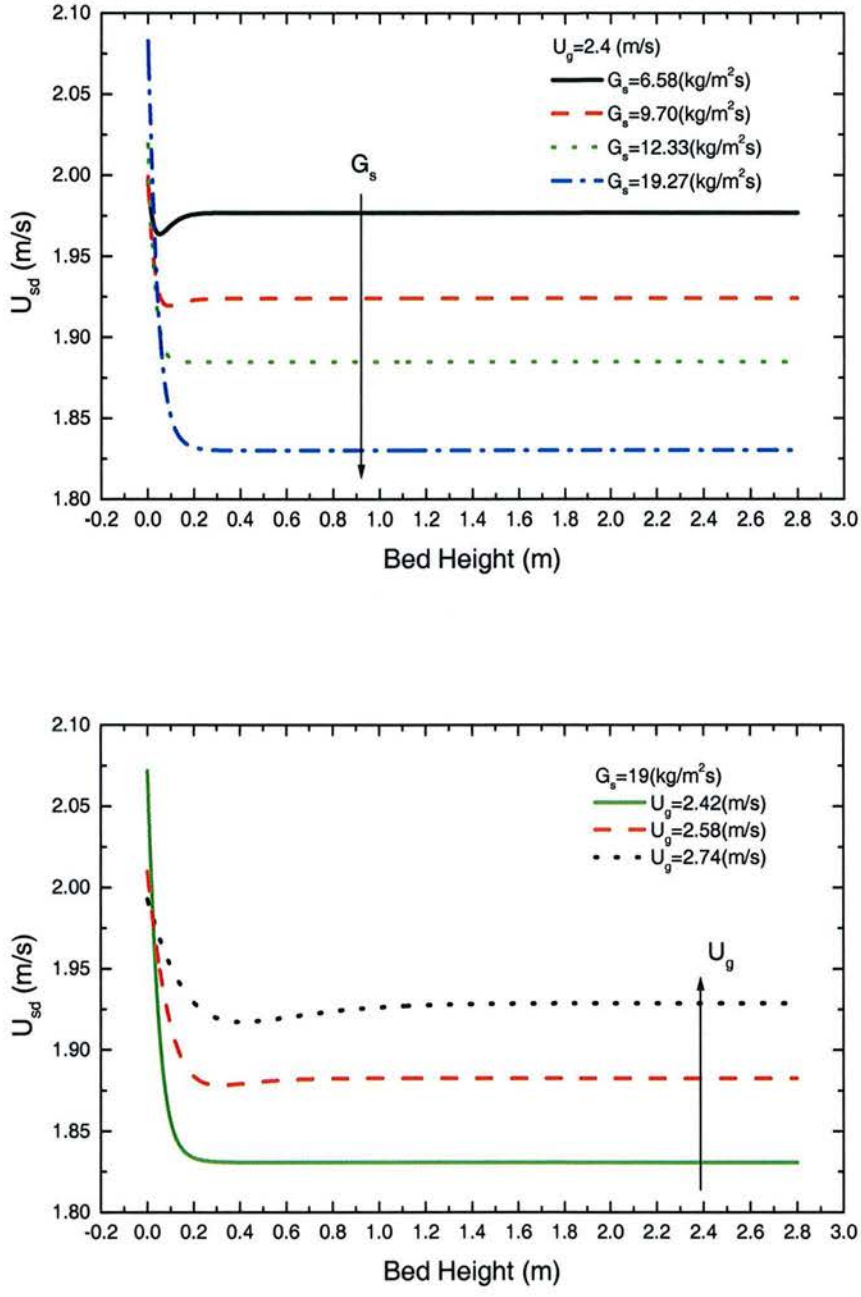

Fig. 5-18 U_{sd} Distribution Along CFB Riser at Different U_g and G_s

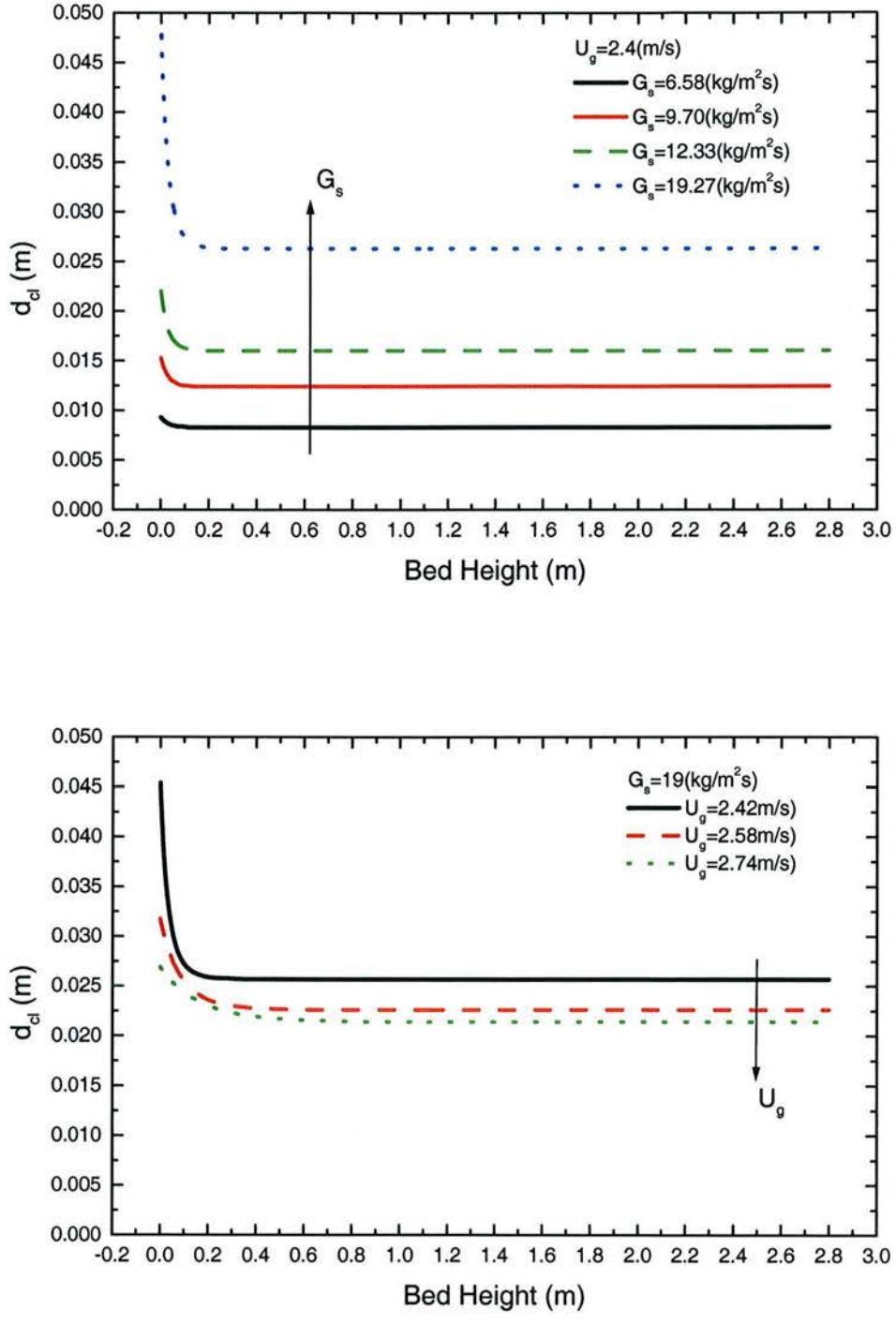

Fig. 5-19 d_{cl} Distribution Along CFB Riser at Different U_g and G_s

Fig. 5-19 is the cluster size distribution along the bed height for different experimental conditions. The cluster size increases with the increasing solid circulation rate, or decreasing superficial gas velocity. Again the cluster diameters are almost constant for most part of the CFB riser, except at the very bottom of the bed.

5.4. Conclusions

- The EMMS model is used and modified to describe the local hydrodynamics of gas and solid particles in a CFB riser. This model divides the heterogeneous gas-solid system in the CFB into two homogeneous gas-solid systems: a dilute phase consisting of gas and discrete individual particles and a dense phase or clusters of particles.
- The numerical solutions of EMMS model gives parameters which describe the detailed structures of gas-solid flow in the fluidized bed, including cluster diameter, cluster phase volume fraction and gas and solid velocities and voidage in the different phases.
- A one-dimensional hydrodynamics model for gas and solid flow in CFB riser is constructed by combining the local EMMS model (5-18) ~ (5-28) and Kunii and Levenspiel's entrainment model for axial voidage distribution (5-38) ~ (5-45). The agreement between experimental results and the predicted values for voidage distribution are reasonable.
- The numerical solutions of one-dimensional hydrodynamics model show that, under experimental operation conditions for VOC adsorption, all hydrodynamic parameters are almost constant for most part of the CFB riser, except at the very bottom of the bed.

6. GAS/SOLID MASS TRANSFER

In CFB riser, the adsorption process of adsorbate from bulk fluid to the surface inside an adsorbent particle involves:

External Transfer: this is the mass transfer process of adsorbate from the bulk fluid to the outside surface of the adsorbent particle.

Intraparticle Transfer: the transfer of adsorbate from the outside surface to the interior of adsorbent particle by both gas diffusion through pores and solid-phase diffusion along the pore walls;

The adsorption-desorption of adsorbate molecules at active sites: This is usually a very fast process as it approximates the order of the collision frequency of gas molecular on the solid surface. So the adsorption equilibrium is generally assumed between the gas and solid surface inside the pore of adsorbent particle.

So the rate of adsorption of gaseous adsorbate to the adsorbent particles inside CFB riser is actually the rate of mass transfer process between gas and solid. Based on the compartmentalization of two phases of Li's EMMS model, a multi-scale mass transfer model is constructed to estimate the external mass transfer process between gas and solid particle in CFB riser, it is then combined with the intraparticle mass transfer model and adsorption isotherm to give a complete description of the VOCs adsorption process inside CFB riser.

6.1. External Mass Transfer

One of the many advantages claimed for CFB risers, is their excellent gas-solids contacting, implying high gas to particle momentum, mass and heat transfer rates. During the past few decades, most of the studies were focused on the hydrodynamics of CFB system and the usual topics were the axial and radial solids distribution, the solids hold-up and the pressure drop. Few studies dealt with the mass transfer process between the gas and solids inside the CFB reactor. The general idea that the gas-solid contacting is excellent does not follow from the results of published experimental work, and the mass transfer rates are significantly lower than would be expected [51].

6.1.1. Mass Transfer Between Gas And Solid Particles

Inside the CFB riser, small solid particles are suspended by the up-flow gas, and carried over the top of the riser then circulated back to the bottom of the riser via a re-circulating

loop. Generally the gas flows at velocities much higher than the terminal velocity of the individual particles and the particles tend to form clusters, rather than homogeneously distributed in the riser. The formation of such clusters affects the hydrodynamic conditions drastically and reduces the apparent mass transfer coefficient[52, 53].

The mass transfer coefficient for a single sphere particle with diameter d_p moving through a fluid at relative velocity U_g is given by Ranz and Marshall [54] as,

$$Sh = 2.0 + 0.6\,\mathrm{Re}^{1/2}\,Sc^{1/3} \qquad (6\text{-}1)$$

This relation describes the transport process between the infinite fluid and a single solid particle for Re>5. The first term 2 is the influence of molecule diffusion and the second term is the contribution of convection. Sh, Re, and Sc are the Sherwood, Reynolds, and Schmidt numbers respectively.

$$Sh = \frac{k_g d_p}{D_g}; \qquad \mathrm{Re} = \frac{d_p U_g \rho_g}{\mu_g}; \qquad Sc = \frac{\mu_g}{D_g \rho_g};$$

D_g is the gas phase diffusion coefficient. For a fixed bed of particles with diameter d_p, the Sherwood number may be estimated as[55]:

$$Sh = 2 + 1.8\,\mathrm{Re}^{1/2}\,Sc^{1/3}, \qquad for \qquad \mathrm{Re} > 80 \qquad (6\text{-}2)$$

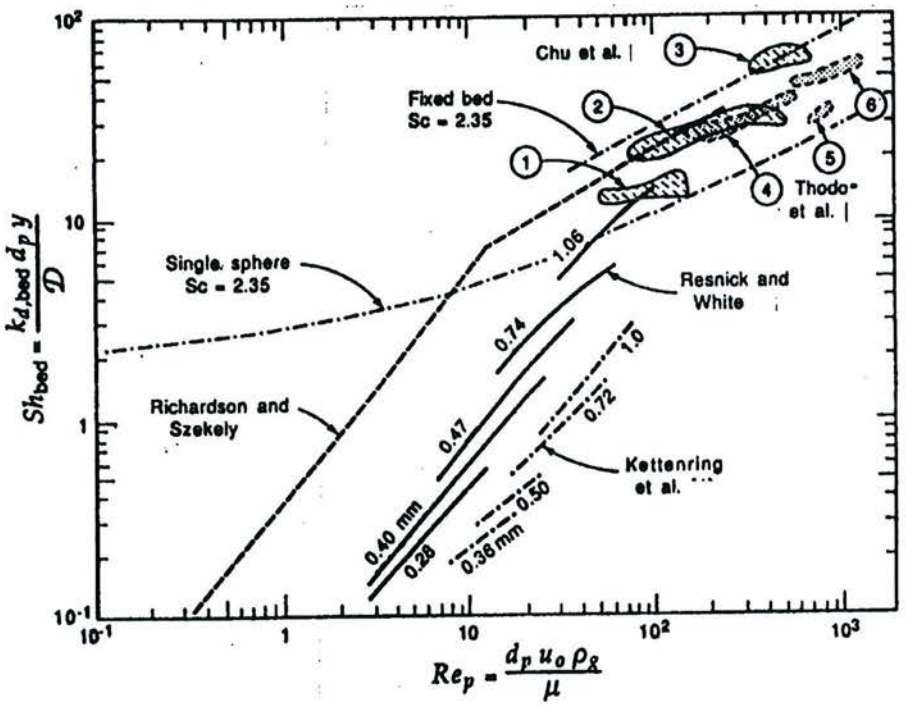

Fig. 6-1. Experimental Findings on MassTransfer in Fluidized Beds (Kunii [55])

The mass transfer coefficient between gas and particles in fluidized bed is difficult to evaluate by a simple relation. The experimental results of mass transfer coefficient for bubbling fluidized bed are shown in Fig 6-1, together with correlations for single particle and fixed bed.

If smaller and smaller solids are completely dispersed in flowing gas, the Sherwood number should approach 2.0, the theoretical minimum for diffusion into a stagnant medium. However Fig. 6-1 clearly shows that the experimental results fall further and further below the theoretical minimum of 2 as the Reynolds number is lowered.

With the higher Reynolds numbers (big particle system), the correlations are similar for fixed bed, fluidized bed and CFB: the mass transfer rate increases with the increase of fluid flow rate and it is higher than that for single particle. For the small Reynolds numbers (small particle system) the result are quite scattered and all are far below the single particle value.

The main reasons for the lower mass transfer rate for small particles system is the heterogeneous space distribution of gas and solids inside the reactor, due to the existence of gas bubbles for the bubble fluidized bed and solids clusters for the CFB. This feature makes the gas-solid system far from plug flow, resulting in lower overall mass transfer rate calculated with the plug flow assumption.

Kunii[55] pointed out that, the mass transfer coefficient measured for the whole bed is model-dependent and it should match the single particle values if the model closely matches the flow conditions in the bed.

6.1.2. Gas/Solid Mass Transfer in CFB Riser

Halder and Basu[56] examined the mass transfer between gas and solid in CFB riser. It is found that the mass transfer coefficient for the freely moving coarse particle in a fast bed of fine solids is lower than that obtained using superficial gas velocities. The slip velocity between gas and solid particle have a strong influence on the mass transfer rate and the correlation proposed for Sherwood number estimation is.

$$Sh = 2\varepsilon + 0.69(\frac{U_s d_p \rho_g}{\mu_g \varepsilon})^{1/2} Sc^{1/3} \tag{6-3}$$

The slip velocity is defined as:

$$U_s = U_g - U_p \varepsilon/(1-\varepsilon) \tag{6-4}$$

The mass transfer model between gas and solid particles in CFB riser is constructed according to the compartmentalization of two phases of Li's EMMS model. The particles inside the CFB riser are considered existing in two different phases: a dilute dispersed phase and a dense cluster phase. The mass transfer between gas and solid particles in dilute and cluster phases could be expressed as:

$$J_d = k_{g,d}(1-f)(1-\varepsilon_d)\frac{6}{d_p}(C_d - C_s) \tag{6-5}$$

$$J_c = k_{g,c} f(1-\varepsilon_c)\frac{6}{d_p}(C_c - C_s) \tag{6-6}$$

J_d and J_c are the mass transfer rate between gas and solid with respect to unit bed volume, $k_{g,d}$ and $k_{g,c}$ are the mass transfer coefficient with respect to unit adsorbent area, C_d and C_c are the gas phase adsorbate concentration in the dilute and cluster phases respectively. C_s is the concentration at the surface of adsorbent particle. Then the mass transfer between the gases of dilute and cluster phase should be considered.

The clusters in the CFB are dynamic, much different from bubbles in the bubbling fluidized bed. The bubbles can only be growing or merging with other bubbles after its formation while traveling through the fluidized bed. The clusters in the fast bed may disperse into dilute phase and the dispersed particles may agglomerate into clusters. The mass transfer between the gases in dilute and cluster phases will be determined by the gas phase mass transfer and this dynamic change of the two phases. Unfortunately, there has not been available model to estimate this influence until now. .

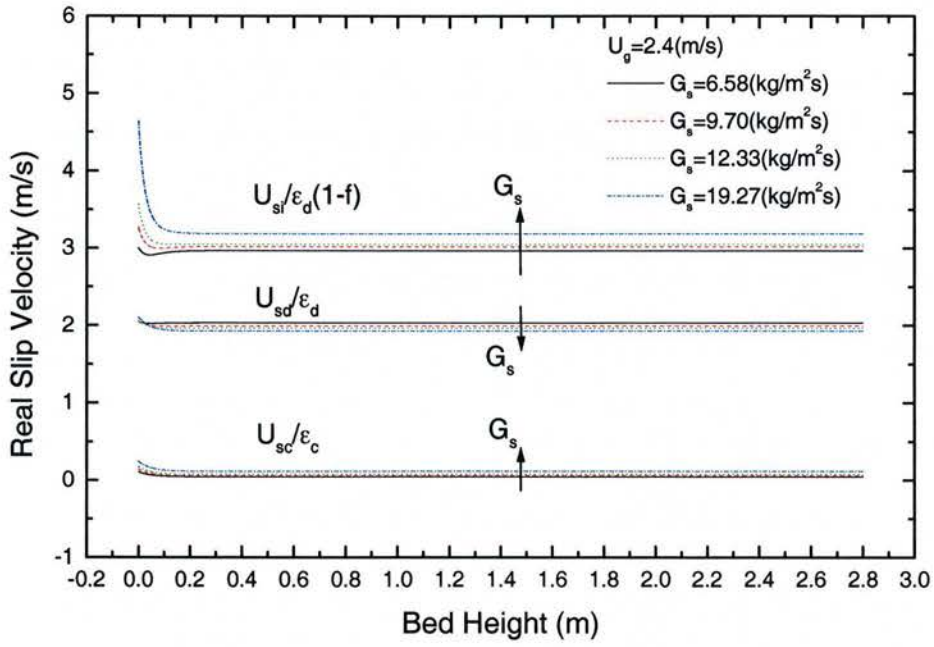

Fig. 6-2 Real Slip Velocities in CFB Riser

Fig. 6-2 shows the real slip velocity between dilute gas and cluster particles and the real slip velocities between the gas and solid particle inside dilute and cluster phases obtained from the EMMS model. The slip velocity between dilute gas and cluster particles is

higher than the other slip velocities, implying the gas-gas mass transfer process between dilute and cluster phases is much faster than the gas-solid mass transfer inside dilute and cluster phases. The slip velocity inside cluster phase is much smaller, around 0.1m/s under experimental conditions; so the adsorbate mass transfer coefficient between gas and solid particles inside clusters is much smaller than that in the dilute phase. Assuming the mass transfer process between the gases of dilute and cluster phases are much faster due to this high slip velocity and the dynamic change of the two phases, then the gas phase concentration in the two phases could be considered as the same, or C_c=C_d=C. The total mass transfer rate between gas and solid particles J should be the sum of that inside the dilute and the cluster phases.

$$J = J_d + J_c = [k_{g,d}(1-f)(1-\varepsilon_d) + k_{g,c} f(1-\varepsilon_c)]\frac{6}{d_p}(C - C_s) \tag{6-7}$$

or

$$J = k_g(1-\varepsilon)\frac{6}{d_p}(C - C_s) \tag{6-8}$$

The mass transfer coefficient in dilute and cluster phase is determined by the slip velocities between gas and solid particles in the respect phases that could be obtained from EMMS model. Halder and Basu's [56] equation is used to estimate this coefficient.

$$Sh_d = \frac{k_{g,d} d_p}{D_g} = 2\varepsilon_d + 0.69(\frac{U_{sd} d_p \rho_g}{\mu_g \varepsilon_d})^{1/2} Sc^{1/3} \tag{6-9}$$

$$Sh_c = \frac{k_{g,c} d_p}{D_g} = 2\varepsilon_c + 0.69(\frac{U_{sc} d_p \rho_g}{\mu_g \varepsilon_c})^{1/2} Sc^{1/3} \tag{6-10}$$

So the integrated mass transfer coefficient between gas and solid particles k_g could be expressed as:

$$k_g = \frac{k_{g,d}(1-f)(1-\varepsilon_d) + k_{g,c} f(1-\varepsilon_c)}{1-\varepsilon} \tag{6-11}$$

Fig. 6-3 shows the calculated results of cross sectional averaged mass transfer coefficient for different voidage in the bed. The calculation starts from U_g and G_s, for a given voidage ε, the parameters U_{sd}, U_{sc}, ε_d, ε_c and f could be obtained from (5-24) ~ (5-34), according to the calculation procedures shown in Fig. 5-3. Then, the mass transfer coefficients in the dilute and cluster phases are obtained from (6-9) and (6-10). Finally, the cross sectional averaged mess transfer coefficient is obtained from (6-11).

The cross sectional averaged mass transfer coefficients are also calculated for homogeneous gas/solid system at the same operation conditions. Now f=0 and the superficial slip velocity is calculated from (6-4). The mass transfer coefficient k_g is

directly obtained from (6-3) and also presented in Fig. 6-3.

It is obvious that this value is much smaller than that calculated with homogeneous gas/solid distribution assumption. This shows the formation of clusters is the main reason for the lower mass transfer coefficient between gas and solid particles in CFB. If $f=0$, or clusters disappears and all the particles are discretely distributed in the fluid, the mass transfer coefficient for the bed k_g will equal that in dilute phase k_{gd}. If $f\neq 0$, k_g will be smaller than k_{gd} as the mass transfer coefficient in the cluster phase k_{gc} is small. This explains why the mass transfer coefficient obtained with superficial gas velocity for the fluidized bed is less than that for a single particle.

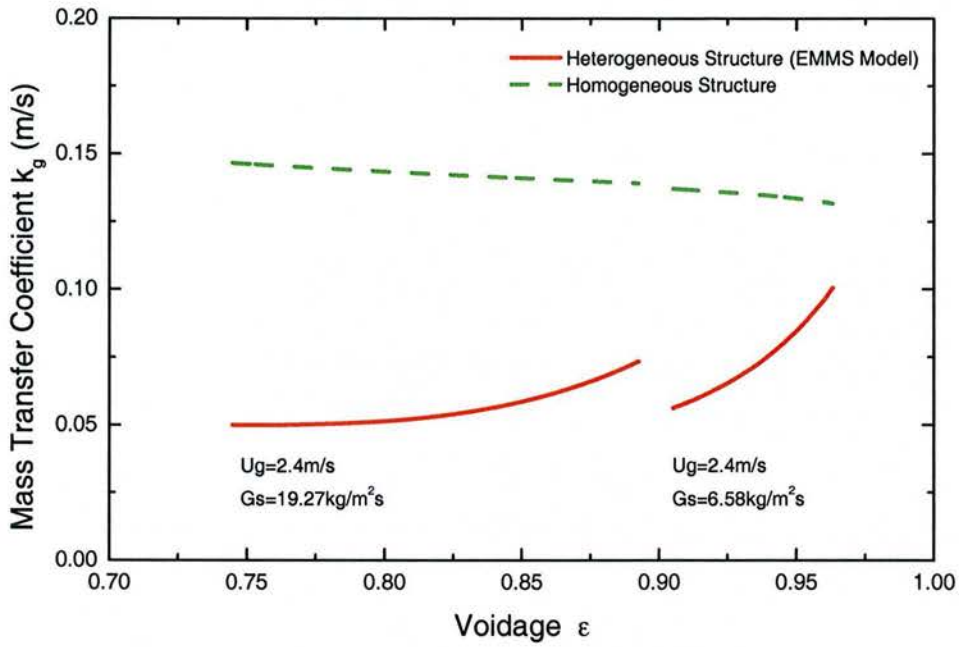

Fig. 6-3 Cross sectional averaged gas/solid mass transfer coefficient in CFB

The external mass transfer coefficients in the cluster phase and dilute phase is obtained from (6-9) and (6-10) with the slip velocities obtained from EMMS model. The corss sectional averaged external mass transfer coefficient distribution along the bed height is then calculated with (6-11).

Fig 6-4 shows the calculated results under two different experimental conditions. The external mass transfer coefficient in the cluster phase k_{gc} is only 1/3 or 1/4 of that in the dilute phase k_{gd}. While the change of k_{gc} and k_{gd} are relatively small along the bed height, the cross sectional averaged value of k_g increases with bed height first, then settles down to a constant value, in accordance with the change of cluster phase volume fraction f along the bed height.

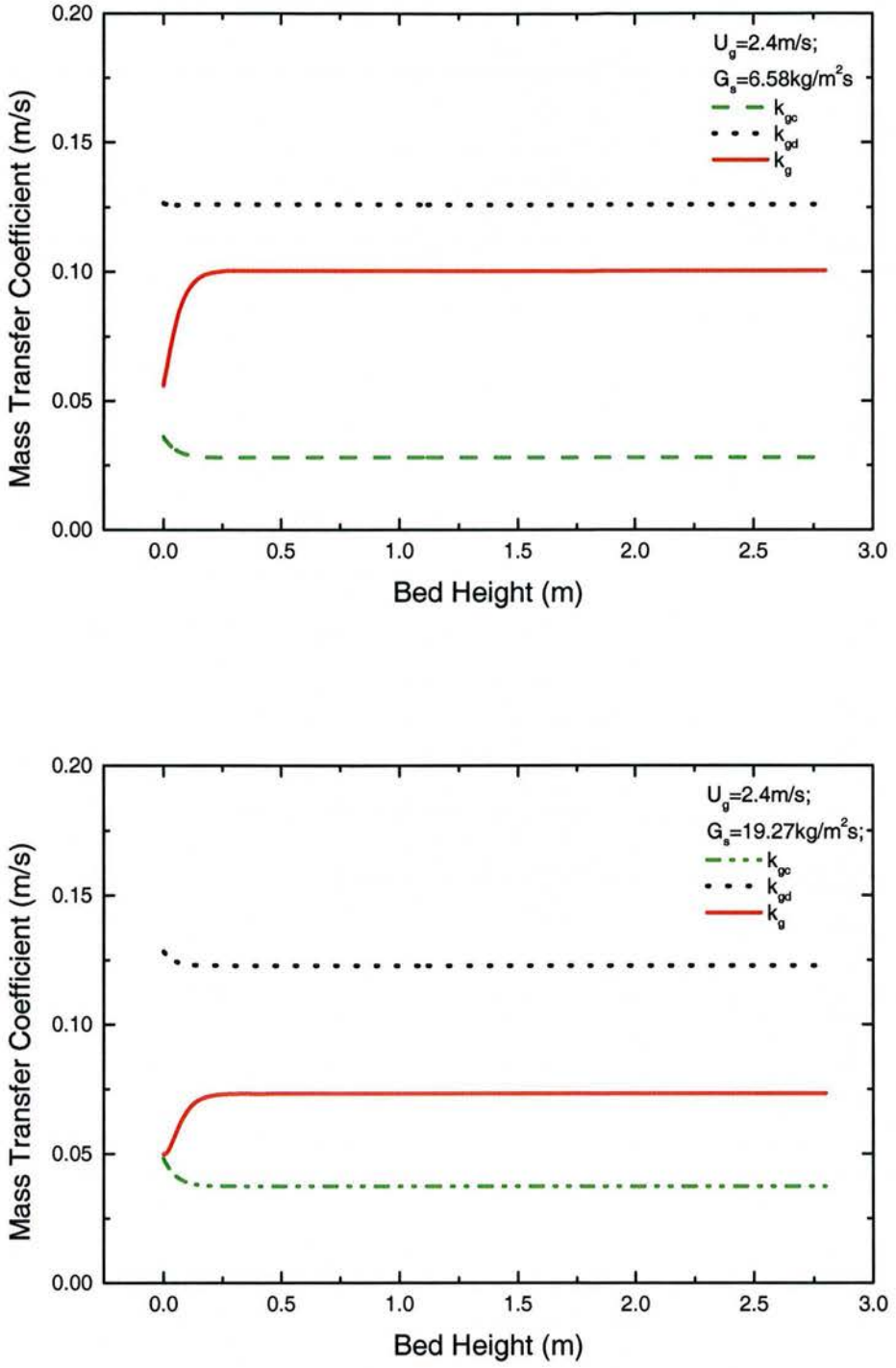

Fig. 6-4 External Mass Transfer Coefficient in the Bed

Fig. 6-5 shows the external mass transfer coefficient distribution along the CFB riser under different operation conditions. k_g is almost constant for most of the bed height except at the very bottom of the bed. The value of k_g is higher for higher superficial gas velocities or lower solid circulation rate.

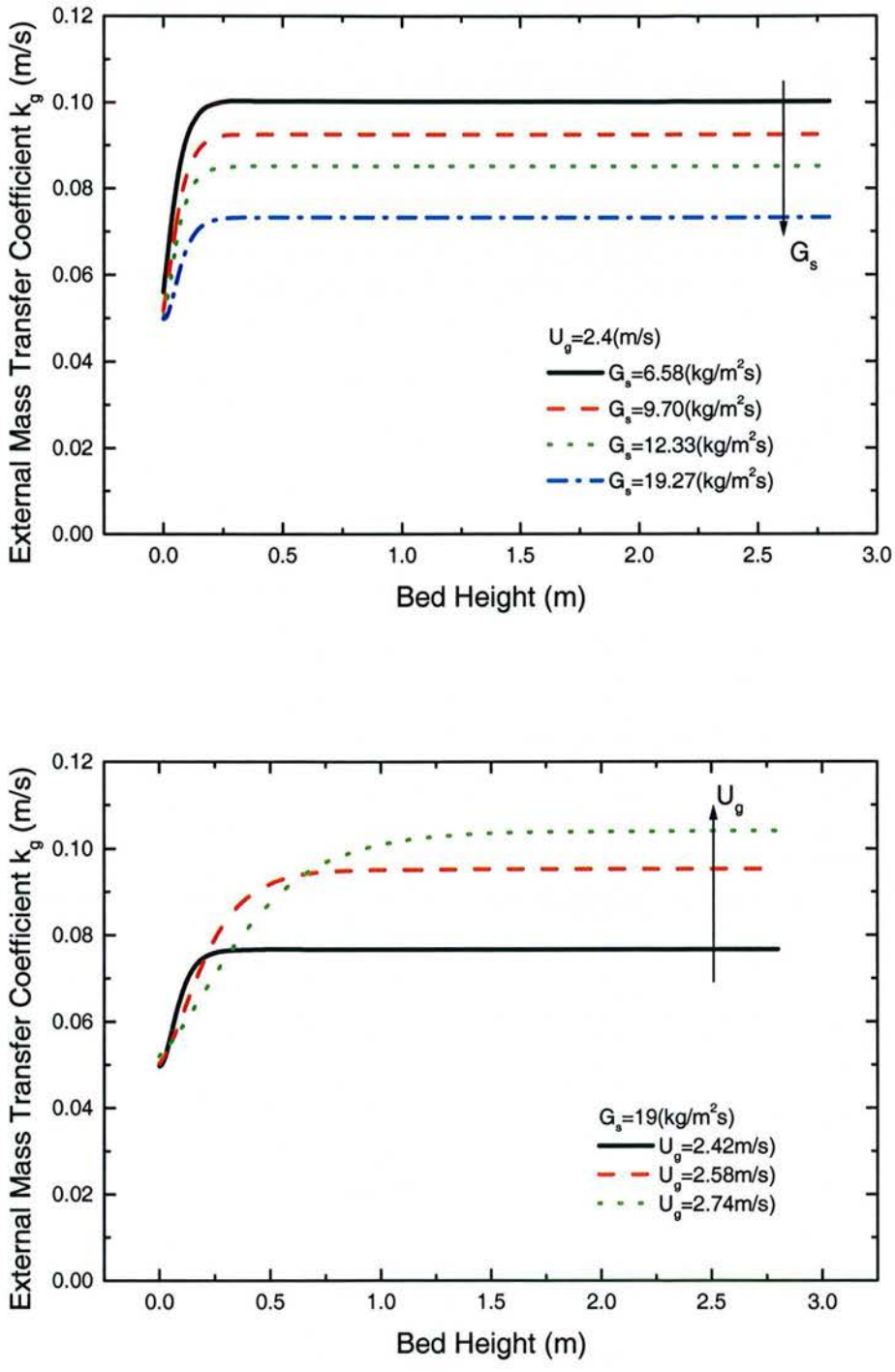

Fig. 6-5 The Changes of External Mass Transfer Coefficient along the Bed Height under Various Operating Conditions

6.2. Intraparticle Mass Transfer In Porous Adsorbent

Rate of adsorption and desorption in porous adsorbent are generally controlled by transport within the pore network, rather than by the kinetics of adsorbate sorption at the solid surface. Since there is generally little bulk flow through the pores, the intraparticle transport is generally considered as a diffusion process and expressed by Fick's first equation with diffusivity D.

$$J = -D\frac{\partial C_r}{\partial r} \tag{6-12}$$

Diffusion of adsorbate inside porous adsorbent may occur by several different mechanisms: pore diffusion through the gas phase, including molecular diffusion and Knudsen diffusion, and surface diffusion through the adsorbed phase, depending on the pore size, the adsorbate concentration and other conditions.

6.2.1. Pore Diffusion

For gas-solid systems, if transport within the macropores occurs only by molecular diffusion, the effective molecular diffusivity $D_{m,e}$ can be calculated from the gas phase diffusivity D_m related with tortuosity τ and particle porosity ε_p as follows:

$$D_{m,e} = \frac{\varepsilon_p}{\tau} D_m \tag{6-13}$$

The molecular diffusivity D_m may be estimated with Chapman-Enskog equation [57] for a binary gas mixture:

$$D_m = \frac{1.58\times10^{-7} T^{3/2}(1/M_1 + 1/M_2)^{1/2}}{P\sigma_{12}^2 \Omega(\varepsilon_{12}/kT)} \qquad (m^2/s) \tag{6-14}$$

Where M_1, M_2 are the molecular weights, P is the total pressure in the atmosphere, $\sigma_{12}=(\sigma_1+\sigma_2)/2$ is the collision diameter from the Lennard-Jones potential, expressed in Angstroms, and Ω is a function of (α/kT), where $\alpha=(\alpha_1\alpha_2)^{1/2}$ is the Lennard-Jones force constant and k is the Boltzmann constant. The molecular diffusivity in multi-component mixture may be estimated from the simple approximate relationship assuming only component 1 diffuses,

$$\frac{D_{1m}}{1-Y_1} = \left(\sum_{j=2}^{n} \frac{Y_j}{D_{1j}}\right)^{-1} \tag{6-15}$$

The molecular diffusivity of a binary mixture is essentially independent of composition. In multi-component mixtures the diffusivity becomes, in principle, concentration dependent, but such variations are generally relatively small so that the assumption of a

concentration-independent diffusivity is usually used.

In molecular diffusion the resistance to flow arise from collisions between diffusing molecules. The effect of pore is merely to reduce the flux as a result of geometric constraint that is accounted for by the tortuosity factor. Molecular diffusion will dominate transport mechanism whenever the mean free path of the gas is small relative to the pore diameter. However, in small pores and at low pressure the mean free path is larger than pore diameter and collisions of molecules with pore walls occur more often than collisions between diffusing molecules. Under these conditions the collision between molecule and pore wall provide the main diffusional mechanism and we have what is known as Knudsen flow.

Knudsen Diffusion Coefficient D_k for the pores with pore radius r_p may be calculated by the following equations[58]:

$$D_K = 97 r_p (T / M)^{1/2} \tag{6-16}$$

where r_p is the mean pore radius, T is in Kelvin, and M is the molecular weight of the diffusing species. In the transition region where both Knudsen and molecule diffusion are significant, the combined pore diffusivity for a binary gas in porous solid at constant pressure is given by

$$\frac{1}{D_p} = \frac{1}{D_m} + \frac{1}{D_K} \tag{6-17}$$

Similar to other activated carbon adsorbents, Ambersorb 600 has a heterogeneous pore size distribution ranging from micropores (pores less than 2 nm), mesopores (pores between 2 and 50 nm) to macropores (pores larger than 50 nm). The micropores are the adsorbent's primary adsorption sites, while the mesopores and macropores are the transport pores which enable the adsorptives to rapidly diffuse into the adsorbent particles. Considering the parallel diffusion process in the different scale pores, the overall pore diffusion coefficient could be estimated as:

$$D_{p,e} = \frac{\varepsilon_{macro}}{\tau} D_{p,macro} + \frac{\varepsilon_{meso}}{\tau} D_{p,meso} + \frac{\varepsilon_{micro}}{\tau} D_{p,micro} \tag{6-18}$$

The same tortuosity is used for the different scale pores and it is estimated with Maxwell's relation[59]:

$$\tau = 1 + \frac{1}{2}(1 - \varepsilon_p) \tag{6-19}$$

In the macropores, the pore size is big enough to assume molecular diffusion as the only pore diffusion mechanism. For the mesopores and micropores, the pore diffusion including molecular diffusion and Knudsen diffusion. As shown in Table 6-1, the molecule diffusivity of toluene in air at 25 ^{O}C is 8.44x10^{-6} m^2/s. Assuming the averaged

pore radius is 0.5 nm and 13 nm for the micropore and mesopore respectively, the effective pore diffusivity calculated from (6-18) is 1.23×10^{-6} (m^2/s) for Ambersorb 600/toluene system.

Table 6-1 Estimation of Pore Diffusity for Toluene-Air Mixture in Ambersorb 600 Adsorbent at Temperature of 25°C

Parameter	Equation	Macropore	Mesopore	Micropore
Pore Diameter d (nm)		d>50	2>d>50	2>d
Voidage ε_p (-)		0.1575	0.1275	0.165
Pore Radius r_p (m)		>2.5E-08	1.30E-08	5.00E-10
Knudsen Diffusivity D_k (m^2/s)	(6-16)	-	2.27E-06	8.73E-08
Molecular Diffusivity D_m (m^2/s)	(6-14)	8.44E-06	8.44E-06	8.44E-06
Tortuosity τ	(6-19)	1.275	1.275	1.275
Pore Diffusivity D_p (m^2/s)	(6-17)	1.09E-06	1.79E-06	8.64E-08
Effective Pore Diffusivity $D_{p,e}$ (m^2/s)	(6-18)		1.23E-06	

6.2.2. Surface Diffusion

Both Knudsen and molecular diffusion mechanisms involve flow through the space within the pore, there is in addition the possibility of a direct contribution to the flux from transport through the physically adsorbed layer on the surface of the macropore, and this is referred to as surface diffusion. Although the mobility of the adsorbed phase will generally be much smaller than that of the gas phase, the concentration is much higher, so a significant contribution to the flux is possible.

Surface diffusion coefficient is not as easily estimated as the other two. It was suggested by Gilliland [60] that the concentration and temperature effects can be represented by:

$$D_s = D_{s0} \exp(-E / RT) \qquad (6-20)$$

On the basis of the correlation of literature data on 30 different systems, Sladek et al.[61] proposed that the activation energy E could be approximated as 45% of the heat of physical adsorption of nonpolar adsorbate and that D_{so} be estimated by

$$D_{s0} = 1.6 \times 10^{-6} \qquad (m^2/s) \qquad (6-21)$$

From the isotherm discussion we know that the averaged value of isosteric heat over the experimental concentration range is 65.15 MJ/mol for Ambersorb 600/Toluene system. The effective surface diffusivity in the adsorbent is then estimated as:

$$D_{s,e} = D_s / \tau_s \qquad (6-22)$$

While there is no reason for τ_s to equal τ_p, the same value is often used in the absence of a better approximation[58]. With τ_s = 1.275, the calculated value of $D_{s,e}$ for the Toluene/Ambersorb 600 system is 9.165×10^{-12} m^2/s.

6.2.3. Mass Transfer Within Adsorbent Particles

Adsorbent particles are heterogeneous systems formed by a porous solid phase and a fluid phase filling the void fraction of the solid. The internal diffusion can be expressed by the two possible simultaneous mechanisms of diffusion, including pore diffusion and surface diffusion. If one considers this combined parallel resistance within the adsorbent particle, a material balance for spherical particle results in the following partial differential equation:

$$\varepsilon_p \frac{\partial C_r}{\partial t} + \rho_p \frac{\partial q_r}{\partial t} = \frac{1}{r^2}\frac{\partial}{\partial r}[r^2(D_{p,e}\frac{\partial C_r}{\partial r} + D_{s,e}\rho_p \frac{\partial q_r}{\partial r})] \tag{6-23}$$

In the above equation, ε_p is the porosity of the adsorbent particle; ρ_p is the density of the adsorbent particle; C_r and q_r are adsorbate gas and solid phase concentration within the pores of particle.

In the dilute range of an adsorption system have a favourable isotherm; the accumulation of adsorbate inside the void of the adsorbent particle can be neglected compared with the solid phase accumulation. (6-23) can be re-written as:

$$\frac{\partial q_r}{\partial t} = \frac{D_e}{\rho_p r^2}\frac{\partial}{\partial r}(r^2 \frac{\partial C_r}{\partial r}) \tag{6-24}$$

$$D_e = D_{p,e} + D_{s,e}\rho_p \frac{dq}{dC} \tag{6-25}$$

For linear isotherm, the partial derivative of isotherm dq/dC is a constant, but for nonlinear isotherm there is no simple relationship. Thus it may be estimated as q_{in}^*/C_{in}, where C_{in} is the inlet VOC concentration and q_{in}^* is solid phase concentration in equilibrium with it. The calculated results show that, the pore diffusion is the dominate feature in the particle and the contribution of surface diffusion is relatively small under experimental conditions. The effective diffusivity D_e obtained from (6-25) is 1.65×10^{-6} m^2/s and 1.44×10^{-6} m^2/s for C_{in}=1900 mg/Nm^3 and 4100mg/Nm^3 at 25 °C respectively. The averaged uptake rate of adsorbate by the unit mass of adsorbent is:

$$\frac{\partial q}{\partial t} = \int_0^{\frac{d_p}{2}} 4\pi r^2 \frac{\partial q_r}{\partial t} dr / (\frac{1}{6}\pi d_p^3) \tag{6-26}$$

Substituting (6-24) into (6-26) we get:

$$\frac{\partial q}{\partial t} = \frac{6}{d_p}\frac{D_e}{\rho_p}(\frac{\partial C_r}{\partial r})_{r=\frac{d_p}{2}} \tag{6-27}$$

If the parabolic concentration distribution of gas (solid) is assumed inside the adsorbent particle, (6-27) becomes:

$$\frac{\partial q}{\partial t} = \frac{60}{d_p^2}\frac{D_e}{\rho_p}(C_s - C_p^*) \tag{6-28}$$

C_p^* is the gas phase concentration in equilibrium with the solid phase concentration q. (6-28) can also been expressed as:

$$\frac{\partial q}{\partial t} = k_p \frac{6}{\rho_p d_p}(C_s - C_p^*) \tag{6-29}$$

$k_p=10D_e/d_p$ is the intraparticle mass transfer coefficient. It is a function of initial gas phase concentration only at specified temperature and shows slight decrease with increasing initial gas phase concentration. Fig. 6-6 is the calculated values of intraparticle mass transfer confficient for Toluene in Ambersorb 600 adsorbent. It is between 0.0254 ~ 0.0222 m/s for C_{in} between 1900 ~ 4700 mg/Nm^3.

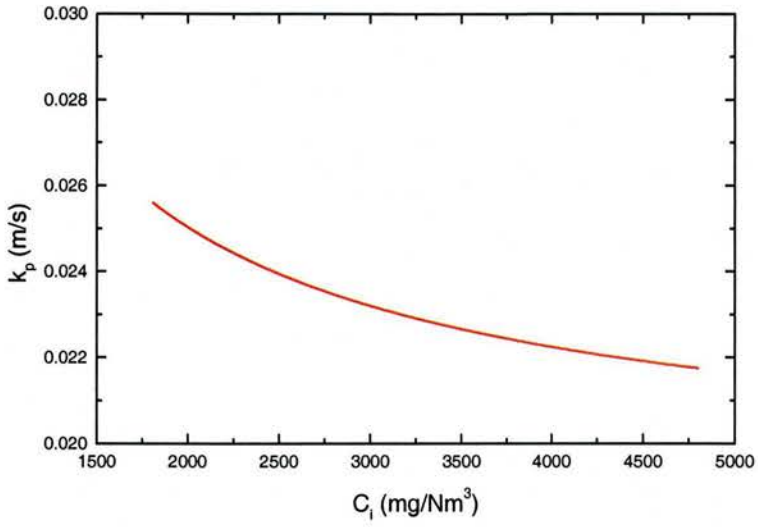

Fig. 6-6 Intrparticle Mass Transfer Coefficient

6.3. Gas/Solid Mass Transfer In CFB Riser

6.3.1. Overall Mass Transfer Coefficient

For unit bed volume in CFB riser, the mass transfer rate calculated from particle side is:

$$J = (1-\varepsilon)\rho_p \frac{\partial q}{\partial t} = k_p(1-\varepsilon)\frac{6}{d_p}(C_s - C_p^*) \tag{6-30}$$

This mass transfer rate should be equal to that calculated from the gas side with equation (6-8). From (6-8) and (6-30) we can eleminate the concentration at the surface of particle C_s and and get the mass transfer rate from gas to adsorbent particle in unit bed volume as:

$$J = K(1-\varepsilon)\frac{6}{d_p}(C - C_p^*) \tag{6-31}$$

In (6-31), K is the overall mass transfer coefficient, including external mass transfer and intraparticle mass transfer process.

$$\frac{1}{K}=\frac{1}{k_p}+\frac{1}{k_g} \tag{6-32}$$

If $k_g>>k_p$, that is, intraparticle mass transfer process is the controling step, then $K=k_p$ and K could be considered as constant along the CFB riser. If $k_g<<k_p$, that is, external mass transfer process is the controling step, then $K=k_g$ and K is increasing with the bed height at the bottom regian of CFB riser, while it could be considered as a constant for the rest of the bed.

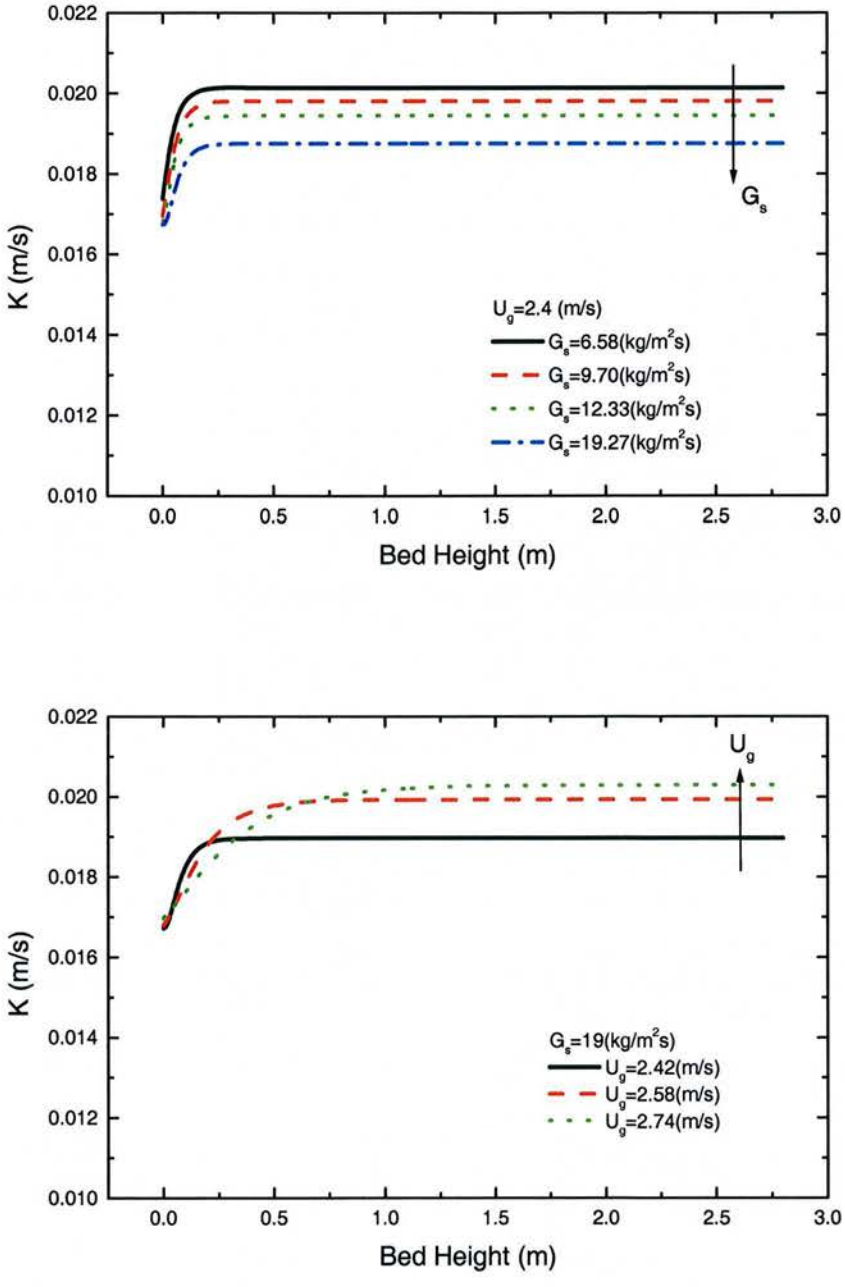

Fig. 6-7 Overall Mass Transfer Coefficient Distribution Along CFB Riser

The calculated results for k_p and k_g under experimental conditions show that the difference between k_p and k_g is less than one order of magnitude, while the value of k_g (0.05-0.1m/s) is higher than that of k_p(0.022-.0.026m/s). So both external and intraparticle mass transfer process should be considered for the adsorbtion of adsorbate in CFB riser. Fig. 6-7 shows the mass transfer coefficient distribution along the CFB riser under different operation conditions. K is almost a constant for most of the bed height except at the very bottom of the bed. The value of K is higher for higher superficial gas velocities or lower solid circulation rate.

6.3.2. Gas Dispersion

Gas dispersion in an empty riser is much smaller than that in the presence of circulating solids [62,63]. The axial dispersion increases strongly as soon as solid particles enter the riser, for any G_s>0. The experimental data for G_s<100 kg/m^{2}s show that, the gas dispersion appears to increase as the solids mass flux increases (at fixed gas velocity) or as the gas velocity decreases (at fixed solids mass flux). The gas mixing becomes evident as the suspension density increases, mainly due to the more intense solids down flow along the riser walls [63]. Li and Wu [64] found that the axial gas dispersion coefficient D_{gz} could be expressed as:

$$D_{gz} = 0.1953\varepsilon^{-4.1197} \qquad (\text{m}^2/\text{s}) \qquad (6\text{-}33)$$

Many gas back mixing experiments have been reported for, low velocity fluidized beds, as extensively reviewed by Potter [65] and Van Deemter [66]. Relatively few gas back mixing experiments have been carried out in transported, high velocity fluidized bed. The experiments of Cankurt and Yerushalmi [67], Yang et al [68], Helmrich et al [69] and Bader et al [70] supported the idea that the gas back mixing substantially decreased beyond the turbulent regime, so that plug flow of gas may be assumed for fast fluidized bed. This conclusion was questioned by Weinstein et al [71] and Li and Weinstein [58]. They found considerable gas back mixing in the fast bed. As in all fluidized regimes, gas back mixing is mainly determined by the down flow of solids particles, the plug flow assumption is only valid for the gas up-flow in the dilute core, not for the whole cross section. It is also found that axial dispersion in the bottom relatively dense region is greater than in the transition and dilute zones [58]. This again, confirms the trends of D_{gz} expression proposed by Li and Wu [64].

Compared with axial mixing, the lateral mixing of gas in CFB is relatively poor. In contrast with the axial mixing, it is generally accepted that lateral mixing in a single-phase flow is higher than that in a gas-solids suspension. The experimental results of Zheng et al [72] show that: the degree of lateral dispersion is maximum in single phase flow; addition of particle to establish a dilute transport regime in the riser leads to a damping of gas turbulence and a consequent reduction of D_{gr}; further increasing in gas solids suspension density lead to an increase in the degree of turbulence and enhances gas mixing.

Two types of theoretical models have been used to describe the gas mixing in the CFB riser. One is the plug flow with dispersion model, which is the same as used for single-phase fluid flow. The other is the core-annulus two regions model, which assumes a turbulent single phase inside the core flows upward while the gas in the annulus is considered as stagnant or flowing upward/downward. The first model is used in this study for the modeling of VOC adsorption in CFB riser. Li and Wu's expression (6-33) is used to calculate the axial gas dispersion coefficient in CFB riser.

6.4. Conclusions

- The external mass transfer coefficient between gas and adsorbent particles in the CFB riser could be estimated by equation (6-11) from that for single particle and hydrodynamic parameters being obtained from EMMS model. The formation of clusters is the main reason for a lower mass transfer coefficient between gas and solid particles in CFB. This coefficient is higher for higher superficial gas velocity and lower solid circulation rate.
- The intraparticle adsorbate mass transfer includes pore diffusion (molecule diffusion and Knudsen diffusion) and surface diffusion process. The pore diffusion is the dominant feature and the contribution of surface diffusion is relatively small under experimental conditions.
- Under experimental conditions, the difference between external and intraparticle mass transfer coefficients is less than one order, while the value of intraparticle mass transfer coefficient is relatively small, or intraparticle mass transfer process is the limiting step. The mass transfer coefficient K is almost a constant for most of the bed height except at the very bottom of the bed.
- Li and Wu's expression (6-33) could be used to estimate the axial gas dispersion coefficient in CFB riser.

7. VOCs ADSORPTION IN CFB RISER

One of the advantages of CFB adsorption process for gas cleanup is that it is a stable continuous operation process with high gas throughput, so it could be used for treatment of large flow rate gas streams. Fig.7-1 is a conceptual schematic diagram of a CFB adsorption system proposed for dilute VOC controlling. Inside a CFB riser, small solid adsorbent particles are suspended by the up-flow gas, and carried over the top of the riser while the adsorption process is taking place. The adsorbent particles are then separated from gas and re-circulated back to the bottom of the riser via a re-circulation loop. Part of the circulated adsorbents is desorbed in a regenerator and fed back to the adsorber to maintain a relatively lower solid phase concentration in the system. A concentrated VOC stream is obtained from the desorber that could be recovered or incinerated in the following process.

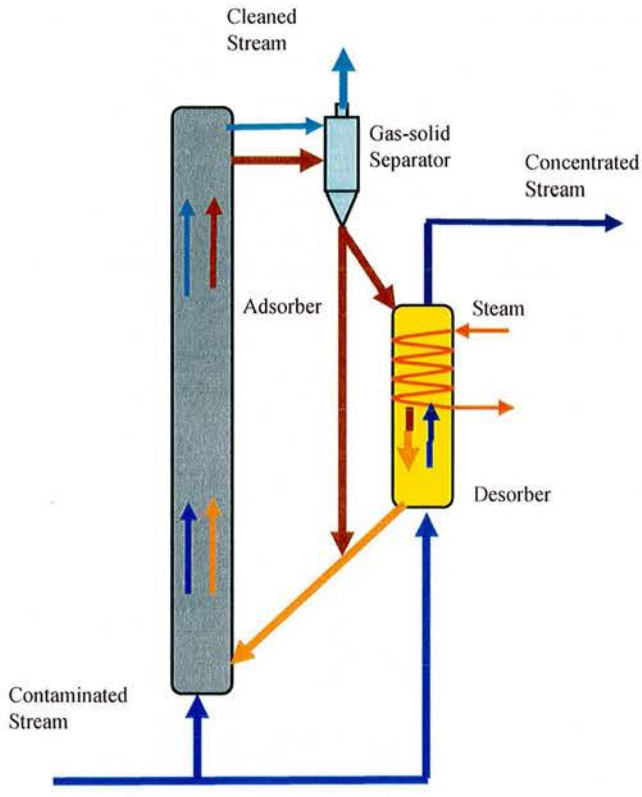

Fig. 7-1 Schematic Diagram of CFB Adsorption System

The CFB are usually operated in the fast fluidization regime with high gas and solids throughput. The heat transfer inside the CFB is much faster and nearly isothermal conditions can be obtained. With improved gas–solid contacting and higher operation

velocity than in a bubbling fluidized bed, the CFB adsorption process is thus an alternative for emission reduction of dilute VOCs. Despite of the advantages, the CFB reactor has not been used in industries for adsorption process until now. This mainly results from the lack of knowledge on hydrodynamics and transfer process involved in the CFB reactor. In this chapter we will analyze the adsorption process inside the CFB riser and discuss the influence of operating parameters on the performance of the adsorber. These are the fundamentals for the design and operation of CFB adsorption process.

7.1. Adsorption In CFB Riser

7.1.1. One Dimensional Adsorption Model

In the CFB riser, the solids are essentially in a state of complete mixing and the gas passes through the solids more or less by plug flow [73]. The main assumptions for setting up the one dimensional adsorption model, which describes the VOC adsorption process along the CFB riser, include:

- isothermal Conditions are assumed throughout the CFB riser;
- Gas is plug flow with axial dispersion;
- Solid particles are completely mixed in CFB system;
- The influence of adsorption on the mass fluxes of gas and sorbent particle density are negligible;

In a stable continuous adsorption system, the solid-phase concentration is constant and the gas phase concentration is a function of bed height only. Considering a infinitesimal element of space in the CFB riser, the mass flows of adsorbate in the gas phase are:

Flow in: $U_g F C$

Flow out: $U_g F(C + \frac{dC}{dz} dz)$

Dispersion in: $- F[D_{gz} \varepsilon \frac{dC}{dz} + \frac{d}{dz}(D_{gz} \varepsilon \frac{dC}{dz})dz]$

Dispersion out: $- F D_{gz} \varepsilon \frac{dC}{dz}$

Adsorbed by adsorbent: $F \frac{6(1-\varepsilon)}{d_p} K(C - C_p^*)dz$

C_p^* is the gas phase concentration in equilibrium with the solid phase concentration of adsorbent particles in CFB riser. The mass balance for adsorbate in a differential element height of CFB riser gives:

$$\varepsilon D_{gz}\frac{d^2C}{dz^2}+[U_g+\frac{d(D_{gz}\varepsilon)}{dz}]\frac{dC}{dz}+\frac{6(1-\varepsilon)}{d_p}K(C-C_p^*)=0 \tag{7-1}$$

From the discussion of gas dispersion in CFB riser we know that the axial dispersion coefficient D_{gz} is a function of ε and is estimated by Li and Wu's relation.

$$D_{gz}=0.1953\varepsilon^{-4.1197} \qquad (\mathrm{m^2/s}) \tag{6-33}$$

Then the partial derivative of $(D_{gz}\varepsilon)$ can be written as:

$$\frac{d(D_{gz}\varepsilon)}{dz}=-3.12D_{gz}\frac{d\varepsilon}{dz} \tag{7-2}$$

The cross sectional averaged voidage is estimated by Kunii and Levenspiel's entrainment model.

$$\varepsilon=\varepsilon^*-(\varepsilon^*-\varepsilon_a)e^{-\alpha Z} \tag{5-44}$$

The partial derivative of ε is:

$$\frac{d\varepsilon}{dz}=a(\varepsilon^*-\varepsilon_a)e^{-az}=a(\varepsilon^*-\varepsilon) \tag{7-3}$$

With (7-2) and (7-3), equation (7-1) is then rewritten as:

$$\varepsilon D_{gz}\frac{d^2C}{dz^2}+[U_g-3.12aD_{gz}(\varepsilon^*-\varepsilon)]\frac{dC}{dz}+\frac{6(1-\varepsilon)}{d_p}K(C-C_p^*)=0 \tag{7-4}$$

The dimensionless form of (7-4) is:

$$\varepsilon D_{gz}\frac{d^2Y}{dz^2}+[U_g-3.12aD_{gz}(\varepsilon^*-\varepsilon)]\frac{dY}{dz}+\frac{6(1-\varepsilon)}{d_p}K(Y-Y^*)=0 \tag{7-5}$$

Characteristic voidage ε_a, ε^* and decay constant a are estimated with (5-38), (5-40) and (5-45) respectively. Y^* is the dimensionless gas phase concentration in equilibrium with the solid phase concentration q. The experimental results show that the equilibrium between gas and adsorbent has been established at the exit of the CFB riser. So we take the experimental measurement results of dimensionless gas phase concentration at the exit of CFB riser as Y^* to calculate the axial VOCs concentration distribution along the CFB riser. (7-5) is solved with boundary conditions:

$$\begin{aligned} &Y=1 \qquad at \qquad z=0\\ &Y=Y^* \qquad at \qquad z=H \end{aligned} \tag{7-6}$$

The axial concentration measurement along the CFB riser was performed with the same

gas detector by connecting it to seven gas sampling probes in turn from bottom to the top, which takes about 10~20 minutes. From the discussion of breaking through curve we know that, when the dimensionless time θ is less than 0.7, the solid phase concentration q shows liner increase with θ while the change of gas phase concentration is relatively small. We take these experimental results as from stable adsorption process in the considered time interval and compare them with the calculated results.

The numerical solutions of (7-5) at different operation time are presented together with experimental results in Fig. 7-2. It can be seen that the one dimensional adsorption model can describe the adsorption process inside the CFB riser with reasonable accuracy. The calculated and experimental results agreed well for Z>0.5m. But for Z<0.5m, the agreement are not so good and all the experimental results are little bit lower than the calculate values.

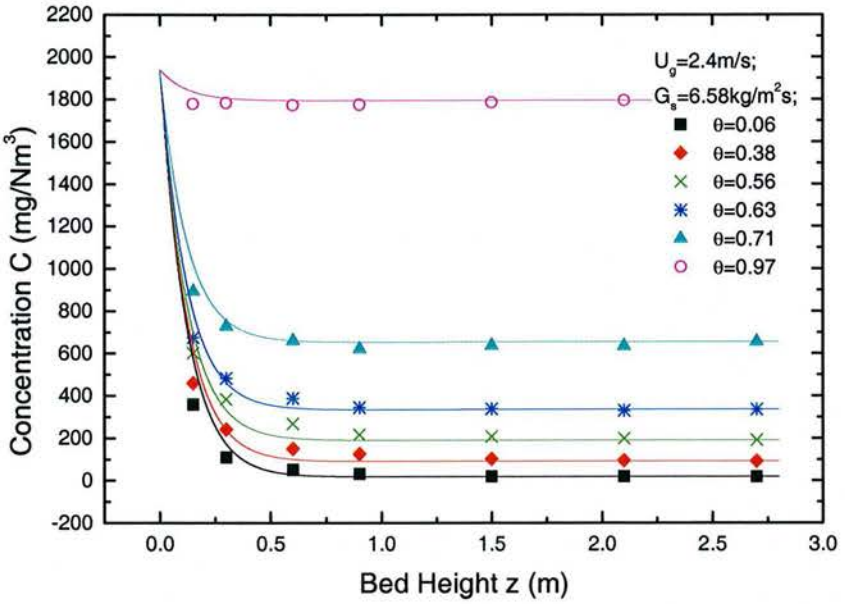

Fig. 7-2 Overall Mass Transfer Coefficient Distribution Along CFB Riser

The most possible reason for that is the underestimation of intraparticle mass transfer coefficient as it is the limiting step for this adsorption process. The intraparticle mass transfer coefficient is estimated with homogeneous pore structure assumption. But Ambersorb 600 adsorbent is produced by pyrolizing the small spherical resin beads and the resulting pore structure inside the particles may not be homogeneous, but heterogeneous. The mass transfer process in the radial direction may be faster than the other directions. So for a porous adsorbent, the intraparticle mass transfer coefficient is difficult to be accurately estimated and it should be measured whenever it is possible.

Both calculated and experimental results show that, the adsorption process for Ambersorb 600/toluene system is very faster. The concentration is significantly reduced

at the bottom of the CFB riser and then settled in less than 1.5 m bed height in all the experiments.

7.1.2. Simplified Analytical Solution

In the CFB riser the axial gas dispersion is relatively small. If we consider the gas is plug flow in the riser, or D_{gz}=0, (7-5) could be simplified as:

$$U_g \frac{dY}{dz} + \frac{6(1-\varepsilon)}{d_p} K(Y - Y^*) = 0 \tag{7-7}$$

From the discussion of mass transfer coefficient in chapter 6 we know that K is almost a constant along the CFB riser except at the very bottom of the bed. Here we take K as a constant and substitut Kunii and Levenspiel's entrainment model [55] for axial voidage distribution (5-44) into (7-7). The integration of (7-7) from z=0 to z=z gives:

$$\frac{Y - Y^*}{1 - Y^*} = EXP\{-\frac{6K}{d_p U_g}[(1-\varepsilon^*)z + \frac{1}{a}(\varepsilon^* - \varepsilon_a)(1 - e^{-az})]\} \tag{7-8}$$

The left hand side of equation (7-8) is the dimensionless residual concentration at bed height z. For a CFB riser, the bed voidage is determined by superficial gas velocity and solid circulating rate, and its value is between 0.8~0.98. So the dimensionless residual concentration distribution in CFB riser will be determined by the mass transfer coefficient K, superficial gas velocity U_g and solid circulating rate G_s.

(7-8) can be further simplified by assuming a constant bed voidage (averaged voidage in the riser ε_{av}) along the CFB riser. Then a much obvious relation between the dimensionless residual concentration and bed height is obtained:

$$\frac{Y - Y^*}{1 - Y^*} = e^{-\frac{6K}{d_p U_g}(1-\varepsilon_{av})z} \tag{7-9}$$

When the dimensionless residual concentration is 0.01, that is, 99% of possible concentration reduction is reached, the bed height is:

$$Z_{99\%} = \frac{d_p U_g \ln 100}{6K(1-\varepsilon_{av})} \tag{7-10}$$

So the required bed height for 99% of possible concentration reduction is proportional to the superficial gas velocity, and inversely proportional to the gas/solid mass transfer coefficient and averaged bed solid volume fraction. For a given superficial gas velocity, the solid circulation rate will determine the bed voidage in the CFB riser. Increasing the solid circulation rate will increase the adsorbent inventory in the CFB riser and decrease the voidage and also the required bed height.

7.1.3. Influence of Operation Conditions

The calculated results from numerical solution and from the simplified analytical solution are almost the same. This indicates that the influence of axial gas dispersion on the adsorption process in the CFB riser is very small and the gas could be considered as plug flow in the riser. As the analytical solution gives much clear relation between dimensionless residual concentration and the operation conditions, (7-8) is used in the following discussion and comparison with experimental results.

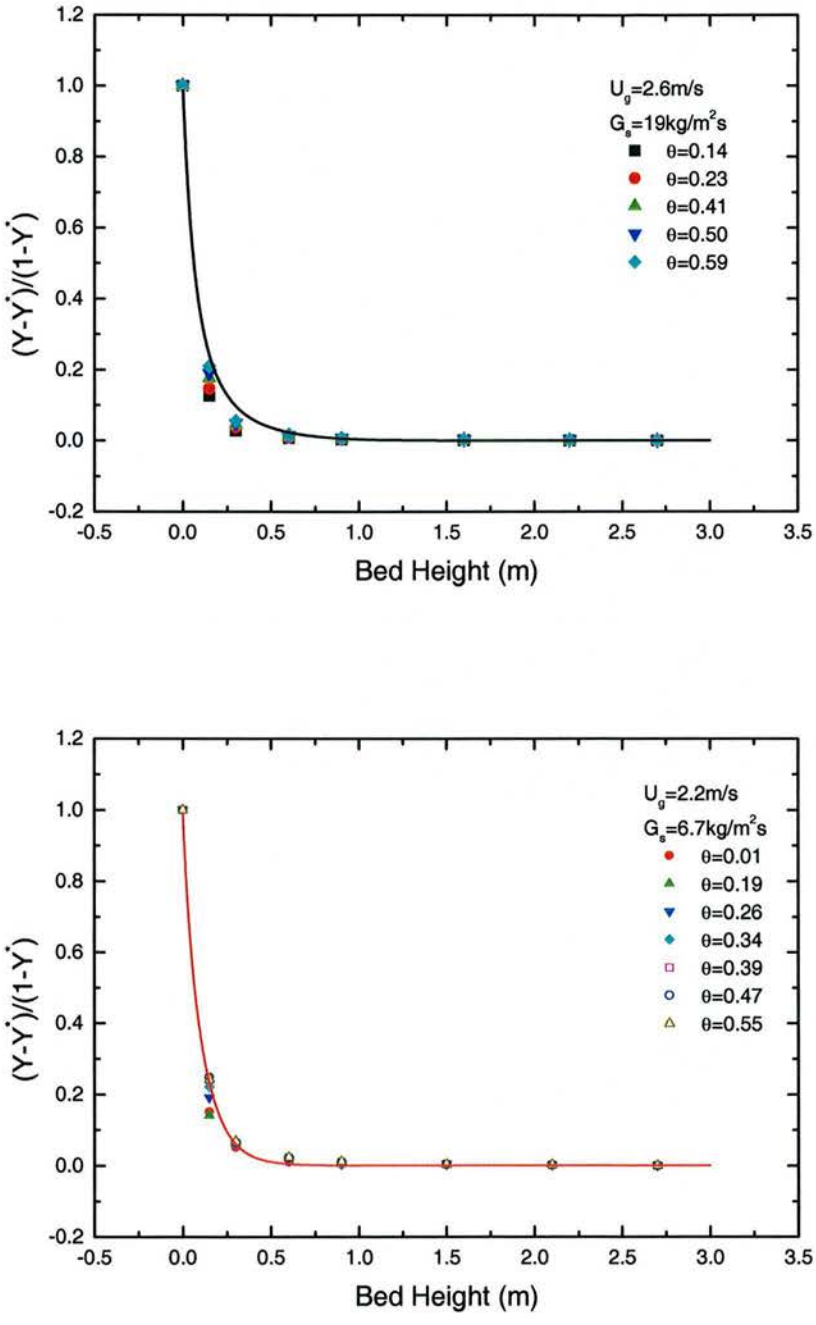

Fig. 7-3 Dimensionless Residual Concentration Distribution

Fig. 7-3 gives the calculated results of dimensionless residual concentration distribution from (7-8) with different solid phase concentrations. The experimental measurement results obtained from the batch-operation CFB adsorption experiments are also presented in the figure. As the adsorption experiment is an unsteady state process, the measurement results are taken from the early stage of test run ($\theta \leq 0.7$) when the change of exit gas-phase concentration with time is relatively small. It can be seen that the axial dimensionless residual concentration distribution with different Y^* can be represented by a same curve at specified U_g and G_s.

Fig. 7-4 shows the calculated and experimental results of residual concentration distribution with different superficial gas velocities. During the adsorption experiment, the superficial gas velocity was changed between 2.4~2.7 m/s while the solid circulation rate was kept almost the same (19kg/m^{2}s). Under this operation conditions, the influence of superficial gas velocity on the dimensionless residual concentration distribution is relatively small.

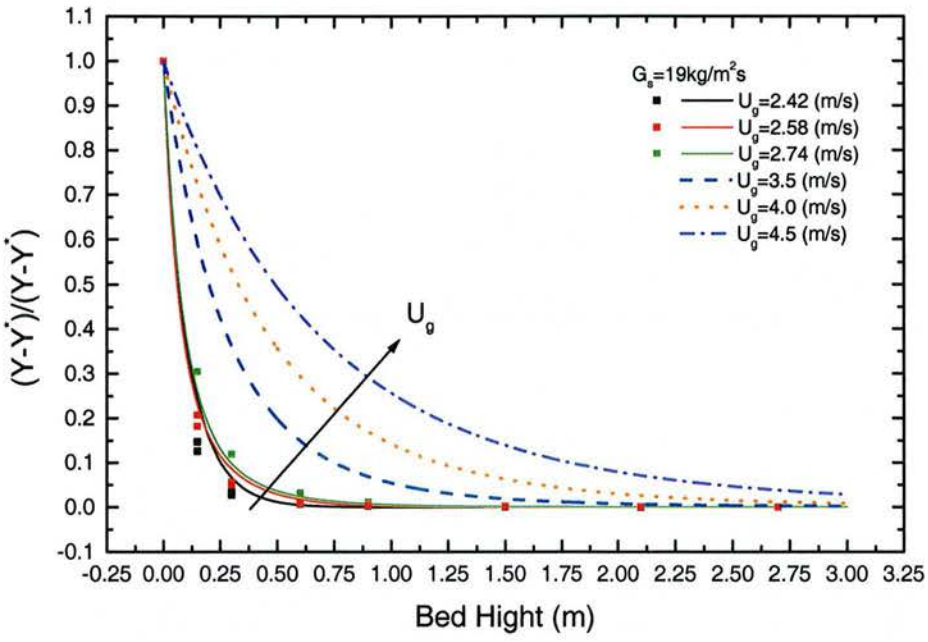

Fig. 7-4 Residual Concentration Distribution with Different Gas Velocities

The model predicted values for higher superficial velocities are also presented in Fig. 7-4. The results show that the superficial gas velocity has a strong influence on the adsorption process in CFB riser. The increase of U_g will increase the gas/solid mass transfer coefficient in the bed, this will result faster reduction of adsorbate concentration along the riser. On the other hand, the increase of U_g will also increase the mass flow rate of adsorbate and the voidage in the CFB riser, this will result in slow reduction of adsorbate concentration along the bed height. It is obvious that the latter influence is much bigger and the reduction of adsorbate concentration along the bed height is slower

for higher superficial gas velocities.

Fig. 7-5 shows the calculated results (line) of residual concentration distribution with different solid circulating rate. Experimental results (scatters) under three different solid circulating rates are also presented. Higher solid circulating rate will reduce the voidage and increase the adsorbent inventory in the CFB riser, resulting rapid VOCs concentration reduction along the bed height. The gas/solid mass transfer coefficient decreases with increasing solid circulating rate, but this influence is relatively small compared with the increase of adsorbent inventory.

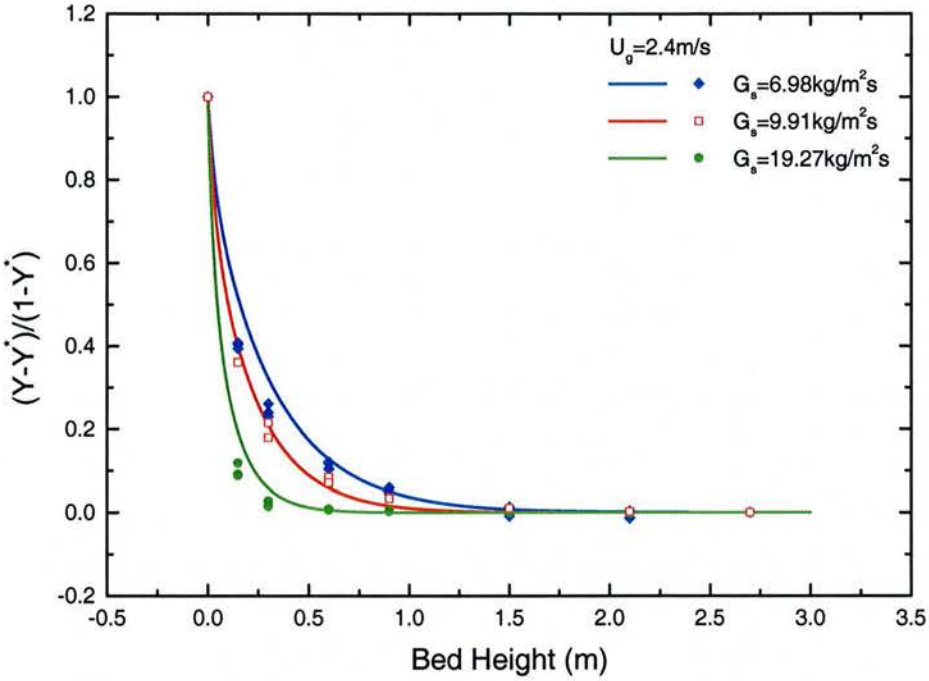

Fig. 7-5 Residual Concentration Distribution with Different Solid Circulating Rate

7.2. Design of CFB Adsorber (Riser)

7.2.1. Determination of Basic Parameters

The information needed in the design of a CFB riser adsorber including:

1 Gas flow rate Q_g;

2 Adsorption isotherm of adsorbate/adsorbent system, $q=f(T,C)$;

3 Initial gas phase VOCs concentration, C_{in};

4 Solid phase VOCs concentration of regenerated adsorbent, q_{in};

5 Outlet VOCs concentration, C_{out} ;

The superficial gas velocity U_g have to be determined first, it should be higher than the terminal velocity of the adsorbent particles u_t. Then, the diameter of the riser is determined from superficial gas velocity U_g and gas flow rate Q_g.

$$d_b = (\frac{4Q_g}{\pi U_g})^{1/2} \tag{7-11}$$

The solid phase VOCs concentration of adsorbent inside CFB riser q is determined by the required outlet VOCs concentration C_{out} with adsorption isotherm. The solid phase concentration of regenerated adsorbent q_{in} should be less than q. Then the minimum solid adsorbent re-circulating rate to the regenerator $W_{c\,min}$ could be obtained from the mass balance of adsorbate:

$$W_{c\min} = (C_{in} - C_{out})Q_g / (q - q_{in}) \tag{7-12}$$

The solid adsorbent re-circulating flow rate to the regenerator W_c is (1.1-1.2)$W_{c\,min}$. With U_g and other gas and solid physical properties, the saturation caring capacity G_s^* is thus determined by (5-35). As the principle of adsorber design is to use less adsorbent to process large quantity of gas, the solid circulating rate G_s should be less then G_{sat}. So the axial voidage distribution in CFB riser is exponential and could be estimated with Kunii and Levenspiel's entrainment model (5-44).

With the averaged bed voidage in CFB riser and mass transfer coefficient K determined in chapter 6, the minimum height of the riser could be estimated with (7-10). Generally higher superficial gas velocity would require higher CFB riser with small diameter. Lower superficial gas velocity will result short bed height with large bed diameter. This calculation process is repeated for different operation conditions to get suitable design.

7.2.2. Gas and Solid Efficiencies

In order to discuss the efficiencies of the adsorber, the gas phase efficiency η_g and solid phase adsorbent efficiency η_s of the adsorber are defined as:

$$\eta_g = \frac{amount\ \ of\ \ adsorbate\ \ actually\ \ given\ \ up\ \ by\ \ gas}{\max imum\ \ that\ \ could\ \ be\ \ given\ \ up} = \frac{C_{in} - C_{out}}{C_{in} - C_p^*} \tag{7-13}$$

$$\eta_s = \frac{amount\ \ of\ \ adsorbate\ \ adsorbed\ \ by\ \ adsorbent}{\max imum\ \ that\ \ could\ \ be\ \ adsorbed} = \frac{q_{out} - q_{in}}{q^* - q_{in}} \tag{7-14}$$

Kunii and Levenspiel discussed continuous fluidized bed adsorption process and point out that, for liner isotherm system, the solid phase efficiency is inversely proportional to the gas phase efficiency. For example, at 99% gas phase efficiency, the solid phase

efficiency is only 1%.

$(1-\eta_g)$ and η_s are actually the dimensionless gas and solid concentrations (Y, X) defined in the discussion of breakthrough curves if $q_{in}=0$. For Ambersorb 600/Toluene system, the relation between gas and solid efficiencies could be obtained from the adsorption isotherm. The result is presented in Fig. 7-6 together with that for linear isotherm system. It is obvious that, for the favorable isotherm system, the solid phase efficiency is much higher than that for liner isotherm system at the same gas phase efficiency. For Ambersorb 600/Toluene system, the solid phase efficiency is 56% at 99% gas phase efficiency.

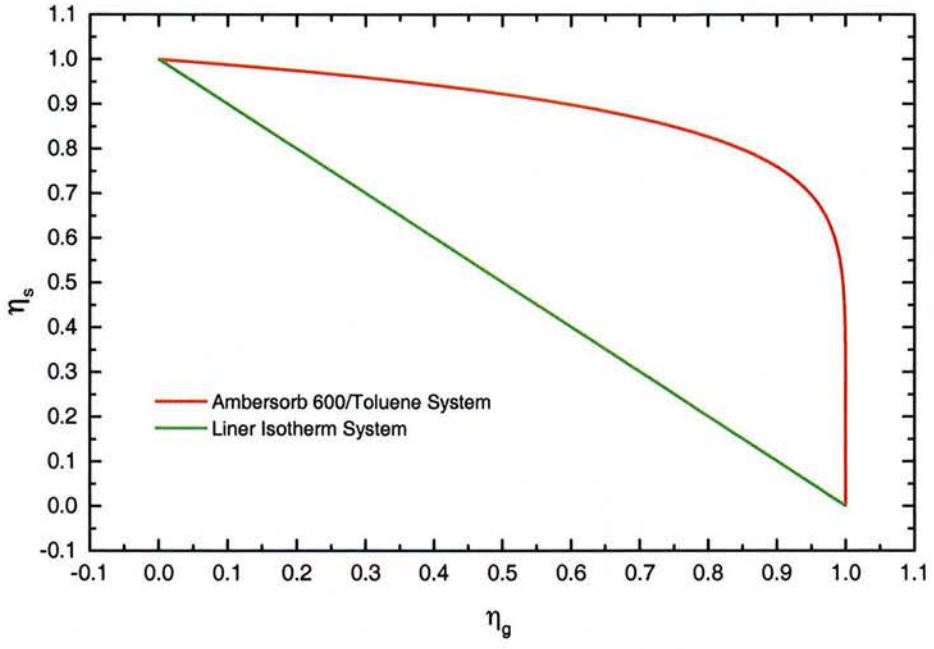

Fig. 7-6 Gas and Solid Efficiencies for different Systems

7.2.3. Multi Stage Adsorber

Fig.7-7 gives an example of operation line in a single stage CFB adsorber. The conditions for the calculation include: the gas flow rate Q_g=10000 Nm^3/h, the initial VOCs concentration C_{in}=2200 mg/Nm^3, the solid phase concentration of regenerated adsorbent q_{in}=10 mg/g. If we want to reduce the VOCs concentration in the gas down to 100 mg/Nm^3, then the maximum solid phase concentration in the CFB system q_1=80 mg/g and the required minimum solid adsorbent re-circulating rate to the regenerator W_c is 300 kg/h. At this operation conditions, the solid phase efficiencyη_s is 66% and the gas phase efficiencyη_g is 98.2%. If a lower outlet gas phase concentration is required, then a higher solid adsorbent re-circulating rate to the regenerator W_c have to be used and the solid phase efficiency will be much lower.

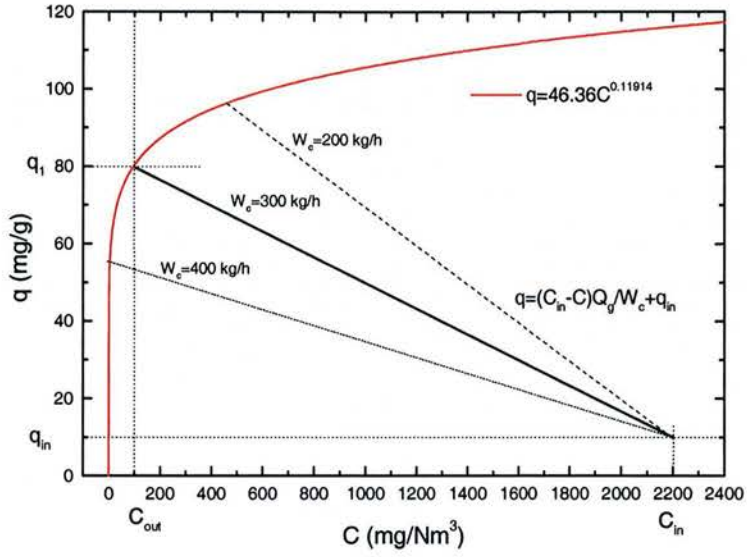

Fig. 7-7 Operation Line in CFB Adsorber

The operation lines for higher or lower W_c are also indicated in Fig. 7-7. It is obvious that, higher adsorbent re-circulating rate to the regenerator results lower outlet gas phase concentration

Though the solid phase efficiency of favorable isotherm system is much higher than that of linear isotherm system, we would like to get higher gas and solid phase efficiencies at the same time. In multi-stage CFB adsorber the overall counter-current flow between the gas and solids could be achieved, resulting higher solid phase efficiency and reduced adsorbent re-circulating rate to the regenerator.

Fig.7-8 shows a possible design of multi-stage CFB adsorber. Each stage CFB in the system is formed by two coaxial tubes. The inner tube acts as the CFB riser while the annulus between two tubes act as the storage and recirculation loop. An overflow tube is also used to control the bed height in the annulus and transport the adsorbent particles down to the next stage.

The regenerated adsorbent particles are added to the top stage CFB first. They will move downward passing through each stage of CFB while circulated

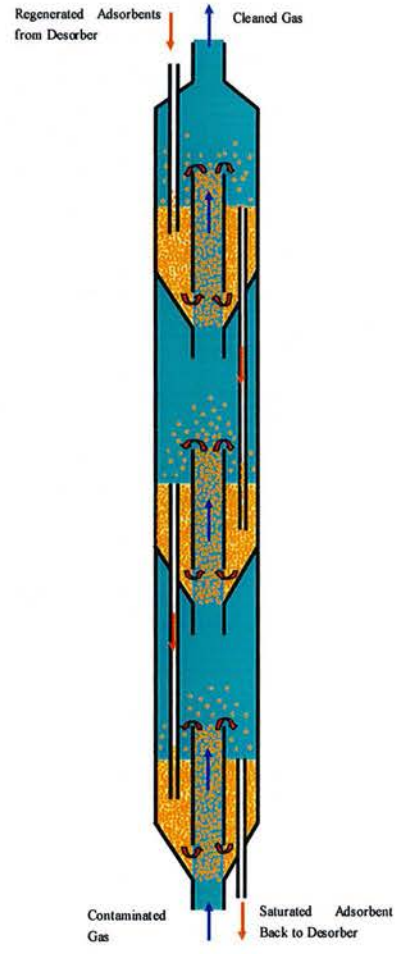

Fig. 7-8 Multi-stage CFB Adsorber

and stayed in each stage for a certain time. The saturated adsorbent is finally discharged from the bottom of the bed and fed back to the regenerator. The gas enters the bottom stage of CFB first and flows upward stage by stage. So the overall counter-current flow between gas and solids adsorbent is formed inside the adsorber.

Fig 7-9 shows the operation lines in a two-stage CFB adsorber. The operation conditions are the same as given in the example of single stage CFB adsorber and the same outlet gas phase VOCs concentration is required. The calculation results show that, the minimum solid adsorbent re-circulating rate to the regenerator W_c is 210 kg/h now. The solid phase efficiency is 95.3% while the gas phase efficiency is the same.

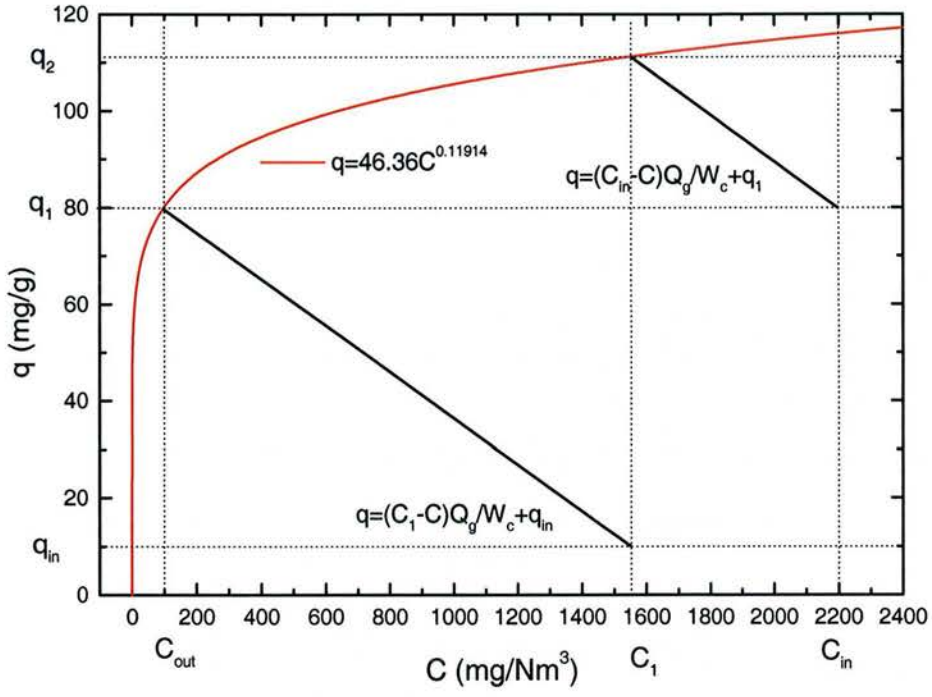

Fig. 7-9 Operation Lines in Two-stage CFB Adsorber

So the multi-stage system can increase the solid phase efficiency and reduce the solid adsorbent re-circulating rate to the regenerator.

7.3. Design of CFB Adsorption Process

For dilute VOCs control, the principle for the design of the adsorber is to use less quantity of adsorbent to process large quantity of gas. So it is suggested that the CFB riser should be operated under relatively dilute solid concentration conditions. The superficial gas velocity should be as high as possible to reduce the diameter of the adsorber. On the other hand, the CFB adsorber should not be very high.

For the design of desorber, the principle is to use less quantity of gas to process large quantity of adsorbent. So the desorber should be designed as a moving bed or bubble fluidised bed reactor.

The cleanup efficiency of the CFB adsorption process is controlled by the solid phase concentration of adsorbent in the CFB adsorber, which is determined by the initial solid phase concentration of regenerated adsorbent and the solid re-circulating rate to the regenerator.

7.3.1. CFB-PSA System

The CFB adsorption could be used for both pressure or temperature swing adsorption processes. This should be determined by the adsorption isotherm of the adsorbate/adsorbent system. The Pressure Swing Adsorption (PSA) process is normally used for steep isotherm system in the operation range and the Temperature Swing Adsorption (TSA) process is used for isotherm system with big temperature difference. Fig. 7-10 gives a conceptual design of CFB-PSA system.

For the CFB-PSA process, the CFB riser is used as the adsorber and operated under ambient temperature and pressure conditions while the desorber is kept at vacuum pressure. The special valves have to be used which can insulated the gas flow between the adsorber and desorber while let the solids passing through. Here a special valve, named Balloon Feeder, is used which is specially designed for CFB applications and can supple high pressure difference with lower solids attrition [74].

In this CFB-PSA system, the regenerated adsorbents are fed into the CFB riser at the bottom and becomes saturated when leaving the top of riser. The adsorbent is then separated from the gas and part of that is fed into the desorber through the Balloon Feeder. The adsorbent is regenerated in the desorber and the released adsorbate is drawn out of the desorber by a vacuum pump, which is then possible to be recovered or incinerated. The regenerated adsorbents come out of the desorber through another Balloon Feeder and re-circulated back to the adsorber.

The contaminated gas is introduced into the CFB riser from the bottom as the fluidizing gas and cleaned by the adsorbents while passing through the riser. The cleaned gas is vented out from the top after separated with the entrained particle by a gas-solid separator.

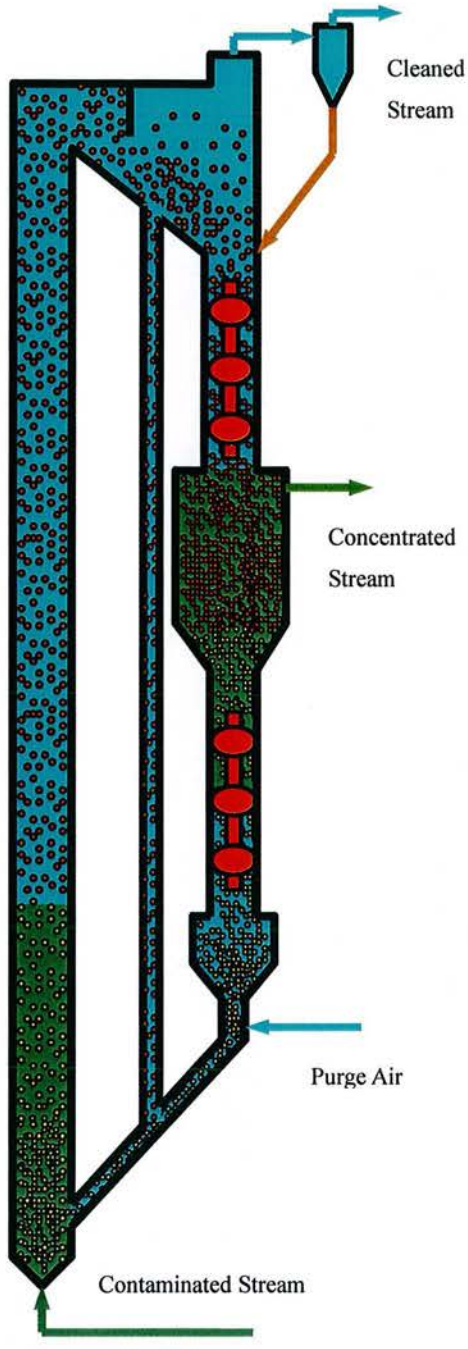

Fig. 7-10 CFB-PSA Process

7.3.2. CFB-TSA System

For the Temperature Swing Adsorption (TSA) process with circulating fluidized bed, the use of special valves is eliminated, but the adsorbent have to be heated up to get

desorbed and cooled down before fed back to the riser. If direct heating is used, steam is often used as heating source and purging gas. If indirect heating is used, a heater for heating up the adsorbent and a purge stream have to be used. Fig. 7-11 shows a possible design of CFB-TSA system.

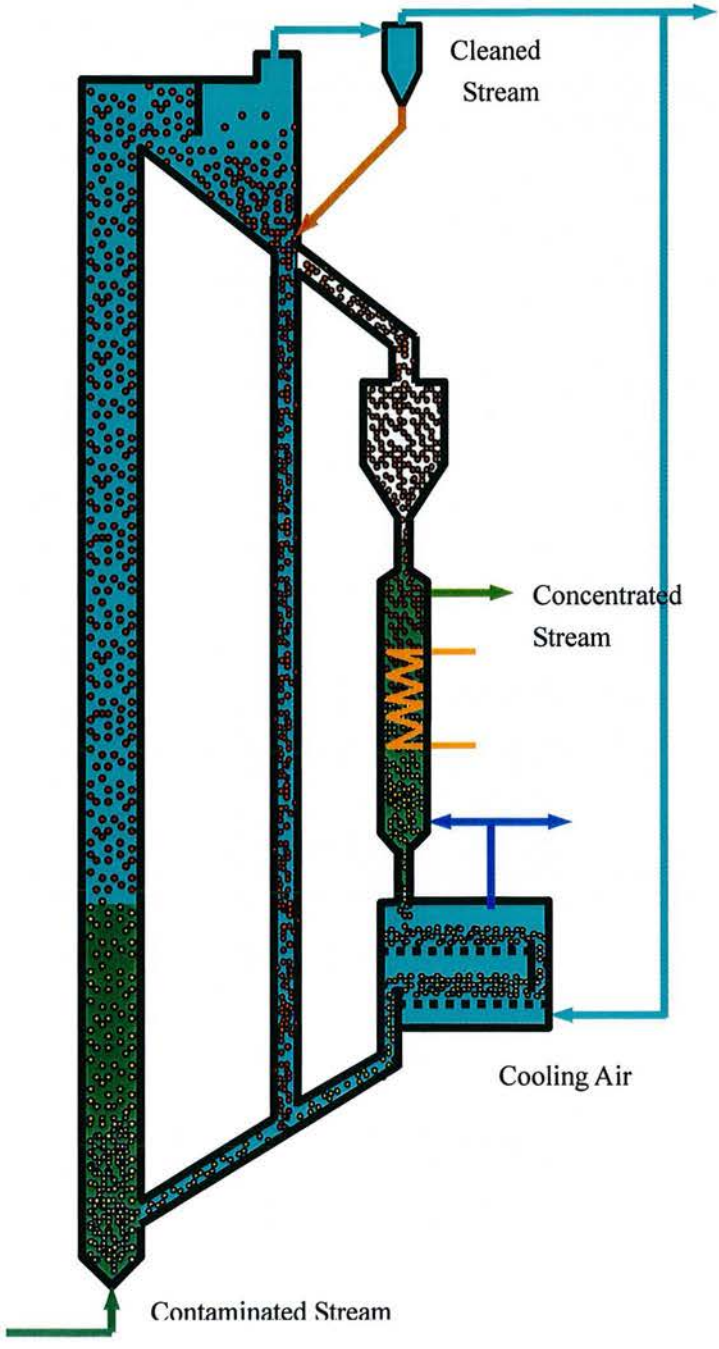

Fig. 7-11 CFB-TSA Process

The contaminated gas comes into the CFB riser from the bottom as the fluidizing gas and gets cleaned by the adsorbents while passing through the riser. The cleaned gas is

vented out from the top after separated with the entrained particle by a gas-solid separator.

In this design, the indirect heating is used. Regenerated adsorbents are feed into the CFB riser from the bottom and becomes saturated when out of the top of riser. The adsorbent is then separated from the gas and part of that is fed into the desorber. The adsorbent particles will release adsorbate in the moving bed desorber under higher temperatures and get regenerated. The Adsorbent particles are then cooled down in a multi-stage bubbling fluidized bed cooler and circulated back to the adsorber. The purge air, which could be part of the cooling air, will bring the released adsorbate out of the desorber. So a concentrated stream is obtained for further processing.

7.4. Conclusions

- The developed one dimensional adsorption model can describe the adsorption process inside the CFB riser with reasonable accuracy. The simplified analytical solution gives the same result and reveals an insight into the relation between dimensionless residual concentration and the operation conditions.
- The axial dimensionless residual concentration distribution with different Y^* can be represented by a same curve at specified U_g's and G_s's. Higher solid circulating rate and lower superficial velocity result in faster reduction of adsorbate concentration along the riser.
- For single stage CFB adsorber, the solid phase efficiency for favorable isotherm system is much higher than that for liner isotherm system at the same gas phase efficiency. For Ambersorb 600/Toluene system, the solid phase efficiency is 56% at 99% gas phase efficiency. Multi-stage system can increase the solid phase efficiency and reduce the solid adsorbent re-circulating rate to the regenerator.
- The design procedures for the CFB adsorber are discussed; conceptual designs of CFB-PSA system and CFB-TSA system are also proposed.

8. CONCLUSIONS AND PROSPECTS

In this study, the topics concerning the CFB adsorption process have been discussed, including adsorption isotherm of adsorbate/adsorbent system; hydrodynamics of gas and solid adsorbent particles in CFB riser, mass transfer between gas and solid adsorbent and adsorption process inside the CFB riser. The main conclusions include:

- The isotherm measurements have been performed for Ambersorb 600/Toluene system at different concentrations and temperatures. Micropore filling mechanism is much more suitable to explain the adsorption behavior of the system. Dubinin-Astakhov equation can be used to describe the adsorption isotherm over the experimental concentration range. The parameters in D-A equation are W_0=0.21×10^{-3} m^3/kg, E_0=17.206 kJ/mol and m=1.17. The isosteric heat is 65.15kJ/mol.

- A batch operation experimental unit is constructed and CFB adsorption experiments have been conducted with different superficial gas velocities, solid circulating rates, gas phase concentrations, fresh and regenerated adsorbent. The study of breakthrough curve shows that, the solid adsorbent particles in the system are well mixed and the gas phase concentration at the exit can be considered as in equilibrium with the solid adsorbent in the system. The solid phase concentration shows liner increase with time when stoichiometric time $\theta<0.7$ while the change of gas phase concentration is much small.

- The EMMS model is modified to include the interaction between dilute particles and dense clusters, resulting in a more reasonable cluster velocities in the CFB riser. While using EMMS model as a local model to describe hydrodynamics at each cross section in the riser, all gas and solid velocities and slip velocities in the dilute phase, cluster phase and between the phases can be obtained. A one-dimensional hydrodynamics model is constructed by combining the local EMMS model and Kunii and Levenspiel's entrainment model for axial voidage distribution. This enables the EMMS model to describe the hydrodynamics of the CFB riser with exponential voidage distribution. The agreement between the calculated results from the one-dimensional model and the results from experimental measurements are reasonable for axial voidage distribution.

- Based on the compartmentalization of two phases of EMMS model, a multi-scale mass transfer model is constructed to estimate the external mass transfer between gas and solid particle in CFB riser. The calculated results shows that the formation of clusters is the main reason for the lower mass transfer coefficient between gas and solid particles. This coefficient is higher for higher superficial gas velocity and

lower solid circulation rate. The study on intraparticle mass transfer shows that, the difference between external and intraparticle mass transfer coefficients is less than one order, while the value of intraparticle mass transfer coefficient is relatively small under experimental conditions.

- The developed one dimensional adsorption model can describe the adsorption process inside the CFB riser with reasonable accuracy. The axial dimensionless residual concentration distribution with different Y* can be represented by a same curve at specified U_g and G_s. Higher solid circulating rate and lower superficial velocity result in faster reduction of adsorbate concentration along the riser.

- The solid phase efficiency for favorable isotherm system is much higher than that for liner isotherm system at the same gas phase efficiency. For Ambersorb 600/Toluene system, the solid phase efficiency is 56% at 99% gas phase efficiency. Multi-stage system can increase the solid phase efficiency; reduce the adsorbent regeneration re-circulating rate and the loading of regenerator. The design procedures for the CFB adsorber are discussed; the possible designs of CFB-PSA system and CFB-TSA system are also presented.

Until now, the understanding about the gas and solid hydrodynamics in CFB riser is far from satisfactory. The knowledge about the transfer and adsorption process in CFB is even less. This study is only a preliminary research on the gas/solid flow, mass transfer and adsorption process in CFB. For this study, tasks that may be further studied include:

- In the discussion of local EMMS model, we assume that the voidage in the cluster phase is the same as that at minimum fluidization. This assumption is not so sound. A much reasonable assumption is that, the real slip velocity between gas and particle in the dilute phase is the terminal velocity of the particle. Then the voidage in the clusters could be obtained from the EMMS model, and also the influence of operation variables. The difficult issue for doing this is the solution of EMMS model will be much complicated.

- During the calculation of one-dimensional model, it is found that the solution of EMMS model can only obtained if the cross sectional averaged voidage ε is not far from the ε values obtained in the experiments. That is to say ε is not independent on operation conditions (superficial gas velocity, solid circulating rate). From EMMS model we may find the variation range of ε in the CFB riser with specified conditions. So what else could be obtained from the EMMS model should be further studied.

- In the study of external gas/solid mass transfer, we assume the gas phase VOCs concentrations in the cluster and diluter phase are the same. This assumption may be reasonable for the adsorption process studied here as the intraparticle mass transfer process is the limiting step. In most CFB reactors the gas phase concentration in the cluster and diluter phase are different. So the established mass transfer model is not complete. If the mass transfer between cluster and diluter gas is considered, the

berry issue is how to evaluate the influence of dynamic change of clusters on this mass transfer process.

- Until now we only gives a one dimensional description of VOCs adsorption process inside CFB. The two dimensional experimental study and modeling should also be conducted to get a much insight understanding of the adsorption and mass transfer process inside the CFB riser.
- This work only studied the adsorption process inside CFB riser. To give a complete evaluation of CFB adsorption process for VOCs emission control, the study for desorption process in moving bed or bubble fluidized bed reactors should be conducted.

NOMENCLATURE

a	Decay constant,
A	Adsorption Potential, (J/mol)
A_r	Archimedes number
C	Gas phase adsorbate concentration, (mg/Nm^3)
C_c	Gas phase adsorbate concentration in cluster phase, (mg/Nm^3)
C_d	Gas phase adsorbate concentration in dilute phase, (mg/Nm^3)
C_D	Drag coefficient,
C_{Dc}	Drag coefficient of particle in cluster phase,
C_{Dd}	Drag coefficient of particle in dilute phase,
C_{Di}	Drag coefficient of cluster,
C_{Dp}	Effective drag coefficient of coarse particle,
C_{in}	Inlet gas phase adsorbate concentration, (mg/Nm^3)
C_{out}	Outlet gas phase adsorbate concentration, (mg/Nm^3)
C_p^*	Gas phase concentration in equilibrium with solid phase concentration, (mg/Nm^3)
C_s	Adsorbate gas phase concentration at the outside surface of adsorbent particle, (mg/Nm^3)
C_{sat}	Saturation concentration of adsorbate vapor at temperature T, (mg/Nm^3)
D	Diffusion coefficient, (m^2/s)
D_b	The inside diameter of CFB riser, (m)
D_e	Effective intraparticle diffusion coefficient, (m^2/s)
$D_{e,m}$	Effective molecule diffusion coefficient, (m^2/s)
D_{gz}	Axial gas dispersion coefficient, (m^2/s)
D_k	Knudson diffusion coefficient, (m^2/s)
D_m	Molecule diffusion coefficient, (m^2/s)
D_p	Pore diffusion coefficient, (m^2/s)
$D_{p,e}$	Effective pore diffusion coefficient, (m^2/s)
D_s	Surface diffusion coefficient, (m^2/s)
$D_{s,e}$	Effective surface diffusion coefficient, (m^2/s)
d_c	Cluster diameter, (m)
d_p	Adsorbent particle diameter, (m)
E_0	The characteristic energy of reference adsorbate, (J/mol)
F	Cross sectional area of CFB riser (m^2)
F_{downer}	Cross sectional area of CFB downer (m^2)

F_c Force exited on a particle in cluster phase (N)

F_d Force exited on a particle in dilute phase (N)

F_i Force exited on a cluster (N)

F_{ig} Force exited on a cluster by gas (N)

F_{ip} Force exited on a cluster by particles (N)

F_r Froude Number

f Cluster phase volumetric fraction

G Adsorbent inventory in the system, (kg)

G_1 Adsorbent inventory in the CFB riser, (kg)

G_2 Adsorbent inventory in the re-circulating loop, (kg)

G_s Solid circulation rate, (kg/m^2s)

G_s^* Saturation caring capacity of the gas, (kg/m^2s)

H Height of CFB riser, (m)

ΔH Isosteric heat of adsorption, (J/mol)

ΔH_{vap} Heat of vaporization, (J/mol)

J Total mass transfer rate between gas and solid particle, (kg/m^3s)

J_c Mass transfer rate between gas and solid particle in cluster phase, (kg/m^3s)

J_d Mass transfer rate between gas and solid particle in dilute phase, (kg/m^3s)

K Overall mass transfer coefficient, (m/s)

K_p Intraparticle mass transfer coefficient, (m/s)

k_L Langmuir constant, (Nm^3/mg)

k_F Frendlich constant,

k_g External mass transfer coefficient between gas and solid particle, (m/s)

$k_{g,c}$ Mass transfer coefficient in cluster phase, (m/s)

$k_{g,d}$ Mass transfer coefficient in dilute phase, (m/s)

M Molecule weight, (g/mol)

m_c Number of particles in unit volume of cluster phase, (m^{-3})

m_d Number of particles in unit volume of dilute phase, (m^{-3})

m_i Number of clusters in unit volume of bed, ($1/m^3$)

N_{st} Energy required for suspending and transporting unit mass of solid, (J/kg s)

N_T Total energy consumption per unit mass of solids, (J/kg s)

N_d Energy dissipated in particle collision per unit mass of solid, (J/kg s)

Nu Nusselt number,

P Pressure, (Pa)

P_{sa} Vapor equilibrium pressure, (Pa)

Pr Prandtl number

ΔP_c	Pressure drop that gas flow through the particles in dense phase (N/m^3)
ΔP_d	Pressure drop that gas flow through the particles in dilute phase (N/m^3)
ΔP_i	Pressure drop that the gas passing between clusters (N/m^3)
Q	Heat of adsorption, (J/mol)
Q_g	Gas flow rate (Nm^3/h)
q	Solid phase adsorbate concentration, (mg/kg)
q_{in}	Inlet solid phase adsorbate concentration, (mg/kg)
q_m	Maximum solid phase adsorbate concentration, (mg/kg)
q_{out}	Outlet solid phase adsorbate concentration, (mg/kg)
q^*	Solid phase concentration in equilibrium with inlet gas phase concentration, (mg/kg)
R	Gas constant, (J/mol K)
Re	Reynolds number,
r_p	Pore radius, (m)
Sc	Schmidt numbers,
Sh	Sherwood number,
T	Temperature, (K)
t	Time, (s)
t*	Stoichiometric breakthrough time, ($t^*=Gq^*/Q_gC_i$), (s)
U_g	Superficial gas velocity, (m/s)
U_{gc}	Superficial gas velocity in cluster phase, (m/s)
U_{gd}	Superficial gas velocity in dilute phase, (m/s)
U_{mf}	Minimum fluidization velocity, (m/s)
U_p	Superficial solid particle velocity, (m/s)
U_{pc}	Superficial solid particle velocity in cluster phase, (m/s)
U_{pd}	Superficial solid particle velocity in dilute phase, (m/s)
U_{sc}	Superficial slip velocity between gas and particle in cluster phase, (m/s)
U_{sd}	Superficial slip velocity between gas and particle in dilute phase, (m/s)
U_{si}	Superficial slip velocity between dilute gas and cluster, (m/s)
u_t	Terminal velocity of particle, (m/s)
V	Volume, (m^3)
w	Weight, (kg)
w_r	Weight of reading, (kg)
W	The volume that the adsorbate occupied in adsorbent, (m^3/kg)
W_0	The maximum volume the adsorbate can occupy, (m^3/kg)
W_c	Solid adsorbent re-circulating flow rate to the regenerator, (kg/h)
X	Dimensionless solid phase concentration, ($X=q/q^*$)
Y	Dimensionless gas phase concentration, ($Y=C/C_{in}$)

Y^* Dimensionless gas phase concentration in equilibrium with solid phase concentration, (C_p^*/C_i)

Z Characteristic length, (m)

Greek symbles

β The similarity coefficient,

δ Temperature variance of relative saturation adsorption capacity, (1/T),

ε Cross sectional averaged voidage in CFB riser,

ε_a Cross sectional averaged voidage at the bottom of CFB riser,

ε_b Averaged bed voidage in CFB riser,

ε_c Bed voidage in cluster phase,

ε_d Bed voidage in dilute phase,

ε_{mf} Bed voidage at minimum fluidization,

ε_p Particle voidage,

ε_{uni} Voidage of homogeneous suspension system,

ε^* Characteristic voidage,

η_g Gas phase efficiency

η_s Solid phase efficiency

θ Dimensionless time, ($\theta=t/t^*$)

μ_g Gas viscusity

ρ_{ad} Adsorbate liquid density, (kg/m^3)

ρ_g Gas density, (kg/m^3)

ρ_m Molecule density, ($kmol/m^3$)

ρ_p Adsorbent particle density, (kg/m^3)

τ Tortuosity

REFERENCES

[1] COUNCIL DIRECTIVE 1999/13/EC of 11 March 1999 on the Limitation of Emissions of Volatile Organic Compounds due to the Use of Organic Solvents in Certain Activities and Installations.

[2] Khan, F. I., Ghoshal, A. K., Removal of Volatile Organic Compounds from Polluted Air, Journal of Loss Prevention in the Process Industries, 2000, 13: 527-545.

[3] Y. Yan, VOCs Cleanup and Recover from Exhaust Gases – Carbon Adsorption and Membrane Separation, Chemical Engineering Advance (in Chinese), 1996, (5): 26-28.

[4] Air Emissions in France, Centre Interprofessionnel Technique d'Etudes de la Pollution Atmospherique, www.citepa.org, 18 April, 2002.

[5] Rowson, H. M., Fluid Bed Adsorption of Carbon Disulfide, British Chemical Engineering, 1963, Vol.8 (3): 180.

[6] Wang, Y., Yong, J. and Kwauk, M., Challenges in Fluidization, In Fluidization'85, Science and Technology, (Eds. Kwauk, M. and Kunii D.), Science Press, Beijing, 1985. 11.

[7] Jin, Y., Zhu, J., Wang, Z., Yu, Z., Fluidization Engineering Principles (in Chinese), Tsinghua University Press, Beijing, 2001.

[8] Keller II, G. E., Adsorption: Building Upon a Solid Foundation. Chemical Engineering Progress, 1995, Vol. 91(10): 56-67.

[9] Danielsson, M. A. and Hudon, V., VOC Emission Control Using a fluidized-Bed Adsorption system. Metal Finishing, 1994, Vol. 92 (6): 89-91.

[10] Slay, J., Goltz, R., Rainwater, B. and Danielsson, M., Volatile Organic Compound Emission Control Using a Fluidized Bed Adsorption System, International Environmental Conference Vol. 2, 1996, TAPPI Press, 1996, Norcross, GA, USA. 601-606.

[11] Biedell, E. L., Hybrid VOC Control Technology Offers Best of Both Worlds, Metal Finishing, 1997, Vol. 95 (11): 24-26.

[12] Cowles, H. and Borenstein, N., Continuous VOC reduction in a fluidized bed adsorber using a new carbonaceous adsorbent, Proceedings of the Air & Waste Management Association's Annual Meeting & Exhibition 1996, Air & Waste Management Assoc, Pittsburgh, PA, USA. 96-TA4B.021996, 15.

[13] Kajiyama, R., Yoyama, T., Inaba, R., Takatsuka, T. and Shibagaki, T., CFB-PTSA Process for Recovering CO_2 From Power Plant Flue Gas, in Proceedings of 4th International Conference on Circulating Fluidized Beds. (A. A. Avidan Ed.), 1993, 478-483.

[14] Pugsley, T. S., Berruti, F. and Chakma, A., Computer Simulation of a Novel Circulating Fluidized Bed Pressure-Temperature Swing Adsorber for Recovering Carbon Dioxide From Flue Gases, Chemical Engineering Science, Dec. 1994, Vol. 49(24A): 4465-4481.

[15] Yang, R. T., Gs Separation by Adsorption Process, Butterworth Publisher, 1987.

[16] Duong, D. Do., Adsorption Analysis: Equilibria and Kinetics, Imperial College Press, 1998.

[17] Zelodowitsch, J. B., Acta Physicochim. USSR, 1935,1, 961.

[18] Urano, K., Koichi, Y. and Nakazawa, J., Journal of Colloid and Interface Science, 1981, Vol.79: 136.

[19] Bering, B. P., Dubinin, M. M. and Serpinsky, V. V., Journal of Colloid Interface Sciences, 1966, Vol. 21: 378-393.

[20] Bering, B. P., Dubinin, M. M. and Serpinsky, V. V., Journal of Colloid Interface Sciences, 1972, Vol. 38: 185.

[21] Comles, H. And Borenstein, N., Continuous VOC Reduction in a Fluidized Bed Adsorber Using a New Carbonceous Adsorbent, 89th Annual Meeting & Exhibition, Air & Waste Management Association, 96-TA4B.02, 1996.

[22] Data Compilation of Pure Compound Properties, Version 9.02, NIST Standard Reference Database 11, Design Institute fpr Physical Property Data (DIPPR) of the AIChE, Gaitherburg, Maryland.

[23] Operating Instructions-Magnetic Suspension Balance, RUBOTHERM.

[24] Choung, J., Lee, Y., Choi, D. and Kim, S., Adsorption Equilibria of Toluene on Polymeric Adsorbents, J. Chem. Eng. Data, 2001, Vol. 46: 954-958.

[25] Kitagawa, H. and Suzuki, K., Fundamentals and Design of Adsorption Process (in Japanese), 1977.

[26] Ye, Z., Adsorption and Separation Process in Chemical Engineering (in Chinese), China Petrochemical Press, Beijing, 1992.

[27] Kunii, D. and Levenspiel, O., Fluidization Engineering, John Wiley & Sons, New York, 1969.

[28] Reh, L., Fluidized Bed Processing. Chem. Eng. Prog., 1971, Vol. 67 (2): 58.

[29] Yerushalmi, J., Turner, D. H., Squires M., The Fast Fluidized Bed, Ind. Eng. Chem. Pro. Des. Dev, 1976, Vol. 15 (1): 47.

[30] Geldart, D., Types of Gas Fluidization, Powder Technology, 1973, Vol. 7 (5): 285-292.

[31] Berggren, J. C. , Bjerle, I., Eklund, H. , Karlsson, H. and Svensson, O., Application of Chemical and Physical Operations in a Circulating Fluidized Bed System, Chemical Engineering Science, 1980, Vol.35 (1-2): 446-455.

[32] Schiller, V. L. & Naumann, A., Uber die Grundlegenden Berechnungen bei der Schwerkraftaufbereitung, Z. Ver. Dtsch. Ing., 1933, Vol. 77: 318-320.

[33] Wen, C. Y. & Yu, Y. H., Mechanics of Fluidization, Chemical Engineering Progress Symposium Series, 1966, Vol. 66: 100-111.

[34] Li, J., Multi-scale Modeling and Method of Energy Minimization in Two-phase Flow (in Chinese), Ph.D. Dissertation, Institute of Chemical Metallurgy, Chinese Academy of Sciences, Beijing 1987.

[35] Li, J. and Kwauk, M., Particle-Fluid Two-Phase Flow. (The Energy - Minimization Multi-Scale Method). Beijing: Metallurgical Industry Press, 1994. 50-55.

[36] Arastoopour, H., Wang, C. and Weil, S. A., Particle-Particle Interaction Force in a Dilute Gas-Solid System, Chemical Engineering Science, 1982, Vol. 37 (9): 1379-1386.

[37] Matsen, T. M., Mechanisms of Choking and Entrainment. Powder Technology. 1982, Vol. 32(1): 21-33.

[38] Lasdon, L. S., Waren, A. D., Jain, A. and Ratner, M., Design and Testing of a GRG code for Nonlinear Optimization, in "ACM Transactions on Mathematical Software," 1978, Vol. 4 (1): 34.

[39] Cheng, C., Energy Minimized Multi-Scale Core-Annual Model for Circulating Fluidized Bed (in Chinese). Ph.D. Dissertation□Institute of Process Engineering, Chinese Academy of Sciences□Beijing, 2001.

[40] Li, Y., Kwauk, M., The Dynamics of Fast Fluidization. In: Fluidization-III, (Eds. Grace, J. and Matsen, J. M.), Plenum Press, 1980. 537

[41] Brereton, C., Stromberg, L., Some Aspects of the Fluid Dynamic Behavior of Fast Fluidized Beds. In: Circulating Fluidized Bed Technology, (Ed. Basu, P.), Halifax, Pergamon Press, 1985. 133.

[42] Bai, D., Jin, Y., Yu, Z., and Zhu, J., The Cross-sectional Averaged Voidage Profiles in Fast Fluidized Bed, Powder Technology, 1992, Vol. 71 (1): 51-57.

[43] Jing, Y., Yu, Z., Qi, C., Bai, D., The influence of exit Structures on the axial Distribution of Voidage in Fast Fluidized Bed, In: Fluidization 88 - Science and Technology, (Eds. Kwauk, M. and Kunii, D.), Science Press, Beijing, 1988, 165.

[44] Weinstein, H., Graff, R. A., Meller, M., Shao, M. J., The Influence of the Imposed Pressure Drop Across a Fat Fluidized Bed. In: Fluidization IV, (Eds. Kasikojima, Kunii, D. and Toei, R.), Japan, 1983. 299.

[45] Li, J. and Weinstein, H., An Experimental Comparison of Gas Backmixing in Fluidized Beds Across the Regime Spectrum. Chem. Eng. Sci., 1989, Vol. 44(8): 1697 - 1704.

[46] Gao, S., Solid Circulating Rate and Axial Voidage Distribution in Fast Fluidized Bed (in Chinese). M.S. Dissertation□Shenyang Research Institute of Chemical Industry, Shenyang, 1990.

[47] Yang, G. L. and Sun, J. K., Transition of flow Regime from Turbulent to Fast Fluidization and from Fast to Dilute Phase Transport, In: Fluidization'91 – Science and Technology, (Eds. Kwauk, M. and Hasatani, M.), Science Press, Beijing, 1991, 37.

[48] Bai, D. and Kato, K., Saturation Carrying Capacity of gas and Flow Regimes in CFB, J. Chem. Eng. Japan, 1995, 28: 179.

[49] Flemmer, R. L. C. and Banks, C. L., On the Drag Coefficient of a Sphere, Powder Technology, 1986, Vol. 48(3): 217-221.

[50] Adanez, J., Gayan, P., Garcia-Labiano, F. and L. F. de Diego, Axial Voidage Profiles in Fast Fluidized Bed, Powder Technology, 1994, Vol. 81 (3): 259-268.

[51] Venderbosh,R. H., Prins, W., Van Swaaij, W. P. M., "Mass Transfer and Influence of the Local Catalyst Activity on the Conversion in a Riser Reactor", The Canadian Journal of Chemical Engineering, 1990, Vol. 77: 262-274

[52] Vollert, J., and Werther, J., "Mass Transfer and Reaction Behaviour of a Circulating Fluidized Bed Reactor", Chem. Eng. Technol. 1994, 17: 201-209

[53] Van der Ham, A. G. J., Prins, W., Van Swaaij, W. P. M., A Small-Regularly Packed Circulating Fluidized Bed, Part 2: Mass Transfer. Powder Technology, 1994, Vol. 79(1): 29-41

[54] Ranz, W. E., Mashall, W. R., Evaporation of Drops. Chem. Eng. Progr., 1952, Vol. 48: 141-146, 173-180

[55] Kunii D, Levenspiel O. Chapter 11: Particle-to-Gas Heat and Mass Transfer. Fluidization Engineering (2nd edition). New York: Wiley, 1991, 257-276

[56] Halder, P. K. and Basu, P., Mass Transfer From A Coarse Particle To A Fast Bed Of Fine Solids, Fluidization Engineering: Fundamentals and Application, AIChE Symposium Series, 1988, 58-67.

[57] Suzuki, Motoyuki, Adsorption Engineering, Kodansha Ltd., TOKYO, 1990.

[58] Satterfield, C. N., Mass Transfer in Heterogeneous Catalysis; Robert E. Krieger: Huntington, NY, USA, 1981.

[59] Maxwell, J. C., Electricity and Magnetism, 2nd ed., Clarendon Press, Oxford. 1892.

[60] Gilliland, E. R., Baddour, R.F., Parkinson, G..P. and Sladek, K.J., Diffusion on Surface. I. Effect of Concentration on Diffusivity of Physically Adsorbed Gases, Ind. Eng. Chem. Fundam. 1974, Vol. 13 (2): 95-99

[61] Sladek, K. J., Gilliland, E.R. and Baddour, R.F., Diffusion on Surface. II. Correlation of Diffusivities of Physically ad Chemically Adsorbed Species, Ind. Eng. Chem. Fundam. 1974, Vol. 13 (2): 100-105.

[62] Van Zoonen, D. Measurements of Diffusional Phenomena and Velocity Profiles in a Vertical Riser, in Proc. Symp. On The Interaction Between Fluids and Particles, Instn. Chem. Engrs., London, 1962, 64-71.

[63] Brereton, C.M.H., Grace, J.R., and Yu, J., Axial Gas Mixing in a Circulating Fluidized Bed, in Circulating Fluidized Bed Technology IV (Ed. Avidan, A.), AIChE, New York, 1998, 137-144.

[64] Li, Y. And Wu, P., A Study on Axial Gas Mixing in a Fast Fluidized Bed, in Circulating Fluidized Bed Technology III, (Ed. Basu, P., Horio, M. and Hasatani, M.), Pergamon Press, Oxford, 1991, 581-586.

[65] Potter, O.E., Mixing, in Fluidization, Chapter 7 (Eds. Davison, J. F. and Harrison, D.), Academic Press, London, 1971, 293- 381.

[66] Van Deemter, J. J., Mixing, in Fluidization, 2nd ed., Chapter 9 (Eds. Davison, J. F., Clift, R. and Harrison D.), Academic Press, London, 1985, 331 - 355.

[67] Cankurt, N. T. and Yerushalmi, J., Gas Backmixing on High Velocity Fluidized Beds, in Fluidization (Eds. Davison, J. F. and Keairns, D. L.), Cambridge University Press, Cambridge, 1978, 387 – 393.

[68] Yang, G., Huang, Z. and Zhao, L., Radial Gas Dispersion in a Fast Fluidized Bed, in Fluidization (Eds. Kunii, D. and Toei, R.), Cambridge University Press, Cambridge, 1983, 145 -152.

[69] Helmrich, H., Schugerl, K. And Janssen, K., Decomposition of $NaHCO_3$ in a Laboratory and Bach Scale Circulating Fluidized Bed Reactor, in Circulating Fluidized Bed Technology I, (Ed. Basu, P.), Pergamon Press, Oxford, 1986, 161-166.

[70] Bader, R., Findlay, J. And Knowlton, T.M., Gas/Solids Flow Patterns in a 30.5 cm-Diameter Circulating Fluidized Bed, in Circulting Fluidized Bed Technology II (Eds. Basu, P. and Large, J. F.), Pergamon Press, Oxford, 1988, 123-137.

[71] Weinstein, H., Li, J. Bandlamudi, E., Feindt, H.J. and Graff, R.A., Gas Backmixing of Fluidized Bed in Different Regimes and Different Regions, in Fluidization VI (Eds. Grace, J. R., Shemilt, L. W. and Bergougnou, M.), Engineering Foundation, New York, 1989, 57- 64.

[72] Zheng, Q. Y., Xing, W. And Luo, F., Experimental Study on Radial Gas Dispersion and Its Enhancement in Circulating Fluidized Bed, in Fluidization VII (Eds. Potter, O. E. and Nicklin, D. J.), Engineering Foundation, New York, 1992, 285-293.

[73] Kwauk, M., Wang, N., Li, Y. Chen, B., Shen, Z., Fast Fluidization at ICM, Circulating Fluidized Bed Technology, Proceedings of the First International Conference on Circulating Fluidized Beds, (Ed. Basu, P.), Pergamon Press, Oxford, November 1985, 33-62.

[74] Li, H. and Kwauk, M., Critical pneumatic Moving Bed Transport and Pneumatically controlled Peristaltic Feeder, 13th International Conference on Hydrotransport – Slurry Handling and Pipeline Transport, Johannesburg, South Africa, in Hydrotransport 13, BDR Group Conf. Ser. Publ., 1996, 20, 357-366.

[75] Li, J., Cheng, C., Zhang, Z. Yuan, J., Nemet, A. and Fett, F. N., The EMMS Model - Its Application, Development and Updated Concepts, Chemical Engineering Sciences, 1999, Vol. 54(22): 5409-5425.

ABOUT THE AUTHOR

SONG, Wenli

1959.11	Born in Weifang, Shandong Province, China.

Education

1978.10～1982.08	Student, Harbin Institute of Technology, Harbin, China.
1982.09～1985.05	Graduated student, Harbin Institute of Technology, Harbin, China.
1998.09～2003.12	Ph. D. Student (in service), Institute of process Engineering, CAS.

Woke Experience

1985.05～1986.05	Engineer, Beijing Research Institute of Coal Chemistry, China Coal Research Institute, Beijing, China.
1986.05～1987.05	Engineer, Herman Research Lab., State Electricity Commission of Victoria, Australia.
1987.05～1997.07	Engineer, Senior Engineer, Biejing Research Institute of Coal Chemistry, China Coal Research Institute, Beijing, China.
1997.08～	Senior Engineer, Multi-phase Reaction Lab. Institute of Peocess Engineering, Chinese Academy of Sciences, Beijing, China

PUBLICATIONS

[1] SONG W, LUO L, GREVILLOT G, TONDEUR D, LI J. Adsorption Experiments with Dilute VOCs in a Circulating Fluidized Bed. 96th Annual Conference & Exhibition of the Air and Waste Management Association. San Diego, USA: June 23-26, 2003.

[2] SONG W, XU Y, BAI Y and LI J. Dissemination of NOx-Suppressed and Smokeless Domestic Stoves and Small-Scale Boilers in Developing Areas. R' 2000-Recovery, Recycling and Reintegration. 5th International Congress and Trade Show. Toronto: June 5-9, 2000.

[3] SONG W, BAI Y, LI J. Configuration Optimization of NOx-Suppressed Smokeless Stoves for Burning Coals in Undeveloped Areas. In: Proceedings of R'99 - Recovery, Recycling and Reintegration, 3rd International Congress with Exhibition. Geneva: Feb.2-5, 1999. Vol. 2: 135 (Keynote Speech)

[4] 宋文立，应幼菊，余洁，姚丹. 煤泥浆流化床燃烧的沸腾层燃烧份额. 煤炭学报, 1998, 21(1): 76-79

[5] 韩龙，宋文立，李静海. 循环流化床过度段高度的简化计算.化工冶金，2000, 21(2): 133–138

[6] LI J, SONG W and BAI Y . Current status of biomass-related pollution and technology in China. In: Proceedings of R'99 - Recycle, Recovery and Re-integration, 3rd International Congress with Exhibition. Geneva: Feb. 2-5, 1999. Vol. 4, 27

[7] XU Y, SONG W, BAI Y, LI J. NOx-suppressed Smokeless Coal Combustion and its Application to Coal-fired Kiln. In: Proceedings of Second International Symposium on Clean Coal Technology. Beijing: China Coal Industry Publishing House, 1999. 755-760

[8] Li J, SONG W, Zhang Y and Cao Z. Environment-related research in multi-phase reaction engineering at ICM. Asia Symposium on Multi-phase Flow. November 2-4, 1999, Osaka.

[9] 段文立，宋文立，罗灵爱. 两段循环流化床吸附有机气体的实验研究. 过程工程学报. (已接受)

[10] SONG W, TONDEUR D, LUO L and LI J. VOC Adsorption in Circulating Gas Fluidized Bed. 8th International Conference on Fundamentals of Adsorption. 2004. USA (accepted).

[11] Song W, Luo L, Tondeur D & Li J. Exploring the Details of Flow Structure in a Gas-Solid Circulating Fluidized Bed by the Modified EMMS Model. (修改中)

获奖

“抑制氮氧化物排放的无烟燃煤技术”2001 年中科院技术发明一等奖，第二获奖人

专利

专利名称	专利号	批准日期	说明
发明专利			
解耦循环流化床燃烧系统及其脱硫与脱硝方法	97112562.7	2002.10.09	第四发明人
实用新型			
一种带有推煤装置的炉排	98201669.7	1999.05.12	第一发明人
一种双侧加煤的抑制 NOx 的无烟燃煤炉	98202954.3	1999.08.14	第二发明人
中间加煤两侧燃烧抑制 NO_X 排放的无烟燃煤炉	98207373.9	1999.10.23	第四发明人
一种机械层状解耦式燃烧炉	01259302.8	2002.06.12	第二发明人

ACKNOLEDGEMENT

This thesis is a result of collaborated research project between Multi-Phase Reaction Laboratory, Institute of Process Engineering, CAS, China and Laboratoire des Sciences du Génie Chimique, CNRS, France.

The research was carried out in the framework of the French–Chinese Collaboratory of Chemical and Environmental Engineering, supported by the French National Centre of Scientific Research (CNRS), Department of Engineering Sciences, and by the Ministry of Science and Technology of China (MOST) as parts of the Key Program for International Cooperation of Science and Technology (2001CB711203).

I also obtained financial support from Association Franco-Chinoise pour la Recherche Scientifique & Technique and China Scholarship Council for my study in France. All these supports are gratefully acknowledged.

I would like to thank Mr. Jinghai LI, my supervisor in China for teaching me his unique idea about the multi-phase system and arranging special time for me to work on this project, away from other tasks.

It is a great pleasure to meet Mr. Daniel TONDEUR, my French supervisor. His sagaciousness, erudition and preciseness have left me deep impression. I learned, from him, not only the knowledge in science, but also the history, the culture and the people of France.

I would like to express my thanks also to Prof. Lingai LUO, another supervisor in France and also Yue DONG and Shi DONG. Their great help and encouragement is an important support for me to finish this work.

Thanks also going to my colleagues and student in MPRL. Ms. Yunru BAI and Prof. Zhuyou CAO have taken over a lot of my work. Mr. Jianguo ZHANG helped me to build up the CFB test unit. I have made valuable discussions with Dr. Shiqiu GAO, Dr. Wei GE and Dr. Ning YANG about the EMMS model.

I have also received worm welcome and great help from the people in LSGC, especial Mr. Michel SARDIN, Mr. George GREVILLOT, Mr. Fengdong YU, Miss Isabelle MONZIE and Mr. Didier BORREMANS. They made my stay in Nancy much more joyful and rememberable.

Finally, I would like to thank my son Xiuhan and my wife Qi for their understanding and support. They have lost a lot of time that we can be together. They have experienced, together with me, the loneliness of separation, the difficulties of living abroad and of course the joys involved.

INSTITUT NATIONAL
POLYTECHNIQUE
DE LORRAINE

Service Commun de la Documentation
INPL
Nancy-Brabois

AUTORISATION DE SOUTENANCE DE THESE DU DOCTORAT DE L'INSTITUT NATIONAL POLYTECHNIQUE DE LORRAINE

o0o

VU LES RAPPORTS ETABLIS PAR :
Monsieur John DODDS, Professeur, Ecole des Mines d'Albi-Carmaux, Albi

Monsieur Hongzhong LI, Professeur, Chinese Academy of Siences de Beijing, Chine populaire

Le Président de l'Institut National Polytechnique de Lorraine, autorise :

Monsieur SONG Wenli

NANCY BRABOIS
2, AVENUE DE LA
FORET-DE-HAYE
BOITE POSTALE 3
F - 54501
VANŒUVRE CEDEX

à soutenir devant un jury de l'INSTITUT NATIONAL POLYTECHNIQUE DE LORRAINE, une thèse intitulée :

« Contrôle de l'émission de composés organiques volatils par adsorption en lit fluidisé circulant »

en vue de l'obtention du titre de :

DOCTEUR DE L'INSTITUT NATIONAL POLYTECHNIQUE DE LORRAINE

Spécialité : **« Génie des procédés »**

Fait à Vandoeuvre, le 28 novembre 2003
Le Président de l'I.N.P.L.
L. SCHUFFENECKER

TEL 33/03.83.59.59.59
FAX. 33/03.83.59.59.55